Minimal Haemodynamic Modelling of the Heart & Circulation for Clinical Application

Bram W. Smith

A thesis presented for the degree of
Doctor of Philosophy
in
Mechanical Engineering
at the
University of Canterbury,
Christchurch, New Zealand.

19 January 2004

To:

Sheena E. Smith

my best friend and wife

Acknowledgements

There have been many people that have helped me along the way with this research. I would first like to thank my supervisors; Geoff Chase, Geoff Shaw and Roger Nokes for their contributions. I am very lucky to have a great group of supervisors that have all been happy to help me when I needed it.

In particular I would like to thank Geoff Chase, my main supervisor. Geoff was always available to discuss issues, particularly when I was having difficulties. He included me in a number of different research areas outside my main topic, which I found very interesting, and spent a lot of time helping me with my writing. His contributions and guidance have been greatly appreciated.

I would also like to thank the following people who all made contributions:

Geoff Shaw, my contact at Christchurch hospital and the person who first proposed the research topic. His help and enthusiasm for the research were invaluable, especially when I was trying to figure out all the medical textbooks. No wonder it takes years of training to be a doctor when the medical textbooks are so difficult to read.

Roger Nokes, who I first contacted to help me with the fluids aspects of my research. He has always been happy to talk and I found my discussions with him to be very useful and enjoyable.

Ian Coope, who always enthusiastically helped me, and developed the optimisation routine I use when Matlab's optimisation routines wouldn't work, using his extensive knowledge and enthusiasm for optimisation.

Tim David, who made valuable contributions helping me understand the fluids problems. His positive feedback when I initially showed him my work was very motivating.

Graeme Wake, who has always been ready to help when I needed it since my undergraduate.

Garage (Gary Wake), who helped with the final proof reading of this thesis

and was able to pick up on a number of errors that the rest of us missed. Also, for the many enjoyable hours of kayaking we did every week that helped me get over the days when I didn't seem to be getting anywhere.

Andrew Rudge, for doing the initial proof reading of each chapter and making some valuable contributions.

Mum, Dad and the rest of my family for their encouragement and support all the way through university, and also Sheena's family for their support and interest.

Most importantly, I would like to thank Sheena, for her support and understanding, and for always being enthusiastic about the research, even though she didn't always understand it.

Contents

List of Figures

List of Tables

Nomenclature

α	Womersley number
ℓ	length of tube or vessel
λ	parameter in EDPVR
μ	blood viscosity
ν	blood kinematic viscosity
ω	heart rate (beats/sec)
ρ	density
θ	angle
ao	aorta
av	aortic valve
BPM	beats per minute, heart rate
CO	cardiac output
CR	constant resistance
CVS	cardiovascular system
e(t)	cardiac driver function
ED	end-diastolic
E_{es}	end-systolic elastance
EDPVR	end-diastolic pressure volume relationship
ES	end-systolic
ESPVR	end-diastolic pressure volume relationship
$\underline{F}$	objective function array
$\underline{F}_1$	part of $\underline{F}$ relating to target function values
$\underline{F}_2$	part of $\underline{F}$ relating to amount model parameters are changed
HR	heart rate, (beats/min)
L	inertance

la	left atrium
lv	left ventricle
lvf	left ventricle free wall
mt	mitral valve
$\underline{M}$	objective function array
ODE	ordinary differential equation
$\underline{p}$	model parameters array
P	pressure
P_0	parameter in EDPVR relating to end-diastolic elastance
P_{ed}	end-diastolic pressure
P_{es}	end-systolic pressure
P_{th}	thoracic cavity pressure
pa	pulmonary artery
PAC	pulmonary artery constriction
pcd	pericardium
pu	pulmonary vein
pul	pulmonary circulation system
pv	pulmonary valve
PV	pressure-volume
Q	flow rate (litres/min)
r	radius
r_0	maximum radius
R	resistance
$R_{pul}(t)$	time varying pulmonary resistance, due to respiration
ra	right atrium
RPAC	release pulmonary artery constriction
rv	right ventricle
RVCC	release vena-cava constriction
rvf	right ventricle free wall
spt	septum
SV	stroke volume
sys	systemic circulation system

tc	tricuspid valve
$\underline{u}$	velocity profile vector
$\underline{v}$	optimisation variables array
V	volume
vc	vena-cava
VCC	vena-cava constriction
V_d	relaxed end-systolic volume
V_0	relaxed end-diastolic volume
VProf	velocity profile method
V_{tot}	stressed blood volume
x	position along length of vessel or tube

Abstract

Characterising circulatory dysfunction in critically ill patients, and choosing a suitable treatment, is a difficult and time-consuming problem often faced by medical staff. A stable, minimal closed loop model of the human cardiovascular system (CVS) is developed with the specific aim of assisting medical staff in understanding, diagnosis and treatment selection. Models found in the literature simulate specific areas of the CVS with limited direct use to medical staff while others are either overly complex, difficult to solve, and/or unstable. This thesis develops a minimal model with the primary goal of accurately capturing dynamic trends in the entire CVS. Focus is not just on the overall structure, but on the individual components, such as elastic chambers and fluid flow elements, to ensure their physiological accuracy. A novel mixed-formulation approach to simulating blood flow in lumped-parameters CVS models is outlined that adds minimal complexity, but significantly improves physiological accuracy. Optimisation is used to determine patient specific model parameters and create patient specific models in reasonable times, taking the model closer to useful clinical application than previous models.

The minimal model is shown to match experimentally measured static and transient CVS dynamics for ventricular and cardiopulmonary interactions. Few other models are verified to simulate dynamic cardiopulmonary interactions, and none were found that simulate dynamic ventricular interactions. The minimal model was also verified to simulate a variety of CVS dysfunctions due to heart disease and shock. By simulating different dysfunctions and reflex responses, the model can be used to improve understanding of the major contributing factors to CVS dysfunction as well as the relative importance of specific elements and reflex actions. The model offers a powerful tool that can be used in conjunction with experimental research to improve understanding of CVS function, and assist medical staff in diagnosis and therapy selection.

Chapter 1

Introduction

Cardiovascular disease is the largest cause of death in western countries [Westerhof, 2003]. Cardiovascular dysfunction can occur in many areas of the cardiovascular system (CVS) as a result of a wide range of causes, such as age, birth defects or illness. While a great deal of research has been carried out investigating CVS function, much is still unknown about the causes and treatment of cardiovascular disease. The CVS is an extremely complex system involving a combination of hydraulic interactions, nervous system responses and other biological influences. These complex interactions mean that although extensive experimental research has been carried out into CVS function, a great deal remains unknown about the cause and effect of these interactions and dysfunctions.

This chapter discusses how a working minimal model of the CVS would be useful to medical staff in patient diagnosis and treatment. The physiology of the circulation system is also discussed, emphasising the dynamics that this model aims to reproduce. Different approaches to modelling the CVS found in the literature are discussed and compared with the aims of this work. From this discussion a minimal model design philosophy is outlined in detail.

1.1 Applications of a CVS Model

While extensive experimental research has been carried out, there is still much to be learned about the function of the CVS system in healthy and dysfunctional circulation systems. Experimental work is mostly carried out on animals and often involves invasive surgery that itself significantly affects CVS function. In addition, data measured from patients with various CVS diseases is not only influenced by the cause of the dysfunction, but by the reflex actions that are activated to maintain blood pressure and cardiac output.

Pin-pointing CVS dysfunction is often difficult because the clinical signs, or the availability and interpretation of physiological measurements, are unreliable, noisy or contradictory. Health professionals must often rely on intuition and experience to make a "clinical" diagnosis in order to decide upon treatment options. Sometimes this approach results in multiple therapies being applied until a suitable treatment is found. Poor outcomes or death can result from failure to correctly diagnose and treat the underlying condition.

A suitable CVS model could be used to assist medical staff in a variety of applications ranging from improving understanding of CVS function to assisting in diagnosing the cause of dysfunctions. Unlike most experimental research, a model can isolate the function of particular areas of the CVS and identify their contribution to the overall haemodynamics. A model could also be used to identify the impact of particular dysfunctions on overall CVS function while ignoring the effects of reflex actions.

This research aims to create a minimal mathematical model of the cardiovascular system to directly assist health professionals in the key areas of understanding, diagnosis and therapy. Medical staff will be able to easily investigate the cause and effect of various types of cardiac dysfunctions. A model that captures many of the essential dynamics of the CVS can also be used as a teaching aid to improve understanding of CVS function. An appropriate computer model of the CVS system could be used to process patient data including blood pressures, respiratory pressures, blood flow rates, ECG signals and heart rate. The model can be used to identify inconsistencies and irregularities in recorded patient data to aid medical staff in choosing suitable fluid, drug, or mechanical interventions to improve patient condition. More specifically, the known effects of treatments such as drug therapies, or mechanical assist devices can be applied to a model that has been customised to simulate a particular patients condition [Frazier et al., 2001; Westaby et al., 2000].

A specific example of modelling particular treatments is the *VentrAssist* cardiac assist device currently being tested in New South Wales, Australia [VentrAssist, 2003]. This small electronic centrifugal pump bypasses the aortic valve, pumping blood directly from the ventricle into the aorta helping to increase circulation and blood pressure [Skatssoon, 2003]. The impact on CVS dynamics of implanting the *VentrAssist* pump could, for example, be tested on the proposed model to determine the feasibility of implants.

1.2 Cardiovascular System Physiology

The CVS can be divided into two key areas: the heart, which pumps the blood, and the circulation system, which channels the blood to every part of the body [Guyton, 1991; Hurst, 1966]. The heart and CVS form an extremely complex system with many books dedicated to explaining all of the hydraulic, nervous and biological interactions. This research focuses on simulating hydraulic function, which means that although the effects of different reflex actions can be simulated, the physiological activation of these actions is not modelled.

1.2.1 The Heart

The heart is made up of two distinct pumps known as the left and the right heart. The right heart pumps deoxygenated blood returning from the body into the lungs where carbon dioxide is removed and oxygen is absorbed into the blood. The left heart pumps oxygenated blood from the lungs to all the tissues in the peripheral circulation, supplying them with oxygen and nutrients. The layout of the heart and the flow of blood through it is shown in Figure 1.1. Each pump consists of an atrium and a ventricle in series. Both are active elastic chambers that contract by increasing wall tension to pump blood. The ventricle provides most of the pumping function and the atrium acts as a booster to supplement ventricle performance. In fact, the heart can operate effectively under resting conditions without the atria functioning, relying solely on the ventricles [Guyton, 1991].

Both ventricles and atria are contained within the pericardium, a relatively stiff walled passive elastic chamber that encapsulates the heart [Glantz and Parmley, 1978]. During contraction, the walls of the cardiac chambers thicken, swelling both inwards to reduce chamber volume, and outwards. The pericardium acts as an outer constraint to this expansion, meaning the myocardium mostly expands inwards, forcing blood out of the ventricle. Without this outer constraint of the pericardium, ventricle performance is reduced [Hoit et al., 1993].

As shown in Figure 1.2 the right ventricle appears attached to the wall of the left ventricle and they share a common section of cardiac muscle wall called the septum. It is because of this common wall, as well as the influence of the pericardium, that the ventricles interact with each other. For example, right ventricle overload is widely investigated, where right ventricle swelling pushes on the left ventricle and impedes its function [Marcus et al., 2001; Lazar et al., 1993].

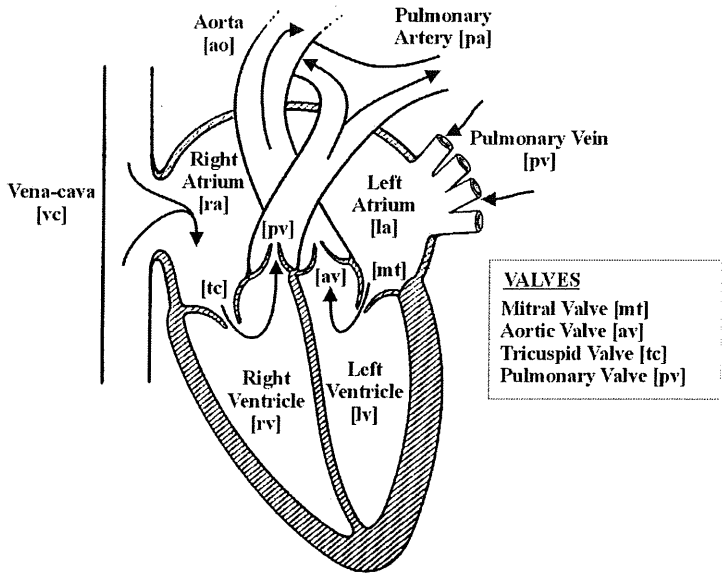

Figure 1.1 Diagram of heart showing directions of blood flow.

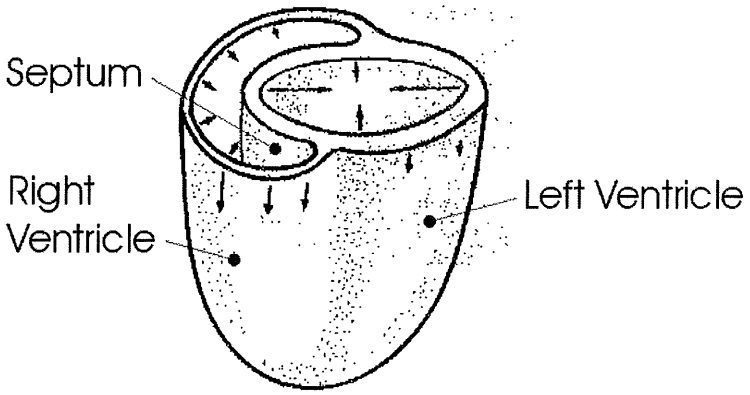

Figure 1.2 A computer reconstruction of a heart showing the right ventricle as appearing to be attached to the side of the left ventricle [Weber et al., 1981].

The heart muscle is known as the myocardium and surrounds each ventricle, contracting when triggered by the sinoatrial node (SA node). An electrical impulse originating from the SA node, the natural pacemaker of the heart, first activates both atria causing them to contract and pump a final burst of blood into the ventricles. About 0.1-0.2s later the signal travels to the ventricles causing them to contract, forcing blood out of the heart [Guyton, 1991].

The function of the heart is dependent on the heart valves which are located at the inlet and outlet of each ventricle. During ventricular contraction the inlet

heart valves close and the outlet valves open, pushing blood into the arterial circulation system. During ventricle expansion, the outlet valves close and the inlet valves open to allow blood to flow into the ventricles from the venous system. Thus, the heart valves ensure blood only flows in a forward direction through the ventricles and are essential for heart function. This dependence means valvular dysfunctions, such as mitral stenosis or aortic insufficiency, can significantly affect heart function causing life threatening consequences [Braunwald, 1997; Parrillo and Bone, 1995].

1.2.2 The Circulatory System

The circulatory system can be divided into two regions. The pulmonary circulation refers to blood flow through the lungs and the systemic circulation refers to blood flow through the rest of the body [Guyton, 1991]. Figure 1.3 illustrates the complex layout of arteries, capillaries and veins that circulate blood to every part of the body. Figure 1.4 shows a simplification of the circulatory system that more closely matches the layout assumed for the proposed model.

Blood exits the heart from the ventricles and enters either the pulmonary or systemic circulation systems through large diameter vessels known as arteries. Deoxygenated blood is pumped from the right heart through the pulmonary artery and into the lungs. Oxygenated blood passes from the left ventricle into the systemic circulation to be distributed to the body. From the arteries, blood flows through consecutively smaller tubes, eventually reaching capillaries, with diameters on the order of microns [Guyton, 1991]. In pulmonary capillaries the blood is oxygenated and in the systemic circulation capillaries oxygen and nutrients are transferred to the body tissues. Blood returning from the capillaries flows through consecutively larger vessels, eventually leading to the veins which take the blood back to the heart. The veins are the main storage area of the circulation containing much of the total blood volume of the body.

The venous system, shown in Figure 1.4, is the largest storage area of blood in the body containing roughly 64% of the total blood in the body [Guyton, 1991]. During ventricular relaxation (diastole) blood returning from the systemic circulation flows from the vena-cava, through the right atrium and tricuspid valve and into the right ventricle, as shown in Figure 1.1. When the right ventricle contracts (systole) the tricuspid valve closes and the pulmonary valve opens allowing blood to flow into the pulmonary artery. Blood flows from the pulmonary arteries into the capillaries and back to the pulmonary veins where it accumulates. When

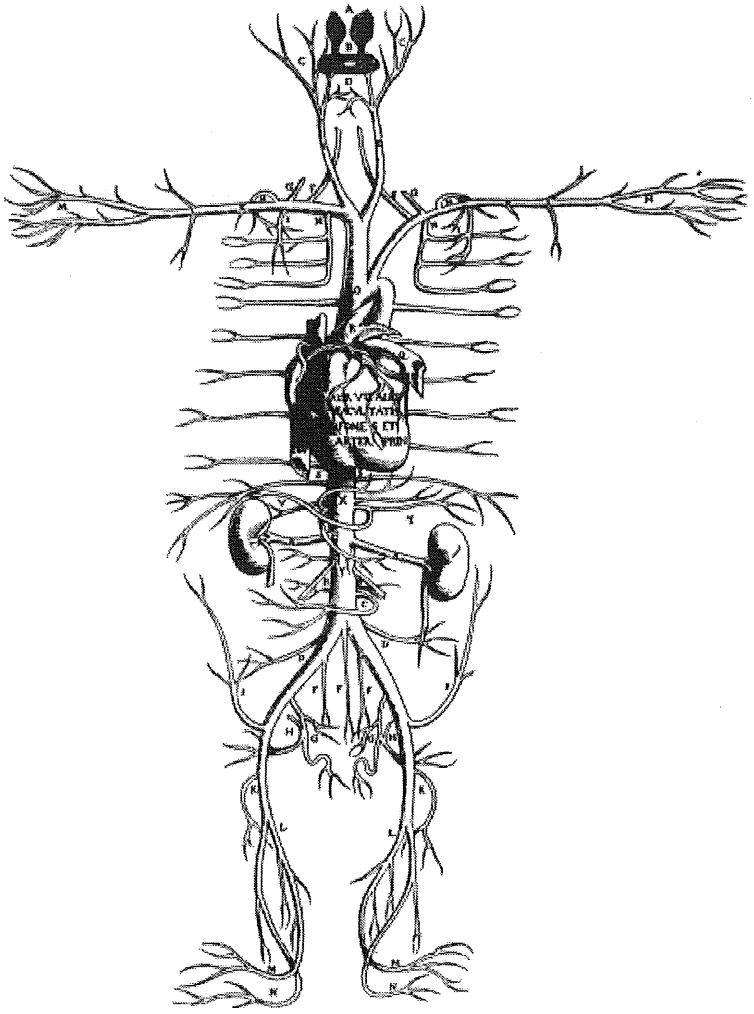

Figure 1.3 Modified sketch of the circulation system originally drawn by Versalius (1514-1564) in his Tabulae Anatomicae [Opie, 1998].

the left ventricle relaxes, the mitral valve opens and blood flows through the left atrium into the left ventricle. As the left ventricular pressure increases during systole, the mitral valve closes and the aortic valve opens, forcing blood into the aorta. Blood enters the aorta and flows into the capillaries of the systemic circulation until finally returning to the vena-cava.

The heart is located, along with the pulmonary circulation, within the thoracic cavity. The pressure in the thoracic cavity varies as the pressure in the lungs varies during respiration. As shown in Figure 1.5, the thoracic cavity pressure is defined as the pressure around the outside of the heart. The intrapulmonary pressure is the pressure inside the lungs. The plot in Figure 1.5 shows the relationship between the variation in the thoracic cavity pressure and the intrapulmonary

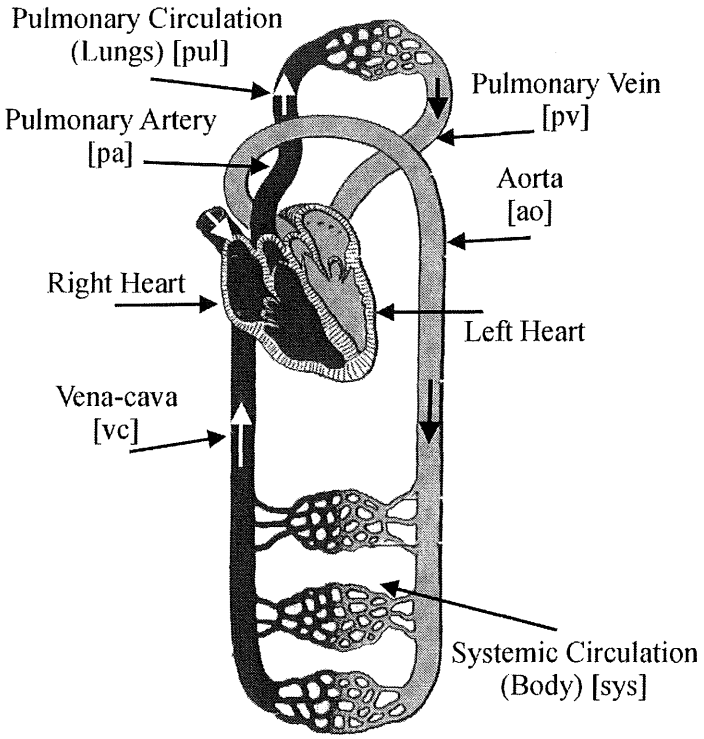

Figure 1.4 Simplified diagram of the human heart and circulation system [Guyton, 1991].

pressure.

Pressure variations in the lungs alter the pressure acting on the outside of the heart, having an impact on its performance. During an intake of breath (inspiration) the diaphragm deflects downwards causing negative thoracic cavity and intrapulmonary pressures as air is sucked into the lungs. When breathing out (expiration) the diaphragm deflects upwards increasing the intrapulmonary pressure to become positive and forcing air out of the lungs, while the thoracic cavity pressure becomes less negative. This variation in intrapulmonary pressure during respiration results in variations in thoracic cavity pressure as shown in Figure 1.5 and influences the function of the heart.

Inspiration causes a negative pressure in the thoracic cavity (about -8mmHg for a normal person) and results in a build-up of blood in the pulmonary circulation system. The opposite effect occurs during expiration when the intrapulmonary pressure is positive and the thoracic cavity pressure is higher (about -5mmHg for a normal person). Air is forced out of the lungs and the higher pressure causes the volume of blood in the pulmonary circulation system to decrease [Scharf and Cassidy, 1989; Guyton, 1991].

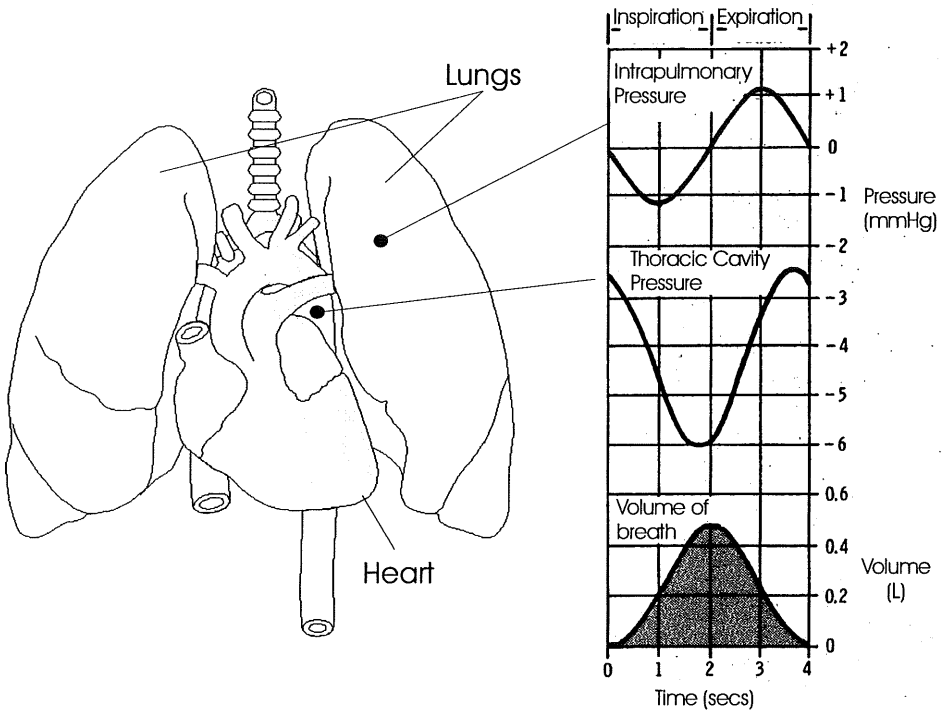

Figure 1.5 Diagram showing the heart located between the lungs and the relative variations in intrapulmonary pressure, thoracic cavity pressure and volume of breath (modified from [Ganong, 1979]).

These cardiopulmonary interactions can have a significant effect on cardiac performance, particularly on cardiac output. During positive pressure breathing, where a patient is mechanically ventilated, the thoracic cavity pressure significantly affects cardiac output [Scharf and Cassidy, 1989]. The positive pressure generated in the lungs by mechanical ventilation causes a significant drop in cardiac output, which can be detrimental to the health of a ventilated critically ill patient, although it does protect the lungs.

1.2.3 Cardiac Function

Indices of cardiac function are used by health professionals to identify the performance of the heart. Three of the most common indicators of cardiac function include the pressure-volume (PV) diagram, cardiac output, preload and afterload. These measures are often used by health professionals to study patient condition.

The PV Diagram

PV diagrams for elastic chambers, as schematically shown in Figure 1.6, are used extensively by medical professionals to explain the pumping mechanics of the ventricle. A lot of information can be interpreted from a PV diagram and it is the method of choice for both medical staff and engineers for analysing ventricle function. Two main characteristics of the PV diagram are the lines plotting the End Systolic Pressure-Volume Relationship (ESPVR) and the End Diastolic Pressure-Volume Relationship (EDPVR) which define the upper and lower limits, respectively, of the cardiac cycle.

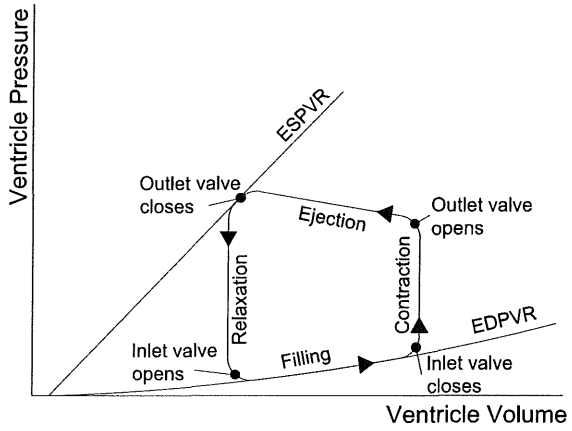

Figure 1.6 An example of a pressure volume diagram.

The cardiac cycle, marked on Figure 1.6 by the triangular arrows, is divided into four parts: filling, contraction, ejection and relaxation. Filling occurs when the upstream pressure in the atrium is greater than the pressure in the ventricle. During contraction, the pressure in the ventricle becomes greater than the pressure upstream, the inlet flow goes to zero, and the valve closes. With both inlet and outlet valves closed a period of isovolumetric ventricular contraction is induced by the cardiac muscle. When the ventricle pressure is above the downstream pressure in the arteries the outlet valve opens and blood is ejected. The ejection phase continues until the flow out of the ventricle stops, the outlet valve closes, and the ventricle relaxes. The ventricle expands isovolumetrically during relaxation until its pressure is again below the upstream pressure and the inlet valve opens to repeat the cycle. Note that the *open on pressure, close on flow* valve law is clearly evident in these fundamental definitions [Opie, 1998; Little, 1978].

The EDPVR for a given ventricle is a measure of the compliance of the ventricle. Compliance, defined as the inverse of elastance (E), is the common term used by medical professionals to describe the PV relationship of an elastic chamber. Figure 1.7 shows how during diastolic failure, otherwise known as a stiffening of the heart wall, the compliance of the heart wall decreases. Heart wall stiffening results in a drop in cardiac output with a detrimental effect to the patients circulation [Opie, 1998].

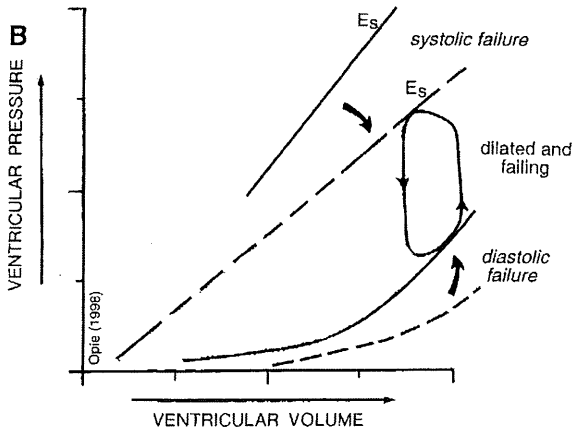

Figure 1.7 Variations in the ESPVR (labelled systolic failure) and the EDPVR (labelled diastolic failure) during heart failure [Opie, 1998].

The ESPVR gives a measure of cardiac contractility, or the strength of contraction, which is roughly defined as the rate at which the myocardium reaches peak wall stress [Guyton, 1991; Opie, 1998]. On the PV diagram, the contractility is proportional to the gradient of the ESPVR. As shown in Figure 1.7, a reduction in contractility causes systolic failure and the slope of the ESPVR line decreases, which results in a reduction in blood pressure and cardiac output. A reduction in contractility is often seen in heart failure when part of the myocardium becomes damaged, and is colloquially referred to as a "floppy heart" [Opie, 1998].

Blood Flow

Stroke volume (SV) is the main measure of blood flow on a beat by beat basis. The stroke volume is defined as the amount of blood pumped from the ventricle in one heart beat. For a more general measure of blood flow, cardiac output (CO) is defined as the amount of blood pumped into the aorta, from the left ventricle, in litres per minute. Cardiac output is therefore equal to the product of stroke

volume and heart rate (HR) [Opie, 1998].

$$CO = SV \times HR \tag{1.1}$$

Cardiac output is an important measure of cardiac function, defining the ability of the heart to pump oxygen and nutrient rich blood to the peripheral tissues. Equation (1.1) highlights the important dependence of the cardiac output on both stroke volume and heart rate. While heart rate is driven by the sympathetic nervous system, the stroke volume is dependent on the function of the myocardium as well as ventricle preloads and afterloads. Ventricle preloads and afterloads give measures of the boundary conditions around the heart, which are influenced by the cardiovascular system as a whole.

Preload & Afterload

The definitions of cardiac preload and afterload used in the literature vary depending on their application. Definitions include ventricle wall stress or strain, end-diastolic and end-systolic pressures, and peripheral resistances, as well as many more combinations [Norton, 2001]. Preload and afterload are generally intended to be measures of ventricular boundary conditions, indicating the state of the ventricle before and after contraction respectively. Preload is a measure of the muscle fibre length, or the amount that the cardiac muscles are stretched, immediately prior to contraction. Afterload is a measure of the cardiac muscle stress required to eject blood from a ventricle, or the pressure the ventricle must pump against. However, outside influences can affect the preload and afterload pressures such as thoracic pressure variations due to breathing.

A more suitable means of measuring preload and afterload is the wall stress of the ventricle, or the pressure across the ventricle wall [Norton, 2001]. However, these transmural pressures are difficult to measure in a patient, while the pressures at inlet and exit from the heart are relatively easier to measure using common invasive sensors. For this reason, venous and arterial pressures around the heart are the most common surrogate measures of ventricle preload and afterload, respectively.

1.3 Cardiovascular System Modelling

Most approaches to modelling the human CVS can be divided into either finite element (FE) or pressure-volume (PV) approaches. The finite element approach involves breaking down each part of the CVS in great detail and utilising finite element calculations to simulate function. The PV approach is a simpler method, grouping parameters and making assumptions to simplify the model as much as possible, while still attempting to simulate the essential dynamics. This section discusses both methods and investigates which approach is best suited to the application of diagnostic assistance and therapy selection.

1.3.1 Finite Element Approach

FE techniques offer micro-scale results that can theoretically be very accurate both in magnitude and in trends. To simulate a section of the CVS, very detailed micro-scale measurements must be taken of its mechanical properties such as elastic properties, dimensions and fibre directions. This information is then used in detailed finite element equations that simulate the dynamics of the component being modelled on a microscale. A great deal of research has been done in this area with significant results helping to improve understanding.

The Bioengineering institute at Auckland University has carried out extensive micro-scale research into the structure of the heart. Work has been carried out both measuring and modelling myocardial structure, coronary blood flow that supplies blood to the heart muscle, and the excitation of the cardiac muscles. This group has mapped the structure of the cardiac muscle, including muscle fibre directions, and created a finite element model of the heart [Nielsen et al., 1991; Legrice et al., 1997; Stevens and Hunter, 2003]. The model is used to give detailed insight into cardiac excitation during contraction [Hunter et al., 1991; Buist et al., 1999].

Other models such as that of Peskin et.al. (1992) attempt to model the complex fluid flow dynamics in the heart, particularly around the heart valves. Glass et.al. (1991) reviews many of the current finite element approaches to investigating cardiac function. Methods are outlined for measuring and simulating the structure, excitation and fluid flow in the heart to varying degrees of precision.

While FE simulation research has made significant contributions to the understanding of cardiac function, its lack of flexibility makes it unsuitable for patient-specific, rapid diagnostic feedback. It is not feasible to obtain the detailed

patient specific measurements of cardiac structure required to create a patient specific model from a living patient. FE models require significant computational time to solve even on the most powerful computers making them unsuitable for immediate feedback. These models focus primarily on the function of the heart and either do not simulate the closed loop function, or simulate it using lumped-parameter models.

1.3.2 The Pressure-Volume (PV) Approach

PV methods are lumped parameter modelling methods where the CVS is divided into a series of elements simulating elastic chambers and other elements simulating blood flow. Elastic chamber elements model the pressure-volume relationship in a section of the CVS, such as a ventricle, an atrium, or a peripheral section of the circulation system such as the arteries or veins. The fluid flow elements connecting these chambers simulate blood flow through different parts of the circulation system. Lumped parameter CVS models are usually illustrated using electrical circuit analogies, hydraulic circuits or a combination of each. Figure 1.8 shows an illustration of the aorta along with a hydraulic representation and an electrical circuit analogy of the aorta.

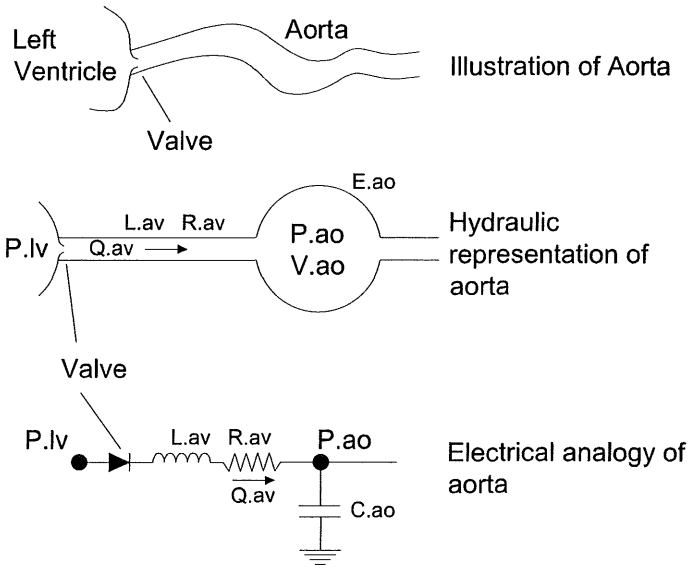

Figure 1.8 Illustration of aorta (top), the hydraulic representation of the aorta (middle) and the electrical analogy representation (bottom).

Electrical Analogies and Hydraulic Representations of the CVS

In electrical circuit models pressure is analogous to voltage, flow rate is analogous to current and volume is analogous to charge. Capacitors are used to simulate elastic chambers, as shown in Figure 1.8 where the capacitor (C_{ao}) simulates the elastic properties of the aorta. A resistor (R_{av}) simulates the pressure drop as blood flows through the aorta and an inductor (L_{av}) simulates inertial effects acting on the blood. Thus, a section of the CVS where fluid flows through an elastic tube, such as the aorta, is modelled as a capacitor, a resistor and, sometimes, an inductor in series. Valves, such as those at the inlet an exit of each ventricle, are represented by diodes.

On a component scale, standard electrical circuits make linear approximations of the pressure-volume relationships and fluid flow properties in the CVS. However, linear models inadequately capture some of the dynamics of many areas of the CVS. For this reason most CVS models adopt non-linear equations to varying degrees to make the models more physiologically accurate. For example, Tsitlik et.al. (1992) investigates using non-linear capacitors to more accurately simulate the physiological function of elastic chambers.

Hydraulic diagrams are an alternative method of illustrating CVS models. Figure 1.8 shows a hydraulic representation of the aorta with the elastic chamber represented by a circle, where the pressure-volume relationship is a function of the chamber elastance. Tubes connecting these chambers show where the fluid dynamics of blood flow are measured.

Figure 1.9 compares two CVS model diagrams of approximately equal size, where Figure 1.9(a) uses an electrical circuit analogy and Figure 1.9(b) uses a hydraulic circuit representation. Electrical circuit analogies are well suited to complex CVS models as standard circuit simulation and analysis techniques can be used when solving the complex dynamics [Tsitlik et al., 1992; Stergiopulos et al., 1999; Melchior et al., 1992]. However, hydraulic circuits offer a more realistic representation of the CVS components and are not constrained by the linear function of most electrical components. In many cases, the governing equations used to simulate electrical circuit and hydraulic models are very similar.

Lumped parameter CVS models using either electrical circuit analogies or a hydraulic representation are generally constructed as a series of Windkessel type circuit. A Windkessel circuit separates the elastic properties of a section of the CVS from the fluid dynamic properties for flow through arteries and veins. A

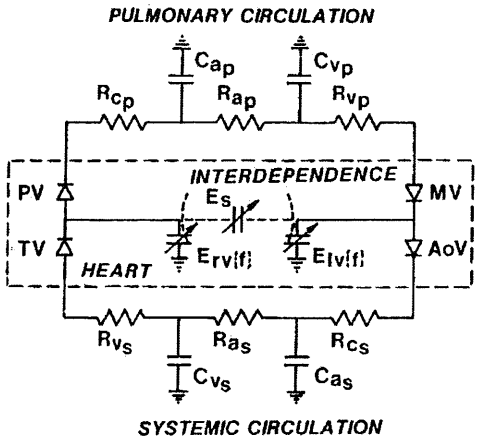

(a) Layout of circulation system used by Santamore et.al. (1991).

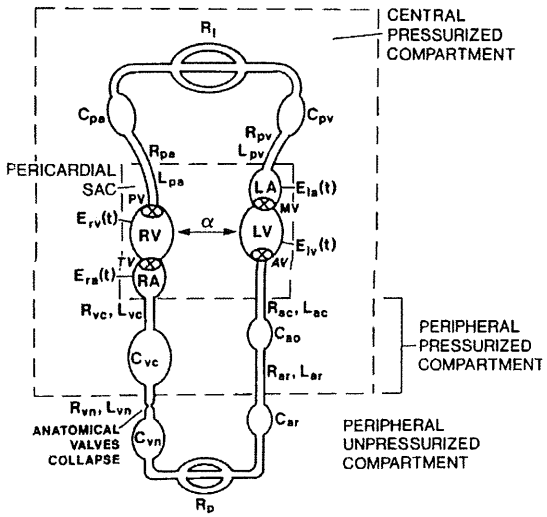

(b) Layout of circulation system used by Beyar et.al. (1987).

Figure 1.9 Comparing two CVS model representation of roughly equal size, electrical circuit analogy (a) and hydraulic representation (b).

rigid tube simulates the fluid dynamic effects and an elastic chamber simulates the compliance of the vessel [Tsitlik et al., 1992; Melchior et al., 1992]. This approach avoids the complex, often unstable, equations that govern fluid flow through an elastic vessel such as the aorta.

For example, the elastic properties of the aorta are simulated using an elastic chamber and the pressure in the chamber is calculated using a relatively simple

pressure-volume relationship. The fluid dynamic properties are simulated as flow through a rigid tube, which has much simpler governing equations than a flexible tube. Similarly, the entire CVS is divided into a series of elastic chambers connected by rigid tubes. In Figure 1.8 the elastic properties are simulated using either the elastic chamber or the capacitor labelled with the subscript ao. The fluid dynamics of blood flow through the aorta are simulated through the sections labelled with the subscript av.

CVS models also come in varying degrees of complexity and focus, with a large range of models that simulate only small areas of the CVS. For example, some authors focus on simulating the function of the left ventricle only [Avanzolini et al., 1985; Hunter et al., 1983; Campbell et al., 1990; Wijkstra and Boom, 1991]. Others investigate the haemodynamic effects of ventricular interaction or interdependence with a number of different approaches used [Chung et al., 1997; Beyar et al., 1987; Amoore et al., 1992; Santamore and Burkhoff, 1991; Sun et al., 1997]. Finally, some researchers attempt to model the entire circuit as a series of passive and active elastic chambers in a closed circuit [Sun et al., 1997; Santamore and Burkhoff, 1991; Beyar et al., 1987; Burkhoff and Tyberg, 1993; Ursino, 1999; Chung et al., 1997; Olansen et al., 2000; Lu et al., 2001]. This research focuses primarily on closed loop models, although some of the theory from smaller models is applied in specific areas of larger closed loop simulations.

Current Closed Loop CVS Models

Figure 1.10 illustrates the lumped parameter closed loop electrical circuit analogy CVS model proposed by Sun et.al. (1997). This model illustrates a common temptation with electrical circuit analogies to build larger complex circuits in the hope of capturing as many of the CVS dynamics as possible. Complex circuits may have the capability for more physiologically accurate simulations, but understanding the individual contributions of each component and choosing suitable parameter values is extremely difficult.

Santamore et.al. (1991) presents an electrical circuit analogy model, shown in Figure 1.9(a), that includes the dynamics of ventricular interaction. However, the model is only verified against static experimental data that shows how one ventricle reacts when the volume of the other is changed. The model is not shown to simulate transient haemodynamic response of ventricular interaction due to sudden variations in the volume of one ventricle.

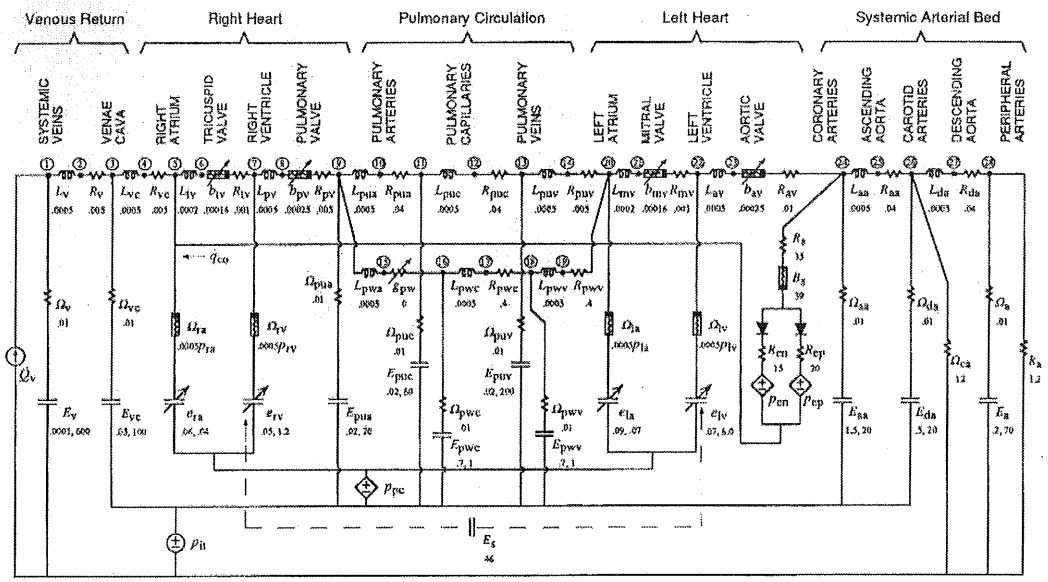

Figure 1.10 Electrical analogy of cardiopulmonary system by Sun et.al. (1997).

Beyar et.al. (1987) presents the closed loop, 10 chamber model shown in Figure 1.9(b) that includes the effects of ventricular interaction and thoracic cavity pressure variations. Limited results show the model captures some of the transient response of the CVS due to dynamic thoracic cavity pressure variations. However, ventricular interaction is verified only against static experimental data.

Burkhoff and Tyberg (1993) present a closed loop model specifically designed for simulating the effects of left ventricle dysfunction. Using this model they are able to comment on the contribution of nervous system reflexes involved in left ventricle dysfunction in CVS dynamics. Similarly, Ursino (1999) presents a model specifically designed for simulating the effects of the baroregulation on CVS function. Nether model accounts for the affects of ventricular or cardiopulmonary interactions. Although both models make contributions to understanding the mechanisms involved in these specific cases, the models are not shown to be general enough to capture other types of dysfunction.

Chung et.al. (1997) present an open loop model of the heart including ventricular interaction due to the septum and the pericardium. The model provides good short term results, however these results are very dependent on accurate calculation of initial conditions. Additionally, accumulation of numerical error causes this model to diverge when simulated over longer periods on the order of 40secs. This problem is caused by too many governing equations over-defining the

model. In spite of this problem, the model was able to produce results for static ventricular interaction that match experimental results. Olansen et.al. (2000) built on this work to create a much more complex closed loop model that once again matched static experimental results for ventricular interaction.

Lu et.al. (2001) also extended this work to include the influence of baroreceptor control of heart rate, myocardial contractility and vasomotor tone. They also added a detailed lumped parameter model of lung function and it's influence on cardiac function. Results show the model roughly captures trends in some CVS haemodynamics. It is also shown to capture the transient haemodynamic response of the CVS due to significant variations in thoracic cavity pressure during forced breathing. However, the examples used for model verification are limited and the model is not shown to be flexible enough to capture a variety of dysfunction. It is also worth noting that this research appears to be still built on the over-defined ventricular interaction model presented by Chung et.al. (1997).

Although all the presented models make contributions to the understanding of various types of dysfunctions, most are not shown to be capable of simulating a range of CVS function and dysfunction. Additionally, it is not shown how any of these models can be of direct use to medical staff for diagnostic assistance. However, these lumped parameter models show how it might be possible to capture various CVS dynamics using a minimal number of equations, parameters and variables such as chamber elastances and arterial resistances. Governing equations are developed in this research that can be simulated on modern, commonly available desktop computers in very reasonable times suitable for immediate feedback.

CVS Models Summary

PV models can rapidly simulate patient-specific CVS dynamics on a standard desktop computer offering the potential for real-time patient specific models. However, the simplicity of these models comes at the expense of accuracy and a PV model may be too simple to capture all of the critical dynamics. Where lumped parameter methods sometimes do not capture enough detail there is a need to include some of the complexity and physiologically accurate equations of the finite element approach. Complexity costs computational power and time, and should therefore only be added where significant benefits are obtained over a simpler method. Hence, the addition of complexity to make a lumped pa-

rameter model more physiologically accurate must be justified by demonstrating significant improvements in physiological accuracy.

The development of the minimal model used in this research is based on a minimalist approach where the model is kept as simple as possible unless the addition of complexity will result in a significant improvement in physiological accuracy. The basic building blocks of the model are the passive and active elastic chambers, and the governing equations for flow between these chambers. The function of the basic model building blocks are investigated individually before assembling these components to create a full closed-loop model. This approach ensures that the individual contributions of each component are known when analysing the performance of the complete model.

1.4 Minimal Modelling Approach

As discussed, there are many examples in the literature of models that simulate and aid in the understanding of specific types of cardiac function. However, these models are not shown to be of direct use to medical staff to assist in diagnosis and therapy selection. In addition, many models in the literature focus on simulating only particular types of dysfunction and not on a general simulation of the CVS. This research aims to not only create a model of the entire CVS to simulate a wide variety of dysfunction, but also to structure the model so that it can be easily applied for use by medical staff. This section outlines a list of specifications that the final model must achieve, followed by an outline of the general philosophy behind this minimal model approach.

1.4.1 Model Specifications

The approach used involves combining the lumped parameter and finite element modelling techniques discussed previously with the requirements of medical staff to create a useful, rapid-feedback, diagnostic assistance system. It is intended that the model will fulfil the following goals:

- A full closed-loop, stable model is required with minimal complexity and physiologically realistic inertia and valve effects.
- Model parameters can be relatively easily determined or approximated for a specific patient using standard, commonly used techniques.

- The model can be run on a standard desktop computer in reasonable time, (eg. on the order of 1-5 minutes)

- Although quantitatively exact results are not necessary, accurate prediction of trends is required.

These goals are set to restrict the model from becoming too complex while ensuring its practicality. The limitations on the patient-specific information, computational power, and solution time means the PV modelling method offers the greatest potential for fulfilling the intended requirements.

In summary, a "Minimal Model" approach to CVS modelling means using a minimal number of governing equations and parameters where other similar models in the literature have been found to use many variables and complex formulae. Using minimal, simple governing equations avoids the instability and non-uniqueness of solution found in the model developed by Chung et.al. (1996) and further used by Olansen et.al. (2000) and Lu et.al. (2001). Using minimal variables avoids problems associated with large complex models such as the one presented by Sun et.al. (1997). Less variables means less parameters that must be defined, and an easier model to analyse and understand.

The general approach of this research is to make the model minimal, stable and easily solved. The CVS is an inherently stable system and therefore stability in the model must be a key feature. Straight forward solution is important, emphasising that the model must be solvable in a reasonable time on a standard commonly available computer. The minimal CVS model will be a closed loop model that is capable of capturing a variety of CVS interactions and dysfunction, and not just focus on special cases.

1.5 Summary

An overall approach to modelling the human CVS is proposed that will create models to help medical staff in the key areas of understanding, diagnosis and treatment of CVS dysfunction. A detailed design philosophy is outlined to create an easily solved, stable, minimal model. Prior CVS models and methods are presented and discussed in detail. Lumped parameter pressure-volume modelling methods are identified as the most suitable method for achieving the target model performance.

This thesis focuses first on the construction of the proposed CVS model starting with a simple model of a single cardiac chamber and concluding with a full closed loop model. Two basic building block of the CVS model are identified, the governing equations for the elastic chambers and the fluid flow between these chambers. The next chapter examines the governing equations for the active and passive elastic chambers. The mathematics and assumptions of the fluid flow between the chambers are then discussed in the following chapter. The method of simulating these dynamics is then discussed followed by simple model verification examples. Subsequent chapters show methods of identifying model parameters to create patient specific models, and simulating CVS function in both healthy and diseased cardiovascular systems.

Chapter 2

Minimal Model

Ultimately, the model presented is intended to simulate the essential haemodynamics of the cardiovascular system including the heart, and the pulmonary and systemic circulation systems. Figure 2.1 shows the model used for this research made up of elastic chambers connected by resistors and inductors in series. The layout of Figure 2.1 can be compared with the simplified representation of the CVS shown in Figure 1.4. The atria have not been added as they contribute only slightly to the main cardiac trends and can be easily added for more specific cases [Guyton, 1991].

The model is divided into blocks of Windkessel like circuits. Windkessel circuits separate the pressure-volume properties and the fluid flow properties of each section of the CVS into different model components [Tsitlik et al., 1992; Melchior et al., 1992]. This method avoids the complex formulae that govern fluid flow through an elastic tube such as the aorta. An elastic chamber, labelled E_{ao} in Figure 2.1, simulates the elastic properties of the aorta, determining the pressure as a function of volume. The resistor (R_{av}) and inductor (L_{av}) simulate the pressure drop and inertial effects, respectively, acting on blood flowing through the aorta.

Each elastic chamber, labelled E in Figure 2.1, simulates the pressure-volume relationship in a particular area of the circulation system. Often this means that an elastic chamber will be simulating a series of physiological chambers. The model presented in Figure 2.1 divides the circulation system into 6 main blood storage areas simulated using elastic chambers.

Two active elastic chambers are used to simulate the left and right ventricles (lv and rv). The ventricles are coupled, via the septum and pericardium, to account for the important ventricular interaction dynamics. The remaining chambers are passive, with constant elastance and simulate the remainder of

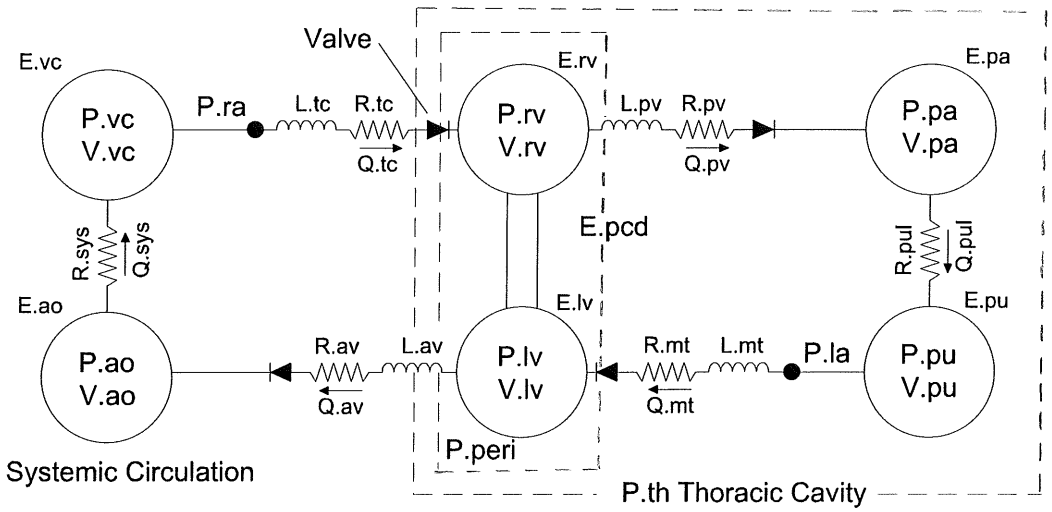

Figure 2.1 The presented closed loop model of the cardiovascular system.

the circulation system. The vena-cava chamber (vc) models the elastance of the larger veins returning from the systemic circulation system as well as the right atrium. Similarly, the pulmonary vein chamber (pu) includes the elastance of the left atrium as well as the large blood storage veins in the pulmonary circulation. The aorta chamber (ao) captures the pressure-volume relationships of the large arteries leading from the left ventricle into the systemic capillaries. In the same way, the pulmonary artery chamber (pa) simulates elastance effects on blood in the large arteries leading to the lungs. With further model developments, the CVS can be divided into more chambers to more accurately capture dynamics where necessary. However, this addition of elastic chambers would increase model complexity and should only be done where the result is a reasonable increase in the physiological accuracy of the model.

Between each elastic chamber in Figure 2.1 is a flow section containing a resistor and in some cases an inductor. Resistances, labelled R, simulate the pressure drop on blood passing through the arteries or valves simulated by each flow section. Inductors, labelled L, simulate inertial effects on the blood flowing through particular areas of the CVS and are used only where the blood undergoes major changes in velocity, such as around heart valves. Diodes mark the location of the one-way valves at the inlet and exit of the ventricles. Once again, as with elastic chambers, resistances and inductors in the model each simulate the dynamics of a large area of the circulation system.

The aortic valve flow section (av) not only simulates the flow through the

aortic valve, but also blood flowing through the aorta. Much like the aortic valve flow section, the pulmonary valve flow section (pv) simulates flow through the pulmonary valve and the arteries before entering the capillaries in the lungs. The tricuspid valve flow section (tc) represents blood flowing through the vena-cava, the right atrium (ra), the tricuspid valve and into the right ventricle. Similarly, the mitral valve flow section (mt) simulates flow through the pulmonary vein, the left atrium (la) and the mitral valve into the left ventricle. The systemic (sys) and pulmonary (pul) flow sections simulate the pressure drops through the small diameter arterioles, capillaries and venules in the body and the lungs respectively.

The dashed line around the ventricles in Figure 2.1 signifies the pericardium that encapsulates both ventricles. The pericardium pressure, labelled P_{peri}, defines the pressure in the pericardium chamber acting on the outside of the ventricles. A further dashed line around the pericardium and the pulmonary circulation system in Figure 2.1 represents the thoracic cavity. The thoracic cavity simulates the rib cage and diaphragm that expands and contracts during respiration to inflate and deflate the lungs. The thoracic cavity pressure (P_{th}) can be either set to a constant to allow focus directly on ventricular function, or varied cyclically to simulate respiration.

The following sections outline the basic concepts and mathematics of the model, including the PV relationships and cardiac driver function. This chapter focuses primarily on the elastic chambers used in the CVS model. Resistive effects, inertial effects and other issues relating to blood flow between the chambers are discussed in subsequent chapters. A single chamber arrangement with constant boundary pressures is investigated first to capture and understand the essential dynamics of a single active cardiac chamber. Ventricular interaction is then included, before developing the full closed loop model with passive elastic chambers. This construction is in accordance with the *start out simple and develop complexity with understanding* philosophy discussed earlier. In subsequent chapters, the model dynamics at each step are checked against known physiological function and well accepted medical references, such as Guyton (1991) and Scharf (1989).

2.1 Single Ventricle Model

A single elastic chamber, as shown in Figure 2.2, was analysed first to examine the dynamics of a single active chamber such as a ventricle. This model is similar to

the Windkessel circuits in the literature, but with a simple elastic chamber rather than the traditional capacitor [Tsitlik et al., 1992; Santamore and Burkhoff, 1991]. A capacitor offers only a linear pressure-volume relationship, or must be modified to produce a more realistic nonlinear relationship [Tsitlik et al., 1992]. An elastic chamber offers a more physiologically realistic representation of CVS chambers with no increase in complexity.

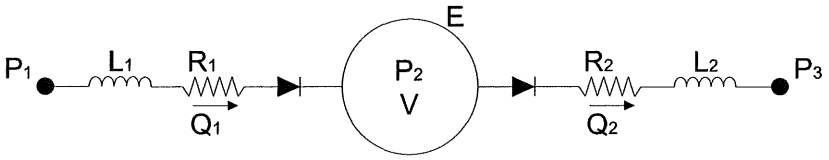

Figure 2.2 Single chamber model.

Fluid entering the elastic chamber flows from a constant pressure source (P_1) through the resistor (R_1), inductor (L_1) and one way valve into the elastic chamber. On exiting the chamber fluid again flows through a resistor (R_2), inductor (L_2) and one way valve before entering a constant pressure sink (P_3). For example, the elastic chamber could simulate the pressure in the right ventricle. This means the pressure source (P_1) would represent the right atrium and the pressure sink (P_3) represents the pressure in the pulmonary artery.

Analysis of the single active chamber model in this way removes transient effects due to pressure variations upstream and downstream of the model and due to ventricular interaction. This leaves only the active elastic chamber and the resistive and inductive effects entering and exiting. This section investigates these effects and interactions. A pressure-volume (PV) diagram is used to define the upper and lower limits of ventricular elastance. These definitions are then used to create a governing pressure-volume relationship for an active elastic chamber. The basic blood flow governing equations are then defined enabling a first order ordinary differential equation for the chamber volume to be outlined.

2.1.1 The PV Diagram

Equations approximating the ESPVR and EDPVR lines are widespread throughout the literature [Hardy and Collins, 1982; Maughan et al., 1987; Hunter et al., 1983; Chung et al., 1997; Santamore and Burkhoff, 1991; Beyar et al., 1987; Amoore et al., 1992]. However, the most common definitions assume the ESPVR

to be a linear function and the EDPVR to be an exponential function of volume [Suga et al., 1973; Weber et al., 1982; Amoore et al., 1992; Campbell et al., 1990]. The most commonly used relationships are defined [Chung et al., 1997; Santamore and Burkhoff, 1991; Beyar et al., 1987]:

$$P_{es}(V) = E_{es}(V - V_d) \tag{2.1}$$

$$P_{ed}(V) = P_0(e^{\lambda(V-V_0)} - 1) \tag{2.2}$$

where Equation (2.1) is the linear relationship between the end-systolic pressure (P_{es}) and volume (V) with elastance (E_{es}) and the volume at zero pressure (V_d). Equation (2.2) represents the nonlinear relationship between end diastolic pressure (P_{ed}) and volume (V). The additional constant parameters P_0, λ, and V_0 define gradient, curvature and volume at zero pressure of the EDPVR curve. The ESPVR and EDPVR lines are plotted in Figure 2.3 along with the cardiac cycle.

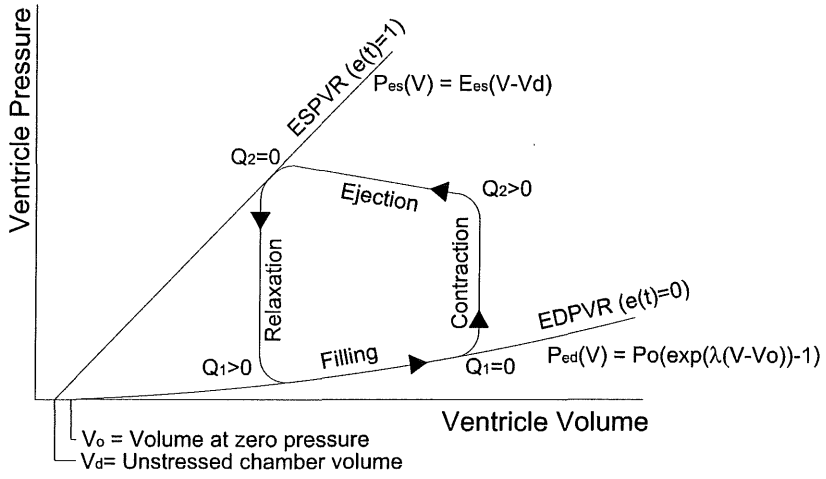

Figure 2.3 Pressure-volume diagram of the cardiac cycle and the variations in end-diastolic and end-systolic pressure-volume relationships.

The ESPVR parameter E_{es} used in Equation (2.1), is widely seen as a measure of the contractility of the ventricle. Suga et.al. (1973) refers to E_{es} as the maximum elastance (Emax) and empirically determines both E_{es} and V_d for a range of canine hearts. The variation in E_{es} is investigated using Epinephrine, a drug that increases the contractile strength of the cardiac muscle. The EDPVR is more complex with 3 variables defining the profile of the curve, as shown in

Equation (2.2). However, the variable P_0 is a good measure of the stiffness of the cardiac muscle. The two parameters, E_{es} and P_0, can be altered in the model to simulate dysfunctions in ventricle contractility and stiffness, respectively.

2.1.2 Cardiac Driver Function

Time varying elastance (E(t)) is commonly agreed as a suitable method of simulating the cardiac muscle activation that enables the heart to pump [Beyar et al., 1987; Chung et al., 1997; Burkhoff and Tyberg, 1993; Santamore and Burkhoff, 1991]. Through time varying elastance, the pressure in an active elastic chamber can vary even with constant volume. Segers et.al. (2000a; 2000b) carried out experiments on healthy humans measuring the variation in elastance with time. That research assumed a linear pressure volume relationship as a function of the nonlinear time varying elastance (E(t)), of the form:

$$P(t) = E(t)(V(t) - V_d) \tag{2.3}$$

where P(t) is the pressure in a cardiac chamber as a function of volume (V(t)) and V_d is the volume at zero pressure.

A more common approach to simulating time varying elastance utilises the ESPVR and EDPVR, shown in Figure 2.3, as the upper and lower limits of cardiac chamber elastance [Santamore and Burkhoff, 1991; Beyar et al., 1987; Chung, 1996]. A cardiac driver function (e(t)) is then defined to vary between 0 and 1, as shown in Figure 2.4. The profile of the driver function represents the variance of elastance between minimum and maximum values over a single heart beat. A driver function value of one (e(t)=1) means elastance is defined by the ESPVR and a value of zero (e(t)=0) uses the EDPVR to define elastance. The driver function profile in Figure 2.3 is defined using the following equation [Chung, 1996]:

$$e(t) = \sum_{i=1}^{N} A_i e^{-B_i(t-C_i)^2} \tag{2.4}$$

where the A_i, B_i, C_i and N are parameters that determine the shape of the driver profile. To produce the simple profile shown in Figure 2.4, values of A=1, B=80s^{-1}, C=0.27s and N=1 were used.

The shape of this driver profile, defining the variation in elastance, can be

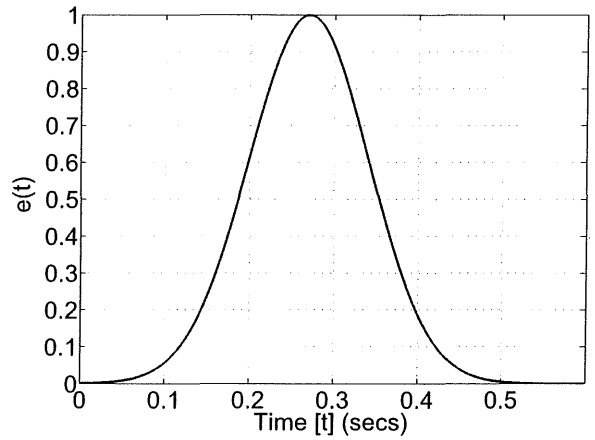

Figure 2.4 The model cardiac driver (e(t)).

compared with graphs of normalised ventricle elastance plotted by Segers et.al. (2000a), as shown in Figure 2.5. Chung et.al. (1996) uses a more complex driver, closer matching the profile defined by Segers et.al. (2000a). Many other variations of this driver can be found in the literature with very similar shapes [Amoore et al., 1992; Beyar et al., 1987; Burkhoff and Tyberg, 1993]. The simple profile used for this research, shown in Figure 2.4, was chosen to keep the model as simple as possible, allowing more focus on other mechanisms contributing to model function.

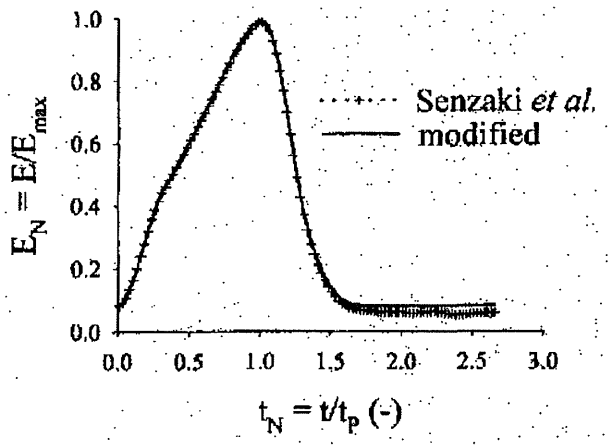

Figure 2.5 Normalised time-varying resistance curve [Segers et al., 2000a].

The pressure in a single active elastic chamber (P_2), as a function of volume and time, is defined as the linear, weighted sum of Equations (2.1) and (2.2). The weighting is defined by the value of the driver function (e(t)) as shown:

$$P_2(V,t) = e(t)P_{es}(V) + (1 - e(t))P_{ed}(V) \qquad 0 \leq e(t) \leq 1 \tag{2.5}$$

$$P_2(V,t) = e(t)E_{es}(V - V_d) + (1 - e(t))P_0(e^{\lambda(V-V_o)} - 1) \tag{2.6}$$

Equation (2.6) is now the governing equation for the time dependent pressure volume relationship in an active elastic chamber, such as a ventricle.

2.1.3 Blood Flow

The blood flow rate through the resistors in Figure 2.2 is primarily dependent on the pressure gradient across the resistor. If the effects of inertia are either ignored or negligible, the equation for the flow rate can be calculated using Poiseuille's equation [Fung, 1990; Beyar et al., 1987; Chung, 1996; Olansen et al., 2000; Guyton, 1991].

$$Q_1 = \frac{P_1 - P_2}{R_1} \tag{2.7}$$

where the resistance (R) is defined by the Poiseuille's equation as $R=\pi r_0^4/8\mu l$, with the variables: radius, r_0, fluid viscosity, μ, and artery length, l. Poiseuille's equation assumes incompressible, Newtonian, laminar, axi-symmetric, fully developed flow through a rigid tube of constant cross-section. These assumptions are reasonable in order to create a simple quasi-static model and are discussed in more detail in Chapter 3. Note, the use of Windkessel circuit components in the model allows the rigid tube assumption, as the elastic properties of each component are simulated in a subsequent elastic chamber.

Valves are modelled simply by maintaining flow rates that are either greater than or equal to zero. If the flow rate calculated using Equation (2.7) is negative, then that flow rate is set to zero. With the flow rate known, the rate of change of volume in the chamber is simply calculated as the net flow through the chamber.

$$\frac{dV}{dt} = Q_{in} - Q_{out} \tag{2.8}$$

Equation (2.8) defines a first order ordinary differential equation governing the volume of the elastic chambers in the model. All flow variables used in the model shown in Figure 2.1 are defined in Table 2.1.

Symbol	Description
Q_{tc}	Flow through the tricuspid valve
Q_{pv}	Flow through the pulmonary valve
Q_{mt}	Flow through the mitral valve
Q_{tc}	Flow through the aortic valve
Q_{pul}	Flow through the pulmonary circulation system
Q_{sys}	Flow through the systemic circulation system

Table 2.1 Flow rate variables from the full closed loop model of Figure 2.1.

2.1.4 Summary of Single Chamber Model

To summarize, for any given volume (V) and time (t), the pressure in the chamber ($P_2(V,t)$) can be calculated using Equation (2.6). The flow rates are then calculated using Equation (2.7) and from the flow rate, the rate of change of volume is calculated using Equation (2.8). These equations define the dynamics of a single ventricle model with resistances at the inlet and outlet. The next step in developing the full closed loop model is to capture the effect of ventricular interaction, using a two chamber model representing both ventricles with constant pressure boundary conditions.

2.2 Ventricular Interaction

Ventricular interaction has a significant impact on cardiovascular dynamics, and is caused by both the septum and the pericardium. The septum is an active, flexible common wall between the left and right ventricle. The pericardium is a relatively rigid, passive wall that encapsulates the entire heart [Hancock, 1995]. Beyar et.al. (1987) use two constant parameters to control the amount that the right ventricle pressure affects the left ventricle pressure and visa-versa. Santamore et.al. (1991) use pressure-volume equations very similar to Equation (2.6), however it is not clear how the elastances of the septum and ventricle walls are calculated from the non-linear PV equations. The presented method of modelling ventricular interaction divides the ventricles into three separate free wall volumes [Chung et al., 1997; Maughan et al., 1987].

Figure 2.6 shows the layout for a two ventricle model including ventricular interaction using an open loop model with constant inlet and outlet pressures. Note that the ventricle interaction model is simply two single chamber models coupled by the septum and pericardium. The double lines between the left and right ventricles indicate the coupling due to the common septal wall. The dashed

line around the left and right ventricles represents the pericardium.

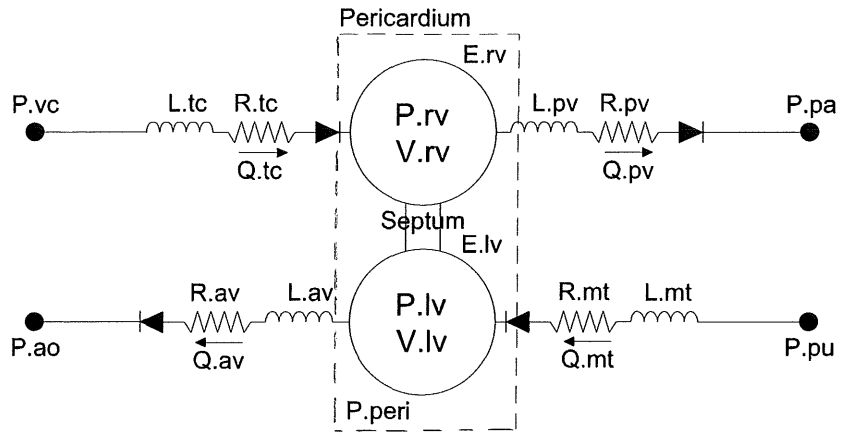

Figure 2.6 Two ventricle open loop model with ventricular interaction.

This model is similar to that shown in Figure 2.1, but with the peripheral chamber pressures held constant. This layout allows focus on the ventricle interaction dynamics without the influence of dynamics in the peripheral circulation. The pressure variations in the peripheral chambers can also be defined as time varying functions, creating more realistic boundary conditions for the ventricles.

2.2.1 Volume Definitions

The volume variables required for this model are defined in Figure 2.7 and Table 2.2. Figure 2.7 shows the left and right ventricle volumes and the three different free walls of the ventricles and the septum. The free wall volumes, V_{lvf}, V_{rvf} and V_{spt}, are not actual physical volumes, but represent fractions of the overall ventricle volumes (V_{lv} and V_{rv}). The volumes are separated to capture the deflection of the cardiac free walls relative to the ventricle volumes.

The left ventricle free wall volume (V_{lvf}), using Figure 2.7, is simply the left ventricle volume (V_{lv}) less the septal volume (V_{spt}).

$$V_{lvf} = V_{lv} - V_{spt} \tag{2.9}$$

Similarly, the right ventricle free wall volume (V_{rvf}) is the sum of the right ventricle volume (V_{rv}) and the septum volume (V_{spt}).

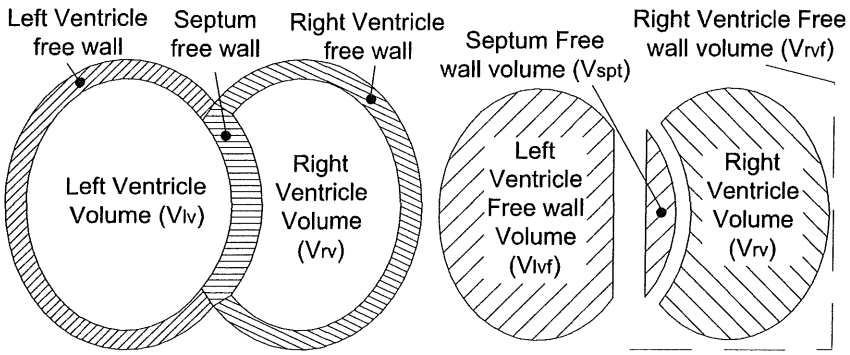

Figure 2.7 Sectioned view of the heart with left and right ventricles and left and right ventricle and septum free walls.

$$V_{rvf} = V_{rv} + V_{spt} \tag{2.10}$$

Finally, the pericardium volume (V_{pcd}) is the sum of the ventricle volumes, or the sum of the ventricle free wall volumes where the septal volume drops out of the definition.

$$V_{pcd} = V_{lv} + V_{rv} = V_{lvf} + V_{rvf} \tag{2.11}$$

The total volume of the pericardium defined in this model excludes the volume of the atria and the myocardium, although the model may be readily augmented to include these details. Note that the septum volume can be negative or positive depending on the relative pressures in the ventricle chambers. Positive septal deflection is into the right ventricle, as shown in Figure 2.7. The relaxed state of the septum is a small amount of deflection into the right ventricle.

Symbol	Description
V_{lv}	Left ventricle volume
V_{rv}	Right ventricle volume
V_{lvf}	Left ventricular free wall volume
V_{rvf}	Right ventricular free wall volume
V_{spt}	Septum free wall volume
V_{pcd}	Pericardium volume

Table 2.2 Volume Variables.

2.2.2 Pressure Definitions

Given the volumes of the chambers, the governing PV relationships can then be used to calculate the pressures, as defined in Equation (2.6). The pressures defined for the two ventricle model are schematically shown in Figure 2.8 and listed in Table 2.3. All pressures are measured relative to atmospheric pressure. The specific pressure relations are defined using Figure 2.8 for the left and right ventricle, and the pericardium using the variables in Table 2.3.

$$P_{lv} = P_{lvf} + P_{peri} \tag{2.12}$$

$$P_{rv} = P_{rvf} + P_{peri} \tag{2.13}$$

$$P_{peri} = P_{pcd} + P_{th} \tag{2.14}$$

where P_{lvf}, P_{rvf} and P_{pcd} are the pressure difference across the wall of the left ventricle, right ventricle and pericardium respectively. The pressure difference across the septum free wall (P_{spt}) is therefore defined using Equations (2.12) and (2.13).

$$P_{spt} = P_{lv} - P_{rv} = P_{lvf} - P_{rvf} \tag{2.15}$$

The pressures across the free walls (P_{lvf}, P_{rvf}, P_{spt} and P_{pcd}) are representations of the stretching force applied to each free wall. These pressures are calculated from the free wall volumes (V_{lvf}, V_{rvf}, V_{spt} and V_{pcd}), which define the deflections, and hence the volumes of the free walls. The relative contributions of each free wall volume to the overall ventricle volumes (V_{lv} and V_{rv}) are calculated using Equations (2.9) and (2.10). The left and right ventricle and septal free wall pressures are a function of the driver, e(t), and the end systolic and end diastolic pressures, P_{ed} and P_{es} respectively, in the same form as Equations (2.5) and (2.6).

$$P_{lvf} = eP_{es,lvf} + (1-e)P_{ed,lvf} \qquad P_{rvf} = eP_{es,rvf} + (1-e)P_{ed,rvf} \tag{2.16}$$

$$P_{spt} = eP_{es,spt} + (1 - e)P_{ed,spt} \tag{2.17}$$

Finally, the pressure across the pericardium wall is defined as a function of the volume of the pericardium. The pericardium is a passive membrane, and is governed by a nonlinear PV relationship [Chung et al., 1997]:

$$P_{pcd}(V_{pcd}) = P_{0,pcd}(e^{\lambda_{pcd}(V_{pcd}-V_{0,pcd})} - 1) \tag{2.18}$$

These equations can be employed to obtain the pressure in the left and right ventricles. Once the ventricle pressures are known the flow rates can be determined and the rate of change of volume calculated. The equations used to calculate the ventricle pressures and rate of change of volumes are outlined in more detail in Appendix 1.

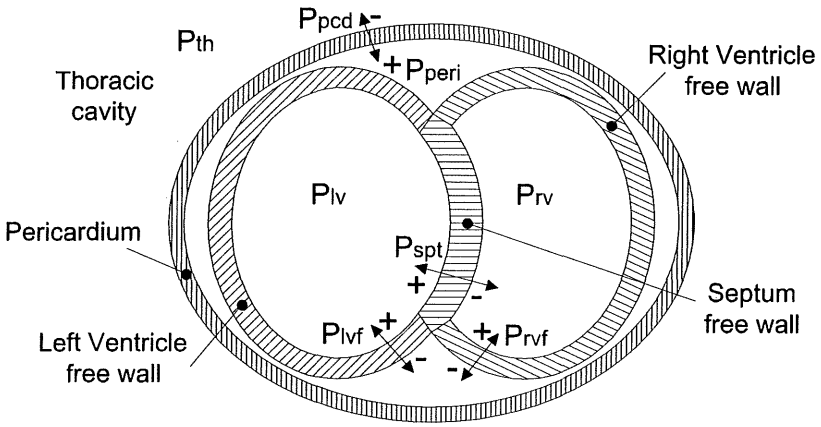

Figure 2.8 Sectioned view of heart enclosed in the pericardium labelling chamber pressures and pressures across walls.

Symbol	Description
P_{lv}	Pressure in the left ventricle
P_{rv}	Pressure in the right ventricle
P_{peri}	Pressure in the pericardium
P_{th}	Pressure in the thoracic cavity
P_{lvf}	Pressure across the left ventricular free wall
P_{rvf}	Pressure across the right ventricular free wall
P_{spt}	Pressure across the septum free wall
P_{pcd}	Pressure across the pericardium wall

Table 2.3 Pressure Variables.

2.3 Peripheral Circulation, Closing the Loop

To capture more of the major governing haemodynamics, the circuit in Figure 2.6 must be closed so that blood can flow around the entire loop, as in Figure 2.1. With the output of each cardiac chamber connected to the inlet of the other, the dynamics of the system will now be affected by peripheral elastances and resistances, capturing the essential dynamics of the pulmonary and systemic circulations.

Although the non-linear PV relation defined in Equation (2.2) may be more suitable to define peripheral elastances, it requires knowledge of three parameters, P_0, λ, and V_0 [Amoore et al., 1992; Ursino, 1999]. To minimise complexity, this research employs the linear PV relationship in Equation (2.1) for the peripheral chambers in Figure 2.1. Equation (2.1) requires knowledge of only two parameters, E and V_d, although V_d is set to zero for this work.

Dividing the peripheral circulation systems into elastic chambers separated by resistances requires a trade-off between complexity and capturing the required fundamental dynamics. Some CVS models in the literature are highly complex attempting to model many of the circulation system chambers. An extreme example of this approach is the model proposed by Sun et.al. (1997) which uses approximately 15 capacitors simulating elastic chambers in the CVS. While complex models may be more capable of capturing some of the complex dynamics than simpler alternatives, separating the individual contribution of each component is very difficult. Other models take a more minimal approach using a similar layout to that shown in Figure 1.9(b) [Beyar et al., 1987; Santamore and Burkhoff, 1991].

The minimal approach presented here divides both the pulmonary and systemic circulation systems into two chambers separated by a resistor. The impact of the thoracic chamber pressure variations resulting from respiration must also be considered. As discussed earlier, the location of the heart in the thoracic cavity between the lungs means that the thoracic cavity pressure (P_{th}) can have a significant effect on cardiac performance. These cardiopulmonary interactions are the subject of many publications, particularly on positive pressure ventilation [Scharf and Cassidy, 1989; Parry-Jones and Pittman, 2003]. For example, positive pressure ventilation through a respirator causes a significant rise in thoracic cavity pressure. The location of the heart means increased thoracic cavity pressure impedes cardiac function and results in reduced cardiac output. Thoracic

pressure is included in the calculations for cardiac pressures in Equation (2.14), however, as shown in Figure 2.1, it will also have an effect on the pressures in the pulmonary chambers.

2.3.1 Pulmonary Circulation

The pulmonary circulation model includes a single elastic chamber to simulate the pulmonary artery (pa) and another to simulate the pulmonary vein (pu) and left atrium, as shown in Figures (1.4) and (2.1). Pulmonary circulation elastic chamber volumes are defined in Table 2.4. Each elastic chamber simulates the pressure volume relationship in these vessels using the following equations:

$$P_{pa}(V_{pa}) = E_{pa}(V_{pa} - V_{pa,d}) + P_{th} \tag{2.19}$$

$$P_{pu}(V_{pu}) = E_{pu}(V_{pu} - V_{pu,d}) + P_{th} \tag{2.20}$$

where P_{pa} and P_{pu} define the pressures in the pulmonary artery and pulmonary vein respectively, and V_{pa} and V_{pu} define the volumes. The elastances of each chamber are defined E_{pa} and E_{pu}. The volume at zero pressure is defined $V_{pa,d}$ and $V_{pu,d}$ for the pulmonary artery and pulmonary vein respectively.

Between the chambers a resistor simulates the pressure drop due to resistance acting on blood flowing through the small diameter capillaries in the lungs (R_{pul}). The resistance and pressure difference between the two chambers is used to calculate the flow rate through the pulmonary circulation.

$$Q_{pul} = \frac{P_{pa} - P_{pu}}{R_{pul}} \tag{2.21}$$

It is important to note that, Equation (2.21) offers only an approximation to fluid flow through the capillaries. Particularly since at the extremely small scale of the capillaries, many of the assumptions associated with Poiseuille's equation are no longer valid. For example, in small vessels, blood behaves in a non-Newtonian manner, which is significantly more complex to simulate. However, at the macro-scale modelled, these assumptions are a reasonable approximation.

Symbol	Description
V_{pa}	Volume of the pulmonary artery
V_{pu}	Volume of the pulmonary vein
V_{ao}	Volume of the aorta
V_{vc}	Volume of the vena-cava

Table 2.4 Peripheral circulation system elastic chamber volume definitions.

2.3.2 Systemic Circulation

The systemic circulation is divided up in the same way as the pulmonary circulation with two elastic chambers simulating the aorta (ao) and the vena-cava (vc), as shown in Figures 1.4 and 2.1. Systemic circulation elastic chamber volumes are defined in Table 2.4. The governing equations for the pressure in the aorta (P_{ao}) as a function of the volume of the aorta (V_{ao}) and the pressure in the vena-cava (P_{vc}) as a function of vena-cava volume (V_{vc}) are defined:

$$P_{ao}(V_{ao}) = E_{ao}(V_{ao} - V_{ao,d}) \tag{2.22}$$

$$P_{vc}(V_{vc}) = E_{vc}(V_{vc} - V_{vc,d}) \tag{2.23}$$

where the elastances of each chamber are defined E_{ao} and E_{vc} and the volume at zero pressure is defined $V_{pa,d}$ and $V_{pu,d}$ for the pulmonary artery and pulmonary vein respectively. Note that unlike the pulmonary chambers, the systemic chambers are not influenced directly by the thoracic pressure (P_{th}), as they are simulating vessels outside the thoracic cavity.

Blood flowing through the small diameter capillaries in the systemic circulation is simulated in the same way as the pulmonary circulation. The resistance (R_{sys}) and pressure difference between the aorta and the vena-cava chambers are used to calculate the flow rate through the systemic circulation.

$$Q_{sys} = \frac{P_{ao} - P_{vc}}{R_{sys}} \tag{2.24}$$

Again note that Equation (2.24), like Equation (2.21), is only an approximation to fluid flow through the capillaries.

2.4 Summary of Minimal Model Construction

This chapter focuses mainly on the pressure-volume relationships in the passive and elastic chambers of the CVS. Time varying elastance is introduced as the method of simulating cardiac function and the mathematical principles involved have been outlined. A description of the entire CVS model is introduced as shown in Figure 2.1, discussing all of the interactions involved.

Initially, a single chamber model is introduced with constant pressure boundary conditions to capture the dynamics of a single ventricle. The single chamber model is then expanded into a two active chamber system to simulate ventricular interaction. The boundary pressures remain constant to once again highlight the function of the ventricles, however these pressures can be varied with time to more accurately simulate ventricle function. Finally, peripheral chambers are added to simulate the pulmonary and systemic circulation systems. This closed loop model can simulate direct ventricular interactions due to the septum and pericardium, as well as series interactions as blood flows from one ventricle to the other through the peripheral circulation systems.

The main overall assumption of this model is the lumped parameter approach which divides the CVS into a series of elastic chambers and blocks simulating blood flow. Numerous assumptions are also made in constructing each of these blocks. This chapter focuses on the elastic chambers and the pressure volume relationships in each chamber. Important assumptions include the profile of the driver function, a structure that excludes both atria, and attempting to model large sections of the CVS, such as the aorta, using only a single chamber. Also, a linear PV relationship is assumed for the chambers simulating the peripheral circulation. It is important to remain aware of these assumptions when using the model as they will restrict the physiological accuracy of the resulting simulations. The elastic chambers described are one of the two main building blocks of this model. The second key area is blood flow between the elastic chambers, through the resistors, inductors and valves in Figure 2.1. This chapter used Poiseuille's equation, which is only a simple approximation of this fluid flow. The next chapter examines the mathematical modelling of blood flow between the elastic chambers in more detail.

Chapter 3

Blood Flow in the Heart

Typical lumped parameter model equations governing arterial flow rate found in the literature either include, or do not include, inertial effects. In both cases, resistance to blood flow is typically assumed constant under varying flow velocity and acceleration. Realistically, resistance varies with time for the pulsatile flow around the heart and its valves, and the amount of this variation is investigated. If the variation in resistance is negligible the well-accepted assumption of constant resistance is valid. However, if the variation in resistance is not negligible, the addition of time varying resistance to the model will produce more physiologically accurate model outputs.

The simplest and most common method of modelling blood flow in the CVS is to calculate flow rate as a function of pressure gradient and constant resistance [Hoppensteadt and Peskin, 2002; Chung et al., 1997; Burkhoff and Tyberg, 1993; Vis et al., 1997; Santamore and Burkhoff, 1991]. To account for the effects of inertia on accelerating blood, many models include inertial effects as well as a constant resistance [Olansen et al., 2000; Beyar et al., 1987; Ursino, 1999; Tsitlik et al., 1992; Hardy et al., 1982; Sun et al., 1997; Avanzolini et al., 1989; Melchior et al., 1992]. Often these models are based on well-accepted electrical circuit analogies with the advantage that electrical circuit analysis techniques can be used to model the CVS [Ursino, 1999; Tsitlik et al., 1992; Santamore and Burkhoff, 1991; Lu et al., 2001; Olansen et al., 2000]. These methods offer the benefit of being well suited to complex circuits such as the CVS, but on a component scale they are only approximations that are not necessarily based on the fundamental mechanical and fluid dynamic principles involved.

This chapter derives the equations governing arterial blood flow near the heart and notes the key assumptions made. The Womersley number is used to investigate where it is necessary to model inertial and time varying resistance

effects and where they can be ignored. A method is developed that uses equations derived from the Navier-Stokes equation to incorporate time varying resistance in lumped parameter CVS models. The method is applied to a simple single chamber model designed to simulate a single ventricular chamber. Models with time varying resistance are then compared with models that assume constant resistance to investigate the differences in performance.

3.1 Equations Governing Flow Rate

This section investigates the equations of fluid motion regularly used in lumped parameter models, how they are derived, and their associated assumptions. Blood flow in parts of the circulation system is approximated as flow through a tube. Figure 3.1 shows an example where the longitudinal position along the tube (x), the tube radius (r_0) and the tube length (ℓ) are labelled. The flow rate equations are derived directly from the Navier-Stokes equation in polar co-ordinates, the form best suited to cylindrical tubes or simple approximations of arteries.

$$\begin{aligned}\frac{\partial u_x}{\partial t} + u_r\frac{\partial u_x}{\partial r} + \frac{u_\theta}{r}\frac{\partial u_x}{\partial \theta} + u_x\frac{\partial u_x}{\partial x} \\ = -\frac{1}{\rho}\frac{\partial P}{\partial x} + \nu\left[\frac{1}{r}\frac{\partial}{\partial r}\left(r\frac{\partial u_x}{\partial r}\right) + \frac{1}{r^2}\frac{\partial^2 u_x}{\partial \theta^2} + \frac{\partial^2 u_x}{\partial x^2}\right]\end{aligned} \tag{3.1}$$

where u_x, u_r and u_θ are the longitudinal, radial and angular velocities respectively, P is the modified pressure relative to hydrostatic, ρ is the density and ν is the kinematic viscosity.

The following assumptions are applied to all equations governing fluid flow used in this thesis and are referred to as the standard assumptions.

- Blood is assumed incompressible (ρ=constant) [White, 1991].
- Although in smaller capillaries blood cannot be modelled using continuous equations, in larger arteries the fluid is assumed to behave in a continuous, Newtonian manner with constant viscosity (μ=constant) [Fung, 1993].
- The arteries through which blood flows are assumed to be rigid with constant cross-sectional area ($\frac{\partial r}{\partial x} = 0$). This assumption fits with standard Windkessel circuit design involving a rigid pipe and an elastic chamber in

series. The rigid tube simulates the fluid dynamics while the elastic chamber simulates the compliance of the artery walls [Tsitlik et al., 1992; Melchior et al., 1992].

- Laminar uni-directional axi-symmetric flow is assumed ($u_r = 0$, $u_\theta = 0$, $\frac{\partial u_x}{\partial \theta} = 0$). Although turbulence can occur around the valves, it takes time to develop, and is assumed not to affect the flow profile significantly.

- The flow is assumed fully developed along the length of the tube meaning the velocity profile is constant with respect to x ($\frac{\partial u_x}{\partial x} = 0$) [Fung, 1993].

- Pressure is assumed constant across the cross-sectional area and the pressure gradient is constant along the length of each section so that the pressure gradient is a function of time only ($\frac{\partial P}{\partial x}(t)$).

These assumptions enable Equation (3.1) to be reduced to the following simplified version of the Navier-Stokes equation:

$$\rho \frac{\partial u(r,t)}{\partial t} = -\frac{\partial P}{\partial x}(t) + \frac{\mu}{r}\frac{\partial}{\partial r}\left(r\frac{\partial u(r,t)}{\partial r}\right) \tag{3.2}$$

where μ is the viscosity ($\mu = \nu\rho$) and u(r,t) is the velocity in the x-direction ($u_x(r,t)$) as a function of radius and time only. Equation (3.2) can be divided into the following 3 forces per unit volume that are applied to the fluid [Fung, 1997].

$$\text{Transient inertial force} = \text{Pressure force} + \text{Viscous force} \tag{3.3}$$

The relative magnitudes of the transient inertial force and the viscous force are important when choosing a suitable governing equation for flow in a section of the CVS.

The two most commonly used equations governing flow rate in lumped-parameter CVS models can be derived from Equation (3.2). When using equations derived from Equation (3.2), all the assumptions listed above are applied, as well as equation specific assumptions that may also apply. The first equation examined is Poiseuille's equation for flow rate, assuming constant resistance and no inertial effects. The second equation examined includes inertial effects, but again assumes constant resistance.

3.1.1 Poiseuille's Equation with Constant Resistance

If the additional assumption of steady fully-developed flow is applied to Equation (3.2), the acceleration term ($\frac{\partial u}{\partial t} = 0$) is removed, leaving a further simplified form of the equation.

$$0 = -\frac{\partial P}{\partial x}(t) + \frac{\mu}{r}\frac{\partial}{\partial r}\left(r\frac{\partial u(r,t)}{\partial r}\right) \tag{3.4}$$

All the density terms have been divided out leaving an equation that is not dependent on density and therefore ignores inertial effects. This equation can be solved to obtain the velocity as a function of radius for flow through a pipe of radius (r_0), as shown in Figure 3.1, under a pressure gradient ($\partial P/\partial x$) [White, 1991; Fung, 1990].

$$u(r) = -\frac{r_0^2 - r^2}{4\mu}\frac{dp}{dx} \tag{3.5}$$

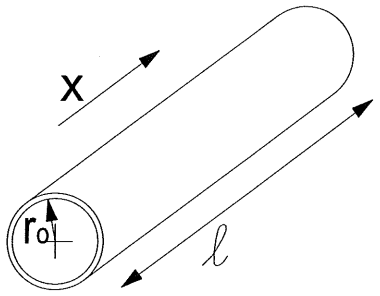

Figure 3.1 Flow through a rigid pipe of constant cross section.

Using Equation (3.5), an equation for the flow rate through a tube can be found by integration.

$$Q = 2\pi\int_0^{r_0} urdr = -\frac{\pi r_0^4}{8\mu}\frac{dp}{dx} \tag{3.6}$$

where the pressure gradient ($\frac{dp}{dx}$) is replaced by the pressure drop along the pipe with upstream pressure ($P_1(t)$), downstream pressure ($P_2(t)$) and artery length (ℓ). .

$$Q(t) = \frac{\pi r_0^4}{8\mu}\frac{P_1(t) - P_2(t)}{\ell} \tag{3.7}$$

By grouping the constants an equation for resistance is derived.

$$R = 8\mu\ell/\pi r_0^4 \tag{3.8}$$

Equation (3.7) can then be simplified to the electrical analogy commonly used in the literature to calculate the flow rate of blood through arteries and valves [Chung et al., 1997; Beyar et al., 1987; Burkhoff and Tyberg, 1993; Ursino, 1999; Olansen et al., 2000; Smith et al., 2003a,b].

$$Q(t) = \frac{P_1(t) - P_2(t)}{R} \tag{3.9}$$

Thus, in addition to the listed standard assumptions, Poiseuille's equation assumes steady fully developed flow, meaning the flow has a fully developed velocity profile and a constant flow rate. Hence, Equation (3.9) does not include inertial effects or the effects of time varying resistance that significantly influence pulsatile flow.

In many parts of the arterial tree, such as the capillaries and the vena-cava, the variation in velocity may be minimal. However, significant changes in velocity will occur around the heart valves and the flow can not be assumed steady during the course of a heart beat. As the ventricle is filling, blood is rushing into the ventricle, however as the ventricle contracts, the inlet valve will shut due to reversing flow rate. Hence, blood passing through the heart valves is periodically stopping during each cardiac cycle and inertial forces must be affecting blood flow [Little, 1978].

3.1.2 Including Inertial Effects

A dynamic equation for flow rate can be found by integrating Equation (3.2) across the cross-sectional area and along the length.

$$\begin{aligned}\int_{x_1}^{x_2}\int_0^{2\pi}\int_0^{r_0} \rho\frac{\partial u(r,t)}{\partial t} r\,dr\,d\theta\,dx \\ = \int_{x_1}^{x_2}\int_0^{2\pi}\int_0^{r_0}\left[-\frac{\partial P}{\partial x}(t) + \frac{\mu}{r}\frac{\partial}{\partial r}\left(r\frac{\partial u(r,t)}{\partial r}\right)\right] r\,dr\,d\theta\,dx\end{aligned} \tag{3.10}$$

where the integration results in the following relation.

$$\rho(x_2 - x_1)\frac{\partial Q(t)}{\partial t} = \pi r_o^2 (P_1(t) - P_2(t)) + 2\pi r_0 \mu (x_2 - x_1)\frac{\partial u(r_0, t)}{\partial r} \tag{3.11}$$

The vessel length (ℓ) is substituted for $(x_2 - x_1)$ and Equation (3.11) is divided by the cross-sectional area (πr_0^2).

$$\frac{\rho \ell}{\pi r_0^2}\frac{\partial Q}{\partial t} = P_1 - P_2 + \frac{2\mu\ell}{r_0}\frac{\partial u}{\partial r}(r_0) \tag{3.12}$$

where $\frac{\partial u(r_0)}{\partial r}$ is the boundary velocity gradient at the wall of the tube. Equation (3.12) can be compared with the equation for flow rate with inertial effects commonly found in the literature [Olansen et al., 2000; Beyar et al., 1987; Ursino, 1999]:

$$L\frac{dQ}{dt} = P_1 - P_2 - QR \tag{3.13}$$

with the constants inertia (L) and resistance (R).

The derivation of Equation (3.13) can be found from electrical circuit analogies for an inductor and a resistor in series, as shown in Figure 3.2. The flow rate of blood through an artery (Q) is analogous to the current (i), or the flow rate of electrons in a wire in an electrical circuit. Likewise, the voltage (V) is analogous to pressure drop $(P_1 - P_2)$ in a fluid flowing through a section of tube. A resistor accounts for the drop in fluid pressure across a section of artery or tube. An inductor in an electrical system limits the rate of change of current and is used to simulate inertial effects on a fluid.

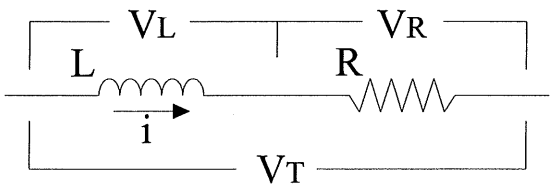

Figure 3.2 Inductor and a resistor in series.

In Figure 3.2 the voltages are labelled across the inductor (V_L), resistor (V_R)

and both (V_T). The voltage across the inductor and the resistor are defined:

$$V_L = L\frac{di}{dt} \qquad V_R = iR \tag{3.14}$$

Therefore, the total voltage (V_T) is equal to the sum of the voltages across the inductor and resistor.

$$V_T = V_L + V_R \tag{3.15}$$

$$V_T = L\frac{di}{dt} + iR \tag{3.16}$$

Using the electrical analogy listed above, the current (i) is replaced with fluid flow rate (Q), and the pressure drop ($P_1 - P_2$) replaces the voltage (V_T). Substituting these variables in Equation (3.16) gives Equation (3.13), summarising the derivation from electrical circuit theory.

By comparing Equation (3.12) with Equation (3.13) the value of the inductance (L) can be found as a function of the fluid properties, making it a measure of the magnitude of the inertial effects on the fluid per unit cross-sectional area.

$$L = \frac{\rho\ell}{\pi r_0^2} \tag{3.17}$$

However, when comparing the resistance terms from Equations (3.12) and (3.13) the following identity is found.

$$QR(t) = -\frac{2\mu\ell}{r_0}\frac{\partial u}{\partial r}(r_0) \tag{3.18}$$

where R(t) denotes resistance that varies with time.

The definition in Equation (3.18) implies that the flow rate (Q) and the boundary velocity gradient ($\frac{\partial u}{\partial r}(r_0)$) are related by a constant ($\frac{r_0}{2\mu\ell}$) multiplied by R(t). If R(t) is assumed constant, meaning the flow is steady, then this relationship is valid. However, for pulsatile flow with time varying resistance (R(t)), when the net flow rate is zero the boundary velocity gradient is not necessarily zero. Figure 3.3 shows an example where the flow rate is zero, but the boundary velocity gradient is non-zero. If the boundary velocity gradient at zero flow rate is not necessarily zero, R(t) will be undefined and unconstrained. This

inconsistency shows that Equation (3.13), which is used to simulate inertial effects in many cases of prior research, is not a suitable governing equation for pulsatile fluid flow with time varying resistance [Olansen et al., 2000; Beyar et al., 1987; Ursino, 1999; Sun et al., 1997]. A more suitable alternative is Equation (3.12) which is derived directly from the equations of motion rather than electrical circuit approximations.

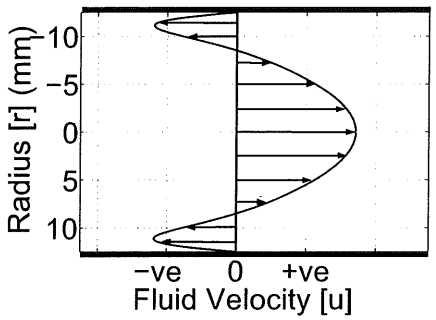

Figure 3.3 The velocity profile at zero flow rate.

3.2 The Womersley Number

The previous two sections have shown the derivation of three different methods of modelling arterial flow, using either of Equations (2.7), (3.12) or (3.13). Equation (2.7) would be the preferred choice where possible as it is simple and easy to implement. However, if including inertial effects by using Equations (3.12) or (3.13) is going to produce significantly more accurate results, then the increase in complexity is justified.

To investigate which of Equations (3.12) and (3.13) should be used to model different types of flow, the Womersley number (α) is used, along with a solution to Equation (3.2) derived by Womersley. The Womersley number is defined as the ratio of the inertial force to the viscous forces in Equation (3.2) [Fung, 1990].

$$\alpha^2 = \frac{\text{transient inertial force}}{\text{viscous force}} = \frac{\omega \mathrm{d}^2}{\nu} \tag{3.19}$$

where ω is a characteristic frequency, defined as the heart rate (HR) and d is a characteristic length, defined as the radius of an artery (r_0). Transient inertial forces represent body forces acting on the fluid limiting its rate of acceleration. Viscous forces represent the effects of wall friction acting to slow the flow of the

fluid. Therefore high values of α, much greater than 1, indicate that transient inertial forces affect the fluid considerably more than viscous forces. Conversely, a low Womersley number, much less than 1, means that viscous forces are the dominate force acting on the fluid flow.

In the CVS, the heart rate (ω) and the kinematic viscosity (ν) do not vary significantly when compared with the variation in the square of the tube radius. Therefore, frequency and kinematic viscosity can be assumed to be constant and the magnitude of the Womersley number in the CVS becomes dependent on radius alone.

The analytical solution derived by Womersley to Equation (3.2) for flow driven by a sinusoidally varying pressure gradient ($\frac{\mathrm{dP}}{\mathrm{dx}}(\mathrm{t})$) is defined [White, 1991; Fung, 1990; Bartlett and Fyfe, 1974]:

$$\frac{\mathrm{dP}}{\mathrm{dx}}(\mathrm{t}) = -\mathrm{dP_{amp}}.\mathrm{e}^{\mathrm{i}\omega\mathrm{t}} \tag{3.20}$$

$$\mathrm{u(r,t)} = \mathrm{dP_{amp}}\frac{\mathrm{i}}{\rho\omega}\left[1 - \frac{\mathrm{J_0}(\mathrm{r}\sqrt{-\mathrm{i}\omega/\nu})}{\mathrm{J_0}(\mathrm{r_0}\sqrt{-\mathrm{i}\omega/\nu})}\right] \tag{3.21}$$

where $\mathrm{dP_{amp}}$ represents the amplitude of the variation in the pressure gradient, ω represents the frequency of oscillation, and J_0 is a Bessel function of order zero. A Bessel function is an analytical solution to a continuous damped harmonic oscillator. Values employed for these constants are outlined in Table 3.1. The amplitude of pressure gradient variation is set as 5mmHg to approximate the pressure drop in the aorta as blood is exiting the left ventricle.

Two different flow cases are modelled for flow through a tube and the profiles of the variations in flow rate and boundary velocity gradient are determined numerically. The first flow case uses a large radius simulating a large Womersley number ($\alpha = 55$), such as flow through the arteries and veins near the heart. The second case uses a small radius simulating a small Womersley number ($\alpha = 0.009$), such as flow through the capillaries, arteriole and venules in the systemic and pulmonary circulation systems [Fung, 1997].

Figure 3.4 shows the results where the top graph plots the variation in pressure gradient with time. The middle graph plots both the flow rate (Q) and the boundary velocity gradient ($\frac{\partial \mathrm{u}}{\partial \mathrm{r}}(\mathrm{r_0})$) overlaid for a small Womersley number. Both lines are scaled to have equal magnitude and it can be seen that the boundary

Description	Symbol	Value
Blood properties:		
Blood density	ρ	1050 kg/m^3
Blood Viscosity	μ	0.004 Ns/m^2
Blood Kinematic Viscosity	ν	3.8x10^{-6} m^2/s
Artery Properties:		
Internal Artery Radius	r_0	0.0125 m
Artery Length	ℓ	0.2 m
Chamber properties:		
Chamber Elastance	E_{es}	1N/m^5
EDPVR Volume Cross-over	V_0	0 m^3
ESPVR Volume Cross-over	V_d	0 m^3
Constant	λ	23000 m^{-3}
Heart Rate	ω	1.33 beats/sec
Constant	A	15 N/m^2

Table 3.1 Constants used in single-chamber simulation.

velocity gradient is directly in phase with the flow rate for small Womersley number flow. The bottom graph shows the same information for a large Womersley number, where the flow rate and the boundary velocity gradient are considerably out of phase.

The results in Figure 3.4 show that for high Womersley number flow, the flow rate lags the pressure gradient. This result is contrasted with the low Womersley number flow where there is no visible lag. Equation (3.19) shows that small Womersley numbers mean inertial forces are small relative to viscous forces, meaning inertial effects can be ignored. The middle plot in Figure 3.4 reinforces this conclusion showing no lag between the driving pressure, the flow rate and the boundary velocity gradient. Therefore, small radius tubes imply low Womersley number flow and thus minimal inertial effects. Hence, Equation (2.7) with constant resistance can be used as the governing equation for fluid flow in the systemic and pulmonary circulation systems where vessel diameters are small and variations in flow rates are minimal.

In the arteries and veins near the heart the Womersley number is large, inertial forces are significant, and therefore they must be included in fluid flow calculations. For large Womersley number flow, inertial effects on the fluid cause the flow rate to significantly lag behind the pressure gradient, as shown in Figure 3.4. Additionally, the boundary velocity gradient is shown to be out of phase with the flow rate. By relating this phase lag to Equation (3.18), it can be seen that resistance must vary with time to accommodate the out of phase variations

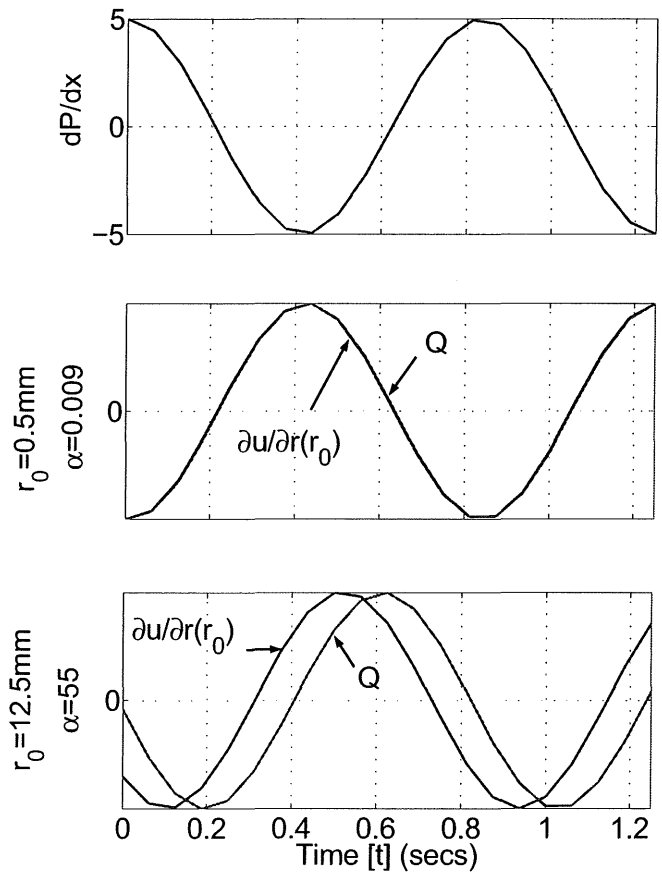

Figure 3.4 Sinusoidally varying pressure gradient driving flow (top), variations in $\partial u/\partial r(r_0)$ and Q for small Womersley number flow, $\alpha = 0.009$, (middle) and large Womersley number flow, $\alpha = 55$ (bottom).

in Q and $\partial u/\partial r(r_0)$. Equation (3.13) assumes constant resistance and is therefore not suitable for modelling this flow, and Equation (3.12) should be used as a more accurate alternative based directly on the Navier-Stokes equation and fluid dynamic principles. Therefore, for large arteries with a high Womersley number flow, both inertial effects and the effects of time varying resistance must be included by using Equation (3.12).

For the full closed loop model, as shown in Figure 2.1, the Womersley number analysis shows that flow through the valves entering and exiting the heart has a high Womersley number. Flow through the valves must therefore include the effects of time varying resistance and inertia. Therefore, flow through the mitral (mt), aortic (av), tricuspid (tc) and pulmonary (pv) sections of the CVS model must be calculated using Equation (3.12). The flow through the capillaries in the systemic and pulmonary circulation systems is low Womersley number flow

and therefore inertial effects and the influence of time varying resistance can be assumed negligible. Thus, flow through the resistors marked R_{sys} and R_{pul} on Figure 2.1 can be governed by Equation (2.7). The result is a more physiologically accurate model mixing lumped parameter equations, such as Equation (2.7), with continuous system equations, such as Equation (3.12).

3.3 Time Varying Resistance

It has been shown that Equation (3.12) should be used when trying to model the effects of time varying resistance and inertial effects. Equation (3.12) gives a first order governing equation for flow rate, but it is posed as a function of the boundary velocity gradient, which is unknown. Equation (3.2), the equation from which Equation (3.12) is derived, is a function of velocity profile and pressure gradient only. When the development of the velocity profile is simulated using Equation (3.2), the velocity profile will be determined at each time step. The flow rate at any time can then be determined numerically by integrating the velocity profile at that time.

$$Q = \int_0^{2\pi} \int_0^{r_0} u(r,t) r dr d\theta \tag{3.22}$$

where u(r,t) is the velocity gradient as a function of radius (r) and time (t).

Therefore, Equation (3.2) is used in this research as a more suitable governing equation for the fluid flow in the arteries near the heart as it can be used to determine the variations in the velocity profile. Although not explicitly defined, the effects of time varying resistance (R(t)) and inertia (L) are implicitly defined in Equation (3.2).

3.3.1 Non-dimensionalisation

The magnitude of the variables used in Equation (3.2) can vary significantly, which will contribute to an accumulation of computational error. For example, the magnitude of the volume is on the order of millilitres ($10^{-6}m^3$) and pressure is on the order of millimeters of mercury ($10^2N/m^2$). The magnitudes of these numbers differs by a factor of 10^8 which is significant enough contribute to excessive computational error. To avoid accumulation of machine error and better pose the problem for the numerical solution method, all equations are non-dimensionalised.

Non-dimensional values are labelled with a star (*) so the non-dimensional form of a dimensional variable x is x^*, which is related to x by it's characteristic value labelled $\overline{x}$.

$$x^* = \frac{x}{\overline{x}} \tag{3.23}$$

The following characteristic values are used:

- The characteristic radius ($\overline{r}$) is set to 12.5mm to roughly approximate the diameter of human heart values [Bellhouse and Talbot, 1969]. The characteristic length ($\overline{\ell}$) is set to 200mm to approximate the effective length and scale of the human aorta.

- The characteristic pressure drop along an artery is set to -10mmHg, to approximate the pressure drop in the arteries around the heart ($\overline{P_2 - P_1}$=10mmHg).

- These definitions allow the definition of a characteristic pressure gradient:

$$\frac{\overline{dP}}{dx} = \frac{\overline{P_2 - P_1}}{\overline{\ell}} \tag{3.24}$$

- The characteristic flow rate is obtained from Poiseuille's equation.

$$\overline{Q} = \frac{\pi \overline{r}^4}{8\mu} \frac{\overline{dP}}{dx} \tag{3.25}$$

- The characteristic velocity is set as the characteristic flow rate divided by the cross sectional area.

$$\overline{u} = \frac{\overline{Q}}{\pi \overline{r}^2} = \frac{\overline{r}^2}{8\mu} \frac{\overline{dP}}{dx} \tag{3.26}$$

- The characteristic volume ($\overline{V}$) is defined as the amount of flow per unit time.

$$\overline{V} = \frac{\overline{Q}}{\overline{t}} \tag{3.27}$$

- The characteristic time is defined as the period of one heartbeat in seconds.

$$\overline{t} = \frac{1}{HR} \tag{3.28}$$

- A characteristic value of resistance ($\overline{R}$) is determined using Equation (2.7)

$$\overline{R} = \frac{\overline{P_2 - P_1}}{\overline{Q}} \tag{3.29}$$

- If only the inertances are used, the characteristic inertance (L) is taken as the average of all inertances ($\overline{L}$ = Average L). If the radius and length of the arteries are known the characteristic inertance is defined from Equation (3.17).

$$\overline{L} = \frac{\rho\overline{\ell}}{\pi\overline{r}^2} \tag{3.30}$$

- The characteristic elastance ($\overline{E}$) is defined as the relationship between the characteristic pressure and volume.

$$\overline{E} = \frac{\overline{P}}{\overline{V}} \tag{3.31}$$

The characteristic variables are substituted into Equation (3.22) to obtain the equation for the non-dimensional value of the flow rate (Q^*).

$$Q^* = \frac{1}{\pi}\int_0^{2\pi}\int_0^{r_0} u^*(r^*, t^*)r^* dr^* d\theta \tag{3.32}$$

Equation (3.13) is non-dimensionalised to produce the dimensionless form of the constant resistance equation governing fluid flow.

$$L^*\frac{dQ^*(t^*)}{dt^*} = \frac{480\nu}{\overline{r}^2 HR}\left(-\frac{\partial P^*}{\partial x}(t^*) - Q(t^*)R^*\right) \tag{3.33}$$

The dimensionless form of the equation for the rate of change of the velocity vector can also be found from Equation (3.2).

$$\frac{\partial u^*(r^*, t^*)}{\partial t^*} = \frac{480\nu}{\overline{r}^2 HR}\left(-\frac{\partial P^*}{\partial x}(t^*) + \frac{1}{8}\left(\frac{\partial^2 u^*(r^*, t^*)}{\partial r^{*2}} + \frac{1}{r^*}\frac{\partial u^*(r^*, t^*)}{\partial r^*}\right)\right) \tag{3.34}$$

Note that the term $\nu/(\overline{r}^2 HR)$, found in both Equations (3.33) and (3.34), is equal to the inverse of the Womersley number squared ($1/\alpha^2$). This result further highlights the significance of the Womersley number in these calculations for relating inertial effects to viscous effects.

These non-dimensional formulae are substituted for the dimensional equivalents in the solution process developed ensuring improved stability. Additional non-dimensional forms of the governing equations for the elastic chambers are required to numerically simulate the model, and these equations are defined in Appendix 1. All state variables, including all chamber volumes and flow rates that include inertial effects, are non-dimensionalised before being used in the model. The output state variables are then dimensionalised at the end, before plotting and analysing. Finally, the use of Equation (3.34) to capture time varying resistance and inertial effects, along with the model terms in Chapter 2, creates a mixed continuous and lumped parameter model that is more physiologically accurate than typically used lumped parameter models.

3.4 Summary

The derivation of the governing equations for flow rate in CVS models has been outlined. The flow through the large arteries and veins around the heart is shown to have a high Womersley number and therefore inertial effects and variations in resistance will be significant. Blood flow through the small diameter capillaries in the peripheral circulation is shown to have a low Womersley number and inertial effects and variations in resistance can be assumed negligible. The most suitable governing equation for high Womersley number flow is found to be Equation (3.34) which captures the time varying resistance and inertia effects. For low Womersley number flow, only Equation (3.9) is required and is much easier to solve numerically.

With the equations governing the elastic chambers outlined in Chapter 2 and the non-dimensionalised fluid flow equations derived in this chapter, the basic building blocks for the model have been established. The next chapter discusses the methods used to numerically simulate and verify the mixed lumped parameter and continuous system model developed.

Chapter 4

Numerical Simulation Methods

The construction of a mixed formulation, minimal model including the governing equations for the passive and active elastic chambers and the fluid flow between them has been outlined in Chapters 2 and 3. This chapter investigates how to numerically simulate these models with their combined lumped parameter and continuous elements. Methods of determining accurate initial conditions to improve computational time are also discussed.

The mixed model is primarily governed by ordinary differential equations (ODEs) such as the rate of change of ventricle volume formula of Equation (2.8). The numerical ODE solver *ode15s* in the mathematical software package MATLAB is used to numerically integrate the model equations. The *ode15s* function is a variable step-size solver for solving stiff problems of the form:

$$\frac{d\underline{x}}{dt} = f(\underline{x}) \tag{4.1}$$

where $\underline{x}$ is a vector of state variables, referred to as the state vector, $f(\underline{x})$ is a function of the state vector that yields the state derivative ($d\underline{x}/dt$), or the rate of change of each state variable.

Equation (4.1) easily admits the mixed model elements developed, including the dynamics of the elastic chambers and fluid flow components. This chapter will bring together all the elements of Chapters 2 and 3 in defining the solution method. The models and methods are developed from a single chamber model and then sequentially expanded to the full closed loop system, as in Chapter 2.

4.1 Basic Model

For the single chamber model of Figure 2.2 with no inertia and constant pressure boundary conditions (P_1 and P_3 constant), the minimal model is governed by

only one ODE:

$$\frac{dV}{dt} = f(V, t) \tag{4.2}$$

where the rate of change of volume (V) is expressed as a function of volume and time (t). The following steps are taken at each iteration of the ODE solver to obtain the overall solution.

- The chamber volume (V) is passed to the ODE function as the only state variable in the state vector ($\underline{x}$=[V]).
- The chamber pressure (P_2) is calculated from the volume using Equation (2.6):

$$P_2(V, t) = e(t)E_{es}(V - V_d) + (1 - e(t))P_0(e^{\lambda(V-V_0)} - 1) \tag{4.3}$$

- Equation (2.7) is used to calculate the flow rates in (Q_{in}) and out (Q_{out}) of the chamber from the pressure differences:

$$Q = \frac{P_1 - P_2}{R_1} \tag{4.4}$$

- Any flow rates that are negative are set to zero to simulate valve function.
- The rate of change of chamber volume (dV/dt) is calculated from the difference between the inlet and outlet flow rates using Equation (2.8):

$$\frac{dV}{dt} = Q_{in} - Q_{out} \tag{4.5}$$

- The derivative of the state vector is passed back to the ODE solver as the state derivative ($d\underline{x}/dt$ = [dV/dt]). The ODE solver then estimates a new volume based on the current volume, the volume derivative and the numerical step size in time.

Models with greater numbers of chambers and complexity are solved in the same way by simply adding the volume of every elastic chamber to the state vector. This simple method summarises the modelling of systems where there are no continuous system elements because inertial effects are assumed to be negligible and variations in resistance are ignored. Valve function is simulated by simply

constraining the flow rate to be greater than or equal to zero. The next section shows how inertial effects and time varying resistance can be added to the model.

4.2 Inertia and Time Varying Resistance

As discussed in Chapter 3, there are three different governing equations for flow rate that can be used to simulate the blood flow in the arteries. Poiseuille's equation, Equation (2.7), allows the calculation of flow rate directly from the pressure gradient. However, Equations (3.2) and (3.13) are first order equations governing the velocity profile and flow rate respectively, and variations in each must be numerically simulated. The following sections discuss the inclusion of inertia with constant resistance, valves, and time varying resistance into lumped parameter CVS models. As discussed in Chapter 3, Equations (3.2) and (3.13) are used in their non-dimensional form as shown in Equations (3.34) and (3.33)

4.2.1 Inertia with Constant Resistance

Equation (3.33) is included as the governing equation for flow rate by simply adding flow rate (Q) to the state vector. For example, a single chamber model that includes inertial effects at the inlet and outlet uses a state vector of the form:

$$\underline{x} = [V, Q_{in}, Q_{out}]^T \tag{4.6}$$

where Q_{in} and Q_{out} are the flow rates in and out respectively. Each iteration of the ODE solver calculates the rate of change of the flow rate as a function of pressure gradient using Equation (3.33). The flow rate is now tracked numerically at each time step in the same way as the volume.

4.2.2 Valve Simulation

In models where inertia is not included and the governing flow equation is defined by Equation (2.7), the valves are simulated simply by setting the flow rate to zero when it is calculated to be zero or negative [Santamore and Burkhoff, 1991]. However, when inertial effects are included in the model, the flow rate (Q) is governed by a first order ODE and setting the flow rate to zero will create a discontinuity, which will cause an unstable numerical solution.

Of the numerous models in the literature, none were found that show how to incorporate valve function into the numerical simulation. Hardy et.al. (1982) propose the valves open on negative pressure gradient, and close on zero flow, but the method of incorporating the non-linearity of the valves into a numerical simulation is not explained. The solution presented here is to allow the system state to change dynamically while solving.

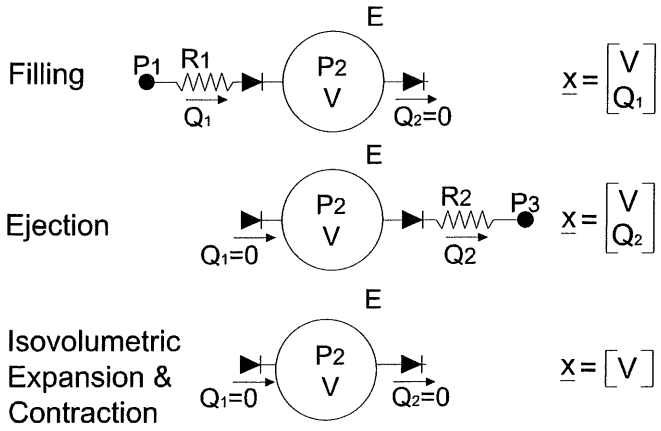

Figure 4.1 The 3 states of a single ventricle system during the cardiac cycle.

Figure 4.1 shows the three different state vectors for a single cardiac chamber that a normal heart cycles through during the cardiac cycle along with their corresponding state vectors ($\underline{x}$). During ejection and filling, the state vector is made up of the volume and the flow rate out or in, respectively. However, during isovolumetric contraction and relaxation, only the volume (V) is required since both flow rates are zero. Hence, different parts of the cardiac cycle require different state variables and are effectively different models. Figure 4.2 shows how the state vector changes at different locations on the cardiac cycle on a PV diagram for a single elastic chamber.

In order to change the state of the system, the state variables employed are triggered to change when either a flow rate or a pressure gradient becomes negative. When a flow rate (Q) becomes negative, it is removed from the state vector to account for the valve closing in the absence of flow. Alternatively, when a pressure gradient becomes negative, favouring forward flow, the associated flow rate is re-included in the state vector to account for the valve opening. Hence, the valve law for the model presented is "*close on flow, open on pressure*" where the valve opens on a negative pressure gradient, but is delayed from closing on a positive pressure gradient due to the inertia of the blood, matching known

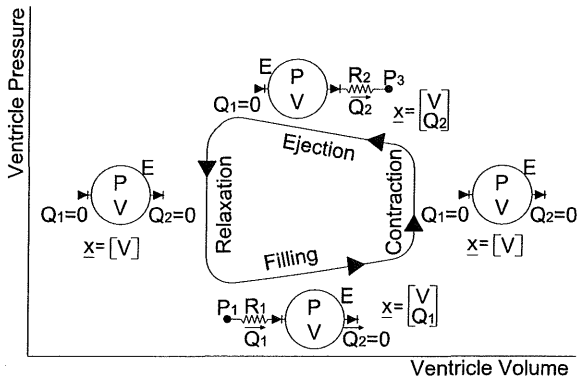

Figure 4.2 The 3 states of a single ventricle system during the cardiac cycle on a PV diagram.

physiological response [Opie, 1998; Little, 1978].

The *events* function in the ODE solvers in Matlab was used to detect when a valve should be opened or closed and break out of the simulation. The state vector of the system is then changed to one of the alternatives in Figure 4.1 and the ODE solver is restarted. For the other variables in the state vector that are not affected, the final value before the solver was stopped is used as the initial condition for the resumed simulation. This method of simulation means that instead of simulating one model for a predefined time period, a series of models are simulated in succession each heartbeat.

4.2.3 Time Varying Resistance

The discussion in Chapter 3 has shown that Equation (3.34), should be used when modelling the effects of time varying resistance and inertia using non-dimensional variables, particularly around the heart. The question is how to add this continuous system equation into a lumped parameter model to replace Equation (3.33). A method is presented where, instead of just determining the flow rate (Q), the velocity profile vector ($\underline{u}$) is added as a series of state variables in the state vector. In this way, not just the flow rate will be determined at each time step, but also the variations in the velocity profile, enabling the boundary velocity gradient and resistance to be determined at any given time.

The velocity profile vector calculated is a discrete representation of the velocity profile, dividing the radius into equally spaced nodes. Equation (3.34) is now used since the velocity profile, not the flow rate, is obtained at each time step.

At each iteration of the ODE solver the rate of change of velocity is calculated at each node using Equation (3.34). A no-slip boundary condition is applied so that the velocity at the boundary is always zero. Thus, where Equation (3.33) is often used to calculate the rate of change of flow rate, Equation (3.34) is now used to calculate the rate of change of the velocity profile vector.

Using this method, the state vector for a single chamber system is of the form:

$$\underline{x} = \left[V, \underbrace{u_{in.1}, u_{in.2}, \ldots, u_{in.j}}_{\underline{u}_{in}}, \underbrace{u_{out.1}, u_{out.2}, \ldots, u_{out.j}}_{\underline{u}_{out}} \right]^T \tag{4.7}$$

where $\underline{u}_{in.i}$ and $\underline{u}_{out.i}$ are the velocity profile in and out of the chamber at node location i, respectively. The following steps are taken at each iteration of the ODE solver using the non-dimensionalised variables:

- The chamber volume (V) and the velocity profiles ($\underline{u}_{in}$ and $\underline{u}_{out}$) are passed to the ODE function as state variables.

$$\underline{x} = [V, \underline{u}_{in}, \underline{u}_{out}]^T \tag{4.8}$$

- The chamber pressure (P_2) is calculated from the volume using the non-dimensional parameters in Equation (2.6).

$$P_2(V,t) = e(t)E_{es}(V - V_d) + (1 - e(t))P_0(e^{\lambda(V-V_o)} - 1) \tag{4.9}$$

- Equation (3.34) is used to find the rate of change of the velocity profiles ($d\underline{u}_{in}/dt$ and $d\underline{u}_{out}/dt$).

$$\frac{\partial u(r,t)}{\partial t} = \frac{480\nu}{\bar{r}^2 HR}\left(-\frac{\partial P}{\partial x}(t) + \frac{1}{8}\left(\frac{\partial^2 u(r,t)}{\partial r^2} + \frac{1}{r}\frac{\partial u(r,t)}{\partial r}\right)\right) \tag{4.10}$$

- The velocity profiles are numerically integrated to calculate the flow rates in (Q_{in}) and out (Q_{out}) using Equation (3.32).

$$Q^* = \frac{1}{\pi}\int_0^{2\pi}\int_0^{r_0} u(r,t)rdrd\theta \tag{4.11}$$

- The rate of change of chamber volume (dV/dt) is calculated as the flow rate in minus the flow rate out.

$$\frac{dV}{dt} = Q_{in} - Q_{out} \tag{4.12}$$

- The time derivative of the state vector ($d\underline{x}/dt$) is passed back to the ODE solver including the rate of change of volume and the rate of change of the velocity profiles.

$$\frac{d\underline{x}}{dt} = \left[\frac{dV}{dt}, \frac{\underline{u}_{in}}{dt}, \frac{\underline{u}_{out}}{dt}\right]^T \tag{4.13}$$

Thus, time varying resistance and inertial effects are included from the continuous system, finite element type formulation into a simple lumped parameter CVS model in a fluid dynamically accurate manner. The actual values of inertia (L) and time varying resistance (R(t)) are not directly calculated in the manner of conventional lumped parameter CVS models. However, this method of tracking the velocity profile automatically incorporates these effects. It is also easily incorporated into lumped parameter CVS models with minimal modification to the ODE solver.

For the velocity profile method, nodes at which velocity is calculated are spaced equally along the radius. Before doing calculations using the velocity profile method, the number of nodes required to gain accurate results must be found. Using many nodes makes the calculations more accurate, but lengthens the computation time required to simulate the model. Figure 4.3 shows a plot of the percentage error of the stroke volume for a single chamber model using different numbers of radial nodes. The accuracy of each different simulation with different numbers of nodes is determined by comparing the stroke volume in the main chamber. The percentage error is relative to the stroke volume at 150 nodes, where the solution has converged and error is negligible. From Figure 4.3, the number of nodes required can be determined based on the allowable error. For all simulations in this thesis using the velocity profile method, 20 nodes were used as this number produces an error of less than 1% without excessive computational cost.

4.3 Ventricular Interaction

When simulating ventricular interaction, the dynamics of the septum, and the effects of the pericardium must be taken into account. As discussed in Chapter

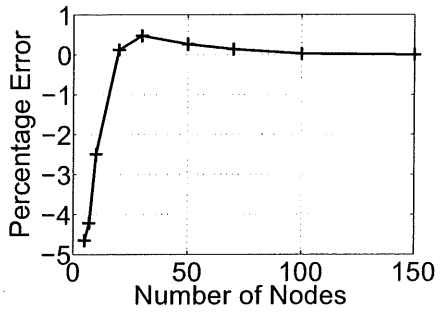

Figure 4.3 Percentage error of stroke volume versus number of nodes on radius.

2, there are many examples in the literature dividing the ventricle volumes to account for the displacement of the septum. However, the author was unable to find methods for determining the displacement of the septum (Vspt) given the non-linear PV relationship of the myocardium defined in Equation (2.6):

$$P(V,t) = e(t)E_{es}(V - V_d) + (1 - e(t))P_0(e^{\lambda(V-V_o)} - 1) \tag{4.14}$$

By combining Equations (2.15), (2.16), (2.17) and (2.6), an equation that relates V_{lv}, V_{rv} and V_{spt} can be found.

$$\begin{aligned} &eE_{es,spt}(V_{spt} - V_{d,spt}) + (1-e)P_{o,spt}(e^{\lambda_{spt}(V_{spt}-V_{o,spt})} - 1) \\ &= eE_{es,lvf}(V_{lv} - V_{spt} - V_{d,lvf}) + (1-e)P_{o,lvf}(e^{\lambda_{lvf}(V_{lv}-V_{spt}-V_{o,lvf})} - 1) \\ &-eE_{es,rvf}(V_{rv} + V_{spt} - V_{d,rvf}) - (1-e)P_{o,rvf}(e^{\lambda_{rvf}(V_{rv}+V_{spt}-V_{o,rvf})} - 1) \end{aligned} \tag{4.15}$$

where the subscript denotes to which cardiac free wall the properties apply. Equation (4.15) can be numerically solved to determine V_{spt} given V_{lv} and V_{rv} via zero finding solutions such as a Gauss-Newton method. The function *fsolve* was used from the Matlab toolbox to solve this equation and find V_{spt}. Note that when simulating the model in the non-dimensional form, Equation (4.15) is of the same form, but with all dimensional variables and parameters substituted with their non-dimensional equivalents.

This method of calculating V_{spt} from the two ventricle volumes means that only V_{lv} and V_{rv} need to be used as state variables. This result is in contrast to the equations used by Chung et.al. (1997) which uses 6 state variables in the state vector. That model included all 3 free wall volumes (V_{lvf}, V_{rvf} and V_{spt}) the left and right free wall pressures (P_{lvf} and P_{rvf}) and the pericardium pressure

(P_{peri}).

$$\underline{x}_c = [V_{lvf}, V_{rvf}, P_{lvf}, P_{rvf}, V_{spt}, P_{pcd}]^T \tag{4.16}$$

where $\underline{x}_c$ denotes the state vector used by Chung et.al. (1996). The three pressures are not necessary in the state vector as they can be calculated at any time from the volumes. Also, it has been shown that the septum volume deflection is not required in the state vector. The inclusion of these variables means the model is over-defined which results in it being numerically unstable and over-constrained. This research uses state vectors with the minimum number of elements required to create a minimal model.

The following steps outline the sequence used in the numerical simulation for modelling ventricular interaction. The state derivative, dV_{lv}/dt and dV_{rv}/dt, is calculated from the state variables, V_{lv} and V_{rv}, at each time step of the simulation:

1. The two state variables V_{lv} and V_{rv} are passed to the ODE function as state variables.

$$\underline{x} = [V_{lv}, V_{rv}]^T \tag{4.17}$$

2. Calculate the pressure in the pericardium (P_{peri}) using Equation (2.14) from the pressure across the pericardium wall (P_{pcd}) using Equation (2.18) and the total volume (V_{pcd}) from Equation (2.11):

$$P_{peri} = P_{0,pcd}(e^{\lambda_{pcd}(V_{lv}+V_{rv}-V_{0,pcd})} - 1) + P_{th} \tag{4.18}$$

3. Determine the septal wall deflection (V_{spt}) by solving Equation (4.15).

4. Given V_{spt} and Equations (2.9) and (2.10), V_{lvf} and V_{rvf} can be determined and used in Equation (2.16) to calculate P_{lvf} and P_{rvf}.

$$P_{lvf} = eP_{es,lvf} + (1 - e)P_{ed,lvf} \qquad P_{rvf} = eP_{es,rvf} + (1 - e)P_{ed,rvf} \tag{4.19}$$

5. The values of P_{lvf}, P_{rvf} and P_{peri} are used in Equations (2.12) and (2.13) to find P_{lv} and P_{rv}.

$$P_{lv} = P_{lvf} + P_{peri} \qquad P_{rv} = P_{rvf} + P_{peri} \tag{4.20}$$

6. The ventricle pressures are then used to calculate the flow rates, and thus, the rate of change of ventricle volumes:

$$\frac{d\underline{x}}{dt} = \left[\frac{dV_{lv}}{dt}, \frac{dV_{rv}}{dt}\right]^T \tag{4.21}$$

These six steps are repeated at each time step to account for ventricular interaction. These steps also show how all of the ventricular interaction equations in Chapter 2 are combined in the numerical simulation.

4.4 Full Closed Loop Model

The full closed loop model simply requires the addition of four additional state variables to the model to account for the four additional peripheral elastic chambers. The resulting state vector, used for simulations that model inertial effects with constant resistance, is constructed as follows:

$$\underline{x} = [V_{pu}, Q_{mt}, V_{lv}, Q_{av}, V_{ao}, V_{vc}, Q_{tc}, V_{rv}, Q_{pv}, V_{pa}]^T \tag{4.22}$$

Alternatively, if each valve incorporates time varying resistance, then each flow rate (Q) in the state vector is substituted with the 20 node velocity profile ($\underline{u}$) for that value.

$$\underline{x} = [V_{pu}, \underline{u}_{mt}, V_{lv}, \underline{u}_{av}, V_{ao}, V_{vc}, \underline{u}_{tc}, V_{rv}, \underline{u}_{pv}, V_{pa}]^T \tag{4.23}$$

All the state variables are defined in Table 4.1.

The choice of using time varying resistance, or constant resistance with inertia is dependent on the available computational time. The time varying resistance method takes approximately twice as long to solve as the constant resistance method for 20 nodes. The constant resistance method is often used to produce approximate results quickly and the time varying resistance model is used to achieve more accurate results.

The flow rate through the pulmonary and systemic circulation systems is assumed to be low Womersley number flow and is therefore governed by Equation (2.7). Thus, by putting all of the above equations together and using an

Symbol	Description
Volumes:	
V_{pu}	Volume of the Pulmonary Vein
V_{lv}	Volume of the Left Ventricle
V_{ao}	Volume of the Aorta
V_{vc}	Volume of the Vena-Cava
V_{rv}	Volume of the Right Ventricle
V_{pa}	Volume of the Pulmonary Artery
Flow Rates:	
Q_{mt}	Flow through the Mitral Valve
Q_{av}	Flow through the Aortic Valve
Q_{tc}	Flow through the Tricuspid Valve
Q_{pv}	Flow through the Pulmonary Valve
Velocity Profiles:	
$\underline{u}_{mt}$	Velocity profile in the Mitral Valve
$\underline{u}_{av}$	Velocity profile in through the Aortic Valve
$\underline{u}_{tc}$	Velocity profile in through the Tricuspid Valve
$\underline{u}_{pv}$	Velocity profile in through the Pulmonary Valve

Table 4.1 Pressure Variables.

ODE solver, a dynamic full closed loop representation of CVS function is created. Appendix 1 shows in more detail the equations used to calculate the state derivative from the state vector at each step of the process.

4.5 Initial Conditions

Another important issue in simulating these models is estimating accurate initial conditions in order to decrease computational time. The model will eventually converge to a steady state solution from any reasonable initial conditions, however the more accurate the initial conditions, the faster the solution converges to a steady state. Two methods were found to determine the initial conditions (ICs) for each volume of the closed loop model. The first determines the volumes at which the system is static without cardiac activation. The second approximates the pressures and resulting volumes for a dynamic system with cardiac activation.

4.5.1 Zero Flow ICs

The first method simply involves calculating the volume of each chamber so that all the pressures are equal. This task is done by solving for the volumes so that flow rates through five of the six resisters are zero. For the flow rate across

a resistor to be zero, the pressures on either side of the resistor must be equal. Consideration must also be made for the total volume of the system (V_{tot}), which must remain constant. The resulting problem involves minimising the following function of the volumes vector.

$$\begin{bmatrix} Q_{mt} \\ Q_{av} \\ Q_{tc} \\ Q_{pv} \\ Q_{sys} \\ \sum Vs - V_{tot} \end{bmatrix} = f\left(\begin{bmatrix} V_{pu} \\ V_{lv} \\ V_{ao} \\ V_{vc} \\ V_{rv} \\ V_{pa} \end{bmatrix}\right) \tag{4.24}$$

where $\sum Vs$ is the sum of all the volumes and the remaining variables are outlined in Table 4.1. Thus, five of the flow rates must be set to zero, meaning the sixth flow rate will also be zero, while making the sum of the volumes equal to V_{tot}.

Calculating the volumes to make all the flow rates zero and consequently all pressures equal, simulates the state of the system in a person whose cardiac function has ceased. Instances where there is no cardiac function occur when attempting to simulate cardio-pulmonary resuscitation (CPR). However, this method does not take into account the build-up of volume in chambers that precede high resistances in the model. For example, typical pressures in the vena-cava (P_{vc}) are on the order of 1mmHg while a typical pressures in the aorta (P_{ao}) is approximately 100mmHg. This method is therefore not suitable for general solutions, but is useful for simulating CPR.

4.5.2 Dynamic ICs

A more accurate method of capturing the ICs involves determining the end-systolic (ES) and end-diastolic (ED) pressures in the ventricles. As discussed, the zero flow ICs defined previously do not account for the damming effect the resistors have on blood flow. The significant difference in pressure between the aorta and vena-cava is caused by blood build-up in the aorta before flowing through the systemic resistance into the vena-cava. The zero flow ICs would calculate these pressures to be equal, which is not an accurate approximation.

A good approximation for the pressure in the veins upstream of the ventricles, such as the vena-cava, is the end-diastolic pressure in the ventricle ($P_{ED}(V_{ED})$).

$P_{ED}(V_{ED})$ can be calculated using the EDPVR as a function of end-diastolic volume (V_{ED}). The value of $P_{ED}(V_{ED})$ is therefore determined using Equation (2.6) with the driver set to zero (e(t)=0). The end-systolic pressure (P_{ES}) is a good approximation to the pressure downstream of the ventricle, such as in the aorta or the pulmonary artery. P_{ES} is a function of end-systolic volume ($P_{ES}(V_{ES})$), however this volume is unknown. The end-systolic pressure can be calculated as a function of the end-diastolic volume ($P_{ES}(V_{ED})$) using Equation (2.6) with the driver set to one (e(t)=1). However, Figure 4.4 shows that $P_{ES}(V_{ED})$ is not a good approximation to $P_{ES}(V_{ES})$. A better approximation is found by using a driver value (e(t)) of 0.5 in Equation (2.6) to roughly approximate $P_{ES}(V_{ES})$.

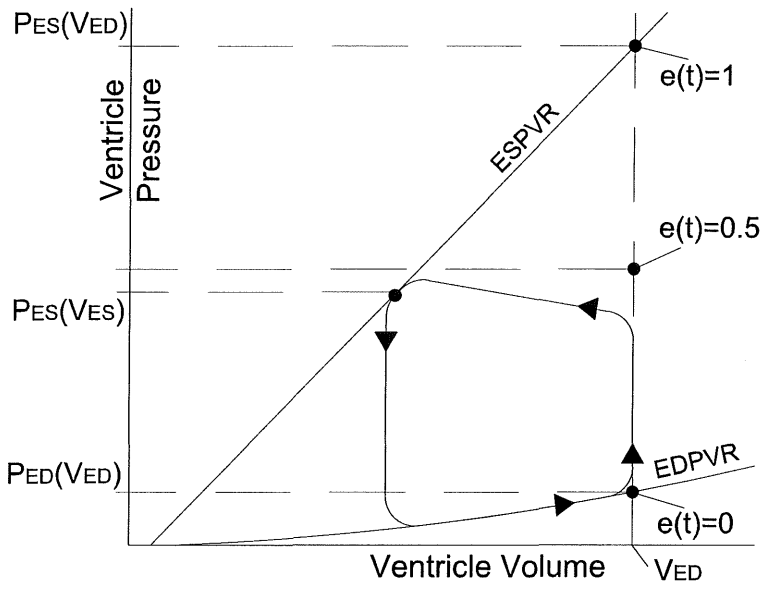

Figure 4.4 Pressure-volume diagram showing ED pressure as a function of ED volume and ED pressure as a function of both ED volume and ES volume.

There are six volumes that must be determined to calculate the best initial conditions for the CVS model, requiring the following six variables and equations to be minimised.

- minimise P_{lv}-P_{pu} for e(t)=0 (across mitral valve)
- minimise P_{rv}-P_{vc} for e(t)=0 (across tricuspid valve)
- minimise P_{ao}-P_{lv} for e(t)=1 (across aortic valve)
- minimise P_{pa}-P_{rv} for e(t)=1 (across pulmonary valve)

- minimise Q_{sys}-Q_{pul}
- minimise $\sum Vs - V_{tot}$

The first two conditions require minimising the pressure difference across the mitral valve (P_{lv}-P_{pu}) and tricuspid valve (P_{rv}-P_{vc}) using ventricle pressures calculated with the driver set to zero (e(t)=0). The second two conditions require the pressure difference across the aortic valve (P_{ao}-P_{lv}) and the pulmonary valve (P_{pa}-P_{rv}) to be minimised while using ventricle pressures calculated with the driver set to 0.5 (e(t)=0.5). The fifth condition states that the flow rate through the systemic circulation (Q_{sys}) must be equal to the flow rate through the pulmonary circulation (Q_{pul}). This fifth condition implies a steady state solution with no net flow rate being transferred from one part of the CVS to another. For example, if Q_{pul} was higher than Q_{sys} it would imply that blood is accumulating in the left ventricle. Finally, the sixth condition defines that the sum of all the chamber volumes must be equal to V_{tot}.

4.6 Summary

The presented method used to numerically simulate the different CVS models has been defined in terms of the pressure, volume and flow rate definitions in Chapters 2 and 3. First, the solution method for the single chamber model is defined and then built up to include ventricular interaction and the full closed loop model. A method of incorporating inertial effects into the model by using flow rate (Q) in the state vector is also outlined. It is shown that this method can be modified so that instead of using Q, the velocity profile ($\underline{u}$) is used in the state vector to obtain more physiologically accurate results. The results will include both inertia and time varying resistance in simulating flow near the heart.

It can be seen that the presented method of numerically tracking the velocity profile instead of the flow rate can be easily adapted into lumped parameter models. This approach creates a more physiologically accurate mixed lumped parameter and continuous system model. However, the constant resistance method of including inertial effects is also outlined as this method is often used to produce approximate results quickly. Once appropriate results are gained using this quicker method, the more computationally intensive time varying resistance model is used to achieve more accurate results.

Two methods of determining accurate initial conditions are defined depending on the type of model being run. Although the model does not require accurate initial conditions they are advantageous in achieving rapid convergence to a steady state solution. This result is in contrast with other models presented in the literature that require accurate initial conditions in order to find a reasonable and/or stable solution. The next chapter looks at model verification, simulating each model and investigating their performance relative to each other and well known trends to verify the model elements and solution methods.

Chapter 5

Model Simulation & Verification

The previous chapters have shown the construction, governing equations and numerical techniques used to develop and simulate the model. The fundamental model elements and dynamics must be verified through comparison with known physiological function and trends. This chapter investigates the results obtained from simulation of the model at different levels of complexity. In addition to checking the hydraulic function and physiological accuracy of the model, a particular focus is ensuring that the model is stable, robust and easy to solve.

The single chamber model is tested first, focusing on verifying the function of the active elastic chambers, valve function and the fluid flow entering and exiting the chamber. Ventricular interaction is tested using the coupled two chamber model with constant boundary conditions. Finally, the full closed loop model including all of these elements is tested and the final results compared with physiological function. The patient specific model parameters used in the numerical simulations in this chapter are extrapolated from those found over several references, producing model results comparable to an average human [Burkhoff and Tyberg, 1993; Chung, 1996; Ursino, 1999]. Most of the data found in the literature is adapted from animal studies as these values are difficult to measure directly in humans.

Table 5.1 lists the mechanical properties of the heart and circulation system. The top three lines define the mechanical properties of the ventricle free walls and septum (V_{lvf}, V_{rvf} and V_{spt}), used in Equation (2.6) to define the PV relationships of these free walls. Only the nonlinear parameters are required for the pericardium properties (V_{pcd}), used in the nonlinear PV relationship of Equation (2.18). The last 4 lines in Table 5.1 give the mechanical properties of the peripheral elastic chambers. Only the linear PV relationship parameters E_{es} and V_d are required to determine the PV relationship in these chambers, as seen in Equations (2.19),

(2.20), (2.22) and (2.23).

To maintain simplicity, Table 5.1 shows that the volumes at zero pressure (V_d and V_0) for all chambers, except the septum volume, are set to zero. The septum volume (V_{spt}) of 2ml at zero pressure accounts for the deflection of the septum in it's relaxed state. The volume at zero pressure accounts for the unstressed volume of blood in the circulation system and by setting these volumes to zero, the unstressed volume is ignored. Of the total 5500ml of blood in the circulation system, about 4000ml is unstressed volume for the average human [Parsons, 2002]. More specifically, unstressed volume is the volume in a chamber that does not contribute to an increase in pressure, or the relaxed volume of a chamber [Kumar and Parrillo, 1995]. With the unstressed volume ignored, the total volume of this model is set to 1500ml.

The resistance and inertance between the elastic chambers is defined in Table 5.2. Table 5.3 lists other properties of the CVS model, including the heart rate, the total stressed blood volume and the fluid dynamic properties of blood. All parameters are loaded into the model in SI units and non-dimensionalised where necessary. However, most output data and graphs are listed with units of millilitres for volume and millimetres of mercury for pressure to match commonly used units found in medical textbooks.

Parameter	E_{es}	V_d	V_0	λ	P_0
Units	$10^6 N/m^5$	$10^{-6}m^3$	$10^{-6}m^3$	m^{-3}	N/m^2
Left ventricle free wall (lvf)	100	0	0	33000	10
Right ventricle free wall (rvf)	54	0	0	23000	10
Septum free wall (spt)	6500	2	2	435000	148
Pericardium (pcd)	-	-	200	30000	66.7
Vena-cava (vc)	1.3	0	-	-	-
Pulmonary Artery (pa)	72	0	-	-	-
Pulmonary Vein (pu)	1.9	0	-	-	-
Aorta (ao)	98	0	-	-	-

Table 5.1 Mechanical properties of the heart and circulation system.

5.1 Single Chamber & Cardiac Dynamics

The single active chamber simulates one of the ventricles, and in this case, data for the right ventricle is used. Constant pressures upstream and downstream of the right ventricle are used (P_1 = 2mmHg and P_3 = 16.5mmHg), matching known average physiological pressures [Guyton, 1991]. The tests in this section

Parameter	Resistance Ns/m^5	Inertance Ns^2/m^5
Mitral Valve (mt)	6.1×10^6	1.3×10^4
Aortic Valve (av)	2.75×10^6	5×10^4
Tricuspid Valve (tc)	1×10^6	1.3×10^4
Pulmonary Valve (pv)	1×10^6	2×10^4
Pulmonary Circulation System (pul)	9.4×10^6	N/A
Systemic Circulation System (sys)	170×10^6	N/A

Table 5.2 Hydraulic properties for flow between chambers.

Description	Symbol	Value
Heart Rate	HR	1.33 beats/sec
Blood density	ρ	1050 kg/m^3
Blood Viscosity	μ	0.004 Ns/m^2
Blood Kinematic Viscosity	ν	$3.8x10^{-6}$ m^2/s
Stressed Volume of blood in CVS	V_{tot}	1500ml

Table 5.3 Constants used in single-chamber simulation.

focus on verifying the dynamics of the specific elements involved. The function of the chamber is shown with the driver function both active and inactive, testing the pressure, volume and flow relationships, as well as the valve function. The robustness of the model is tested using different initial conditions to ensure that the model converges to the same solution. The model is simulated for many consecutive heart beats to check the stability of the steady state solution over a long time. Finally, time varying resistance is added to the model and compared with the function of constant resistance models. Hence, the single chamber model is used to verify the function of the basic elements of the full closed loop model.

5.1.1 Passive Cardiac Chamber

The single chamber model is initially simulated with the driver function inactive to test the response of the passive system from initial conditions. Figure 5.1 plots the response of the model with both active and inactive inertial effects. The initial volume in the active chamber (V) results in a chamber pressure greater than both the upstream and downstream pressures ($P_2 > P_3 > P_1$). The positive pressure gradient across the inlet valve means this valve is closed ($Q_{in} = 0$). The negative pressure across the outlet valve means the outlet valve is open and flow is exiting the chamber ($Q_{out} > 0$). From this initial state with a constant chamber elastance, Figure 5.1 shows that the chamber simply empties until the pressure

in the chamber is less than the down stream pressure.

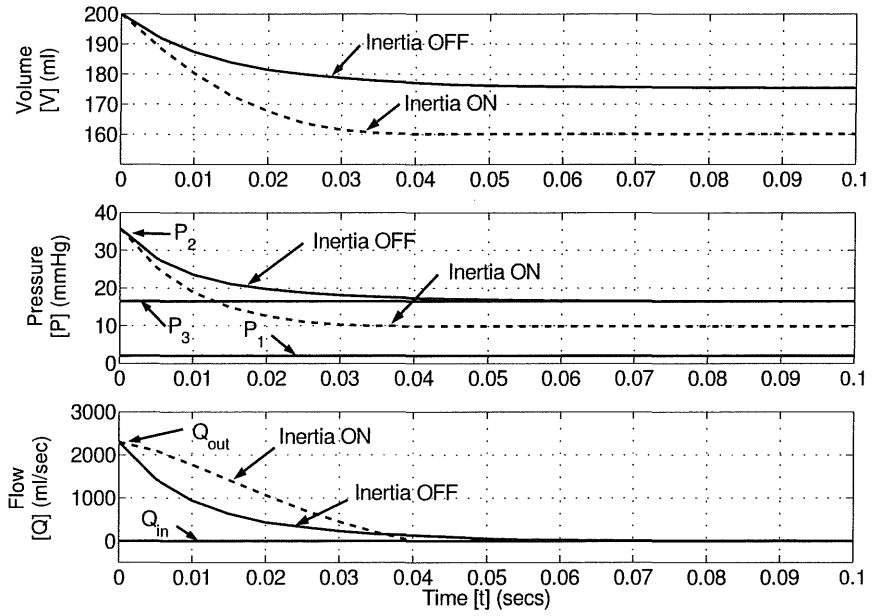

Figure 5.1 Model settling from initial conditions with driver deactivated.

In both cases, as the flow exits the chamber, the volume decreases causing a drop in chamber pressure. Flow continues until the pressure in the chamber becomes equal to the downstream pressure. When inertial effects are not included, the flow stops and the valve closes leaving a chamber pressure equal to the downstream pressure. The inclusion of inertial effects causes the flow rate to decrease more slowly than the non-inertia case and continues flowing even when the pressure gradient becomes positive. This continued flow with inertial effects, against a positive pressure gradient, is due to momentum in the system that limits the rate of change of flow rate [Little, 1978]. The flow continues to empty the chamber so that the pressure drops below the downstream pressure until eventually the flow stops and the valve closes.

5.1.2 Active Cardiac Chamber

The inclusion of the cardiac driver function causes the elastance of the chamber to vary with time and a net flow rate evolves through the system, from P_1 to P_3. Figure 5.2 plots the variation in chamber volume, pressure and flow rates for the single chamber model with inertial effects included. The lines in Figure 5.2 settle from the initial conditions into a repetitive cycle within about one heart beat. The

development of flow entering and exiting the chambers as the pressures change can be seen on the bottom axis. Flow enters the chamber when the chamber pressure is less than the upstream pressure, and exiting flow develops when the chamber pressure is greater than the downstream pressure.

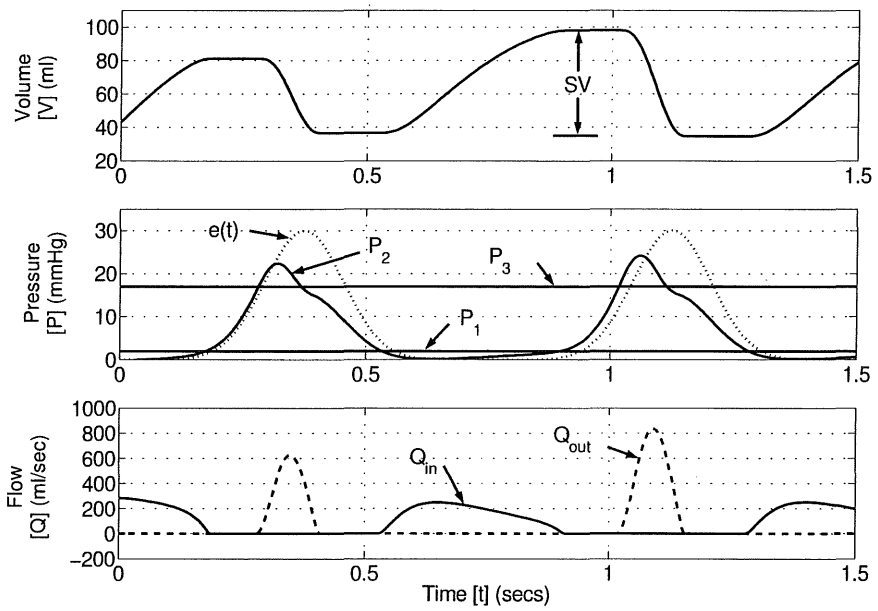

Figure 5.2 Results from single chamber model with driver function included (e(t)).

The driver function (e(t)) is also plotted on the same axes as the pressure variations in Figure 5.2. The impact of variations in chamber elastance (E(t)), as a result of the driver function, can be seen in the chamber pressure variations. The stroke volume (SV) is also labelled on the graph as the difference between the maximum and minimum volumes.

The robustness of the model is tested by running the model from different, relatively extreme, initial conditions and determining if it converges to the same steady state results. Figure 5.3 shows two simulations starting at initial volumes of 10ml and 80ml. These values are set well outside the normal steady state maximum and minimum volumes, as shown in Figure 5.3. The solutions converge to the same steady-state cycle within one heart beat. The stability of the numerical procedure is tested by running the simulation for a long period. Figure 5.4 shows a plot of the pressure and volume profiles over a 40 second period, showing no signs of divergence and emphasising steady state stability. Thus, Figures (5.3) and (5.4) prove the single chamber model is stable, robust and has only one unique steady state solution.

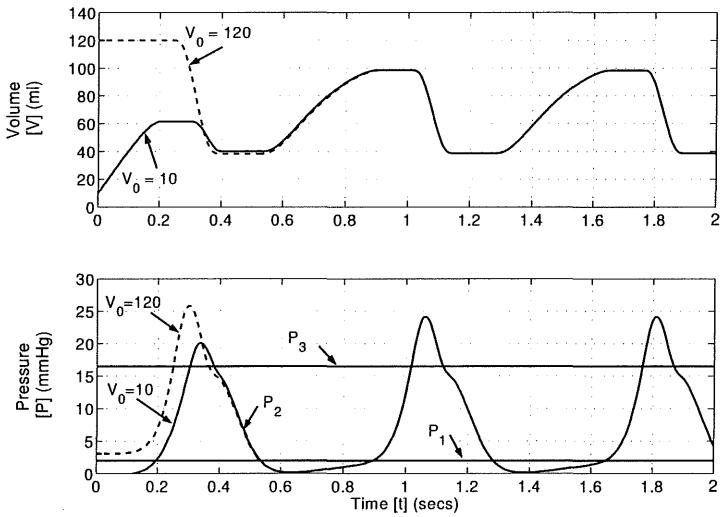

Figure 5.3 Model settling from different initial conditions to the same solution.

The robustness and stability of this model can be compared with that proposed by Chung et.al. (1997). That model requires very accurate initial conditions be determined using a specialised algorithm to obtain stable, realistic results. It was found to produce results that do not fully converge even after 40 seconds of simulation. This lack of convergence was found to be the result of over-defined governing equations that over-constrained the model, as discussed in Chapter 4.

5.1.3 Time Varying Resistance

The velocity profile method developed enables the inclusion of more physiologically accurate variables such as artery radius and length. These parameters replace the conventional lumped parameter resistance and inertance. The radius for this simulation was set to 12.5mm, the average radius of the human heart valves [Bellhouse and Talbot, 1969]. The length was set to 200mm to approximate the effective length and scale of the human aorta.

The velocity profile method is initially verified in comparison with the constant resistance method including inertial effects. The inertial effects in both cases are minimised and the results compared. Inertial effects are minimised by setting the density (ρ) of the blood to a very low value of 1kg/m^3. Substituting $\nu = \mu/\rho$ into Equation (3.19), it can be seen that this density decrease will cause a significant decrease in Womersley number and inertial effects will be negligible. For the constant resistance method, values of R and L are determined using

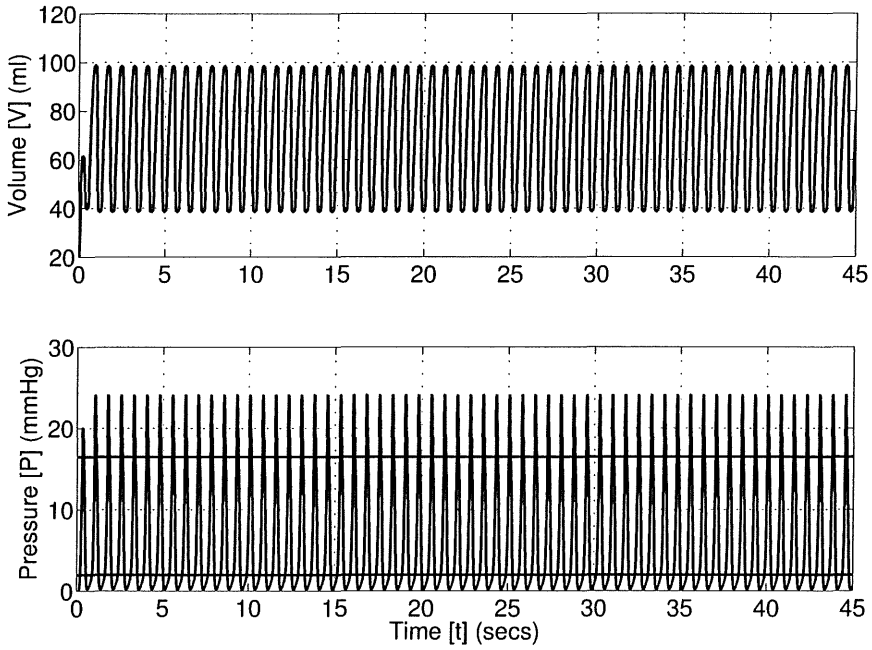

Figure 5.4 Volume and pressure outputs showing long term stability in the single chamber model with inertia.

Equation (3.8) and Equation (3.17) respectively. In both cases, making the inertial effects negligible means that there is now much less restriction on the rate of change of velocity and the velocity profile develops almost instantly to that defined by the Poiseuille solution [White, 1991].

Figure 5.5 shows the results of each method in a PV diagram. There is virtually no difference in performance between the two. This result verifies that the velocity profile method performs in the same way as the constant resistance method under very low inertia conditions, as expected, since density and consequently inertial effects, have been made negligible.

The models are simulated again with the density reset to a normal blood density of 1050kg/m^3, from Table 5.3. Figure 5.6 compares the resulting variations in pressure, volume and flow rates of the two models. Figure 5.7 plots the same simulation results as Figure 5.6 but in a PV diagram, more clearly highlighting the differences in model performance. The velocity profile method results in an approximately 17.5% decrease in stroke volume, and thus cardiac output, in comparison to the constant resistance and inertance case. This decrease is a significant change in the cardiac performance of the model, resulting from using the more physiologically accurate velocity profile method over the widely used constant resistance assumption.

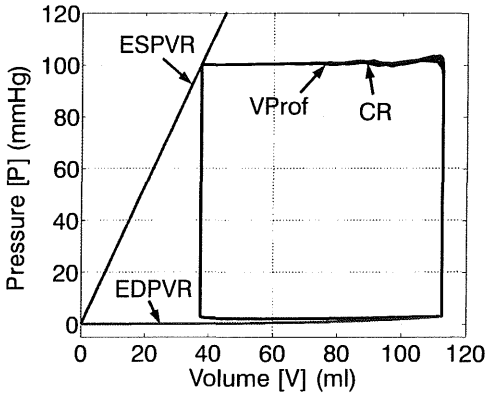

Figure 5.5 Velocity profile method (VProf) and constant resistance method (CR) results overlaid with inertial effects assumed to be negligible.

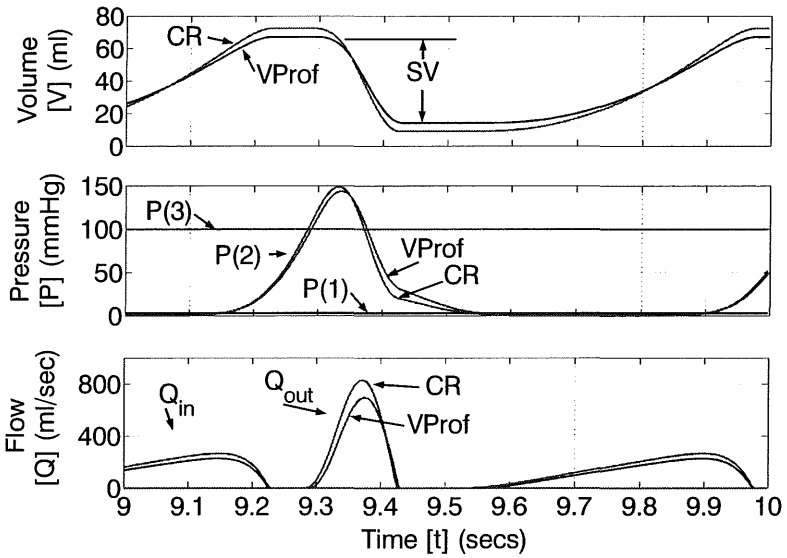

Figure 5.6 Velocity profile method (VProf) and constant resistance (CR) results overlaid with density = 1050kg/m^3.

The relative computational speed of the constant resistance method compared with the velocity profile tracking method was determined by measuring the computational time required for each method. When 100 nodes are used in the velocity profile method, it took 10 times longer to solve than the constant resistance method. When 20 nodes are used, the solution took twice as long to reach a steady state. Therefore, the increase in computational cost for the time varying resistance model is approximately the number of nodes divided by 10,

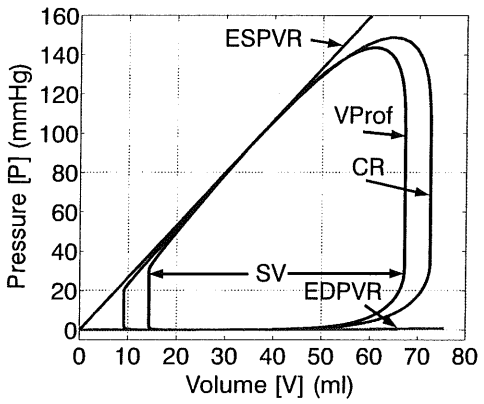

Figure 5.7 Velocity profile method results (VProf) overlaid on constant resistance results (CR) on a PV diagram.

times the solution time of the constant resistance method.

5.2 Two Chambers & Ventricular Interaction

Ventricular interaction in the proposed model results from both the pericardium and the septum. Septum and pericardium properties, used in the two chamber model from Figure 2.6 for this test, are taken from Chung et.al. (1997), as listed in Table 5.1. Figure 5.8 plots the variation in both the septum deflection volume (V_{spt}) and the pericardium volume (V_{pcd}) compared with the left and right ventricle volumes (V_{lv} and V_{rv}). In the case shown, the septal deflection oscillates by 2ml, or about 4% of the ventricle volume, roughly matching results found in the literature [Chung et al., 1997]. This result shows that septal interaction has a measurable impact on cardiac performance, matching clinical expectations.

5.3 Closed Loop Results, Physiological Verification

Full closed loop simulations of the model in Figure 2.1 add an additional four chambers, modelling the peripheral circulation system. Where the pressures upstream and downstream of the one and two chamber models have been assumed constant, these pressures will now vary in the closed loop model. The model should now be capable of simulating a variety of basic CVS trends in a physiologically accurate manner. This section investigates the outputs from the closed loop model, comparing results with known physiological trends. It is therefore testing

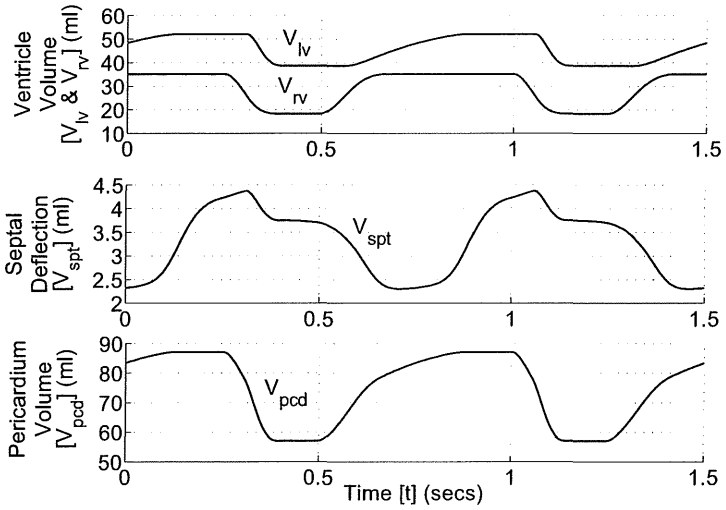

Figure 5.8 Comparing the variations in left and right ventricle volumes (V_{lv} and V_{rv}) with the septum deflection (V_{spt}) and the pericardium deflection (V_{pcd}).

the aggregation of elements tested individually in the one and two chamber model tests.

One of the key constraints in the closed loop model is that the total volume of the system must remain constant. If the total volume of the system varies over the course of a simulation, then the model is unstable. It was found that after long simulations over 100 seconds that the model maintained a constant volume of 1500ml, verifying the stability of the numerical procedure. Where previous tests proved the stability of the numerical procedure for simulating the single chamber model, this test proves the stability of the complete closed loop CVS model.

Figure 5.9 plots the left and right ventricle pressure and volume variations for the closed loop model after it has reached a steady state solution. This plot can be compared with the Wiggers diagram shown in Figure 5.10 [Guyton, 1991]. The model is seen to capture the major dynamics of the CVS including the variations in left ventricle pressure, aortic pressure and ventricle volume.

Since the ultimate goal is simulation of human heart function, particularly in response to changes in therapy, tests to validate simple trends are carried out comparing model outputs with known physiological trends. Figure 5.11 shows the effect of varying ventricle contractility, a measure of cardiac pump function [Maughan and Kass, 1988]. Contractility is varied in the model by changing the end systolic elastance (E_{es}) [Burkhoff and Tyberg, 1993]. Typically, an increase

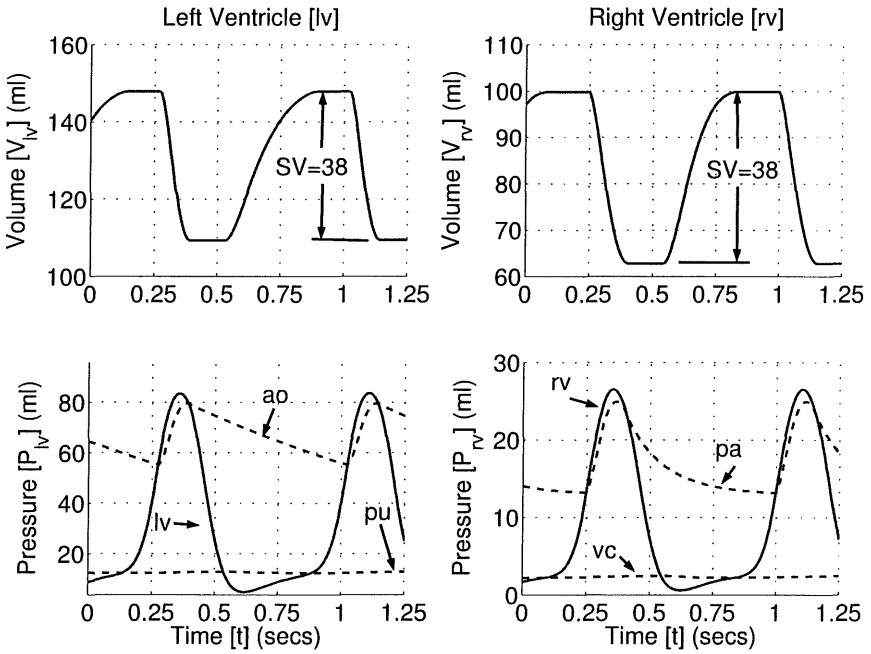

Figure 5.9 Simulation results from the closed loop model with inertia and ventricular interaction.

in contractility results in an increase in cardiac output which correlates with an increase in stroke volume (SV), assuming heart rate remains constant. Figure 5.11 plots a PV diagram for 3 different contractilities showing the desired increase in stroke volume as contractility increases.

A second test shows the effect of changing the systemic circulatory resistance. Readily available clinical data shows that an acute increase in resistance results in reduced cardiac output that varies with the magnitude of the change [Slinker and Glantz, 1989]. Figure 5.12 shows the closed loop model output, as systemic resistance is increased, and decreased. As systemic resistance decreases, stroke volume increases, meaning an increase in cardiac output. The opposite trend occurs as the resistance is increased. Figure 5.13 shows the rise in pressure in the aorta as a result of increased peripheral resistance and the resulting decreased cardiac output (CO), which illustrates the increase in blood pressure (BP) often seen in patients with narrowed or blocked arteries, and the resulting increased systemic resistance. Hence, both figures illustrate that the model captures well-known, basic clinical behaviour in response to changes in systemic resistance.

Finally, the average thoracic cavity pressure in humans is normally about -4mmHg, however if this pressure is increased, as occurs during positive pressure mechanical ventilation, cardiac output is decreased [Guyton, 1991]. Figure 5.14

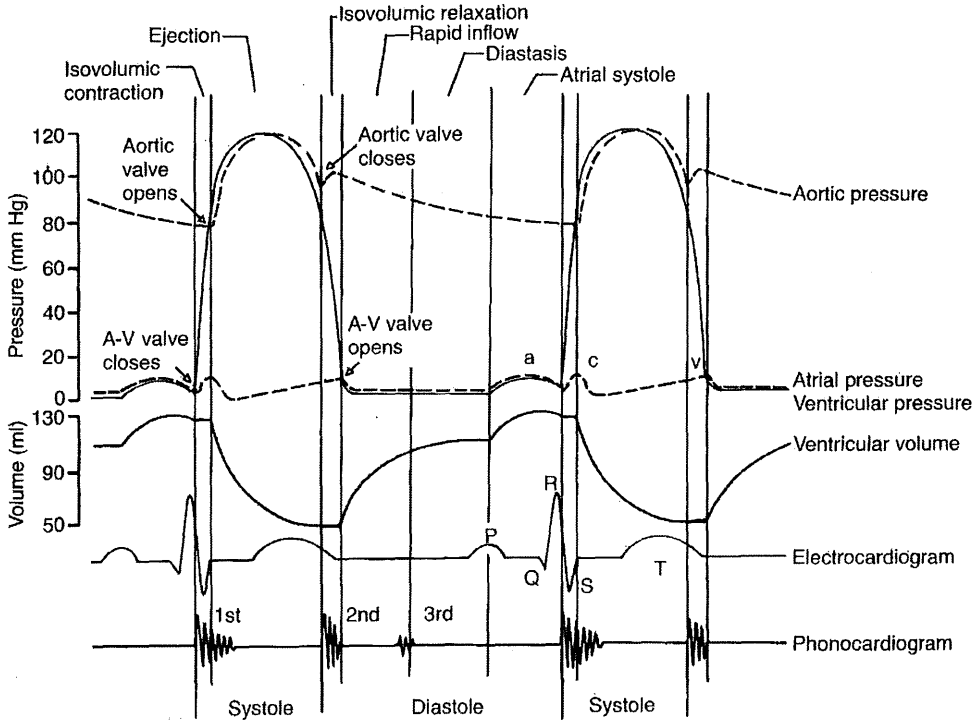

Figure 5.10 The Wiggers diagram showing pressure and volume variations in the left ventricle [Guyton, 1991].

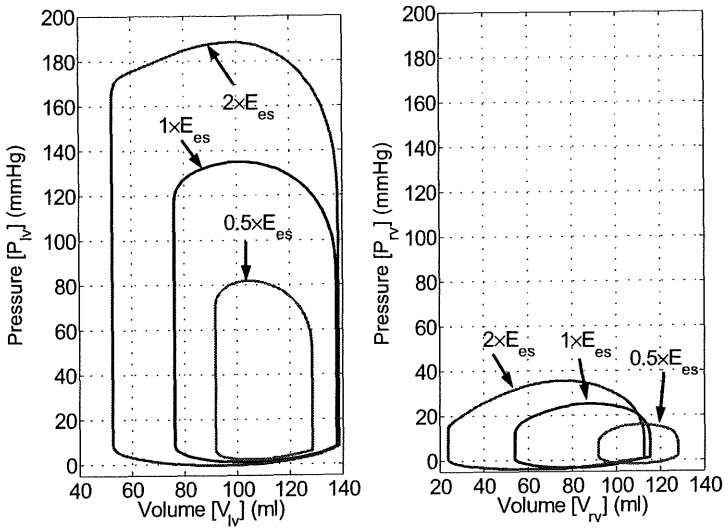

Figure 5.11 The effect of varying ventricular contractility.

shows the model output for both a normal (-4mmHg) and an increased (0mmHg) thoracic pressure where the stroke volume, and thus the cardiac output, is decreased by 9%. This decrease in cardiac output is in good agreement with readily

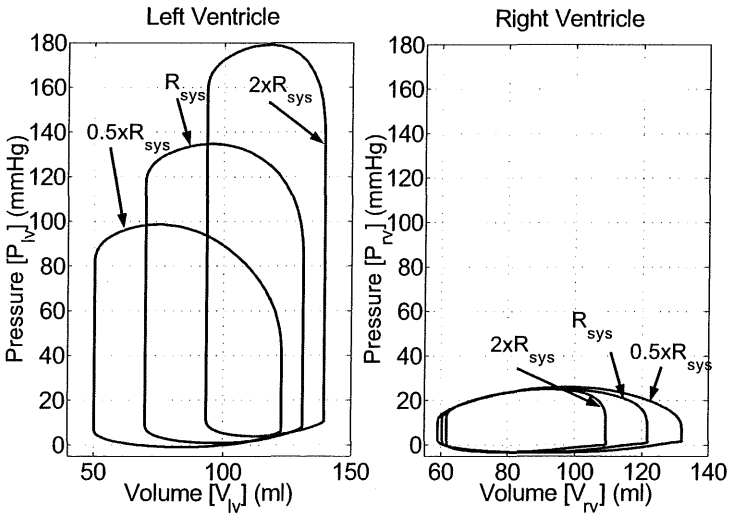

Figure 5.12 Simulation for changes in systemic resistance.

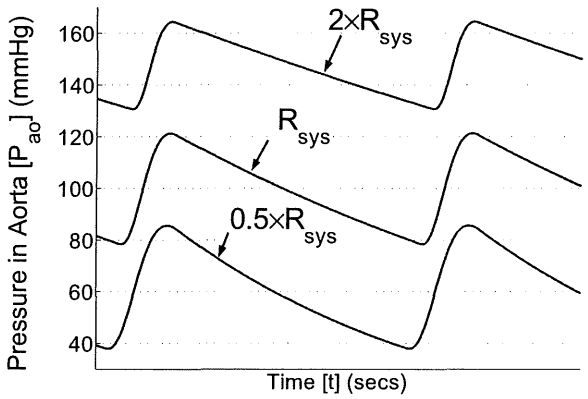

Figure 5.13 Response of aortic pressure to changes in systemic resistance.

available clinical data [Scharf and Cassidy, 1989]. The model is therefore capable of simulating the effect of this common intervention.

5.4 Summary

This chapter has shown the sequential testing and verification of the model from a single active cardiac chamber to a full closed loop model. The function of the cardiac chambers, the valves, inertial effects, time varying resistance, ventricular interaction, and finally, the closed loop model have been verified. The velocity profile method is presented as a more physiologically accurate method of tracking fluid flow in the large arteries and veins near the heart. A 17.5% difference

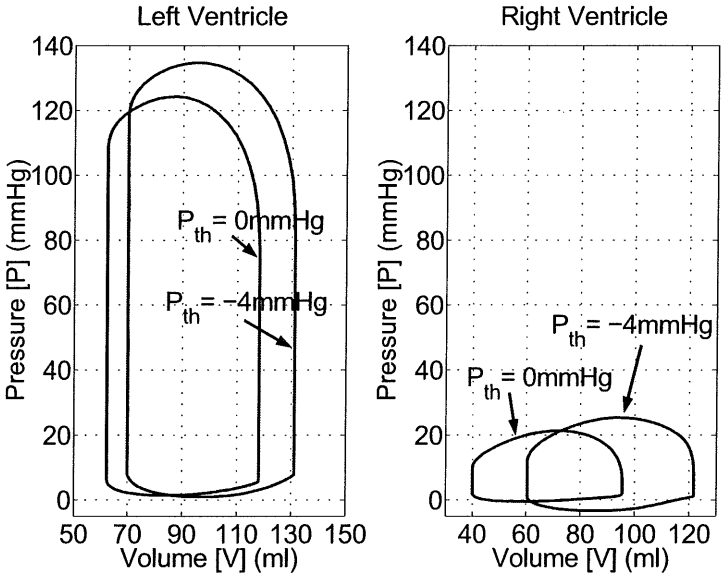

Figure 5.14 Change in stroke volume and PV diagram for a change in thoracic pressure.

in cardiac output for pulsatile flow in larger arteries is found, when comparing this method with the constant resistance method. This significant difference justifies the inclusion of the more physiologically accurate velocity profile tracking method.

The model is shown to be stable on both a component scale, tested using both a single and a two chamber model, and an overall scale, showing a constant total volume throughout simulation. The full closed loop model is simulated producing results that are seen to correlate well with well-known, fundamental physiological function and trends. The good agreement of these results with known clinical data shows the potential of this model in simulating trends in the cardiovascular system in response to physiological changes or intervention. However, even with the minimal model approach, there are still a large number of parameters in the model. This large number of patient specific parameters means the model is still too complex to adjust manually to produce patient specific models. An automated method of determining patient specific parameters is therefore required.

Chapter 6

Optimisation of Model Parameters

It has been shown that the model is capable of capturing major dynamics in the CVS. However, one of the key goals of this research is to model the dynamics of a specific patient. Therefore, the model must be capable of matching a specific patient's CVS dynamics. For example, the model should be equally able to simulate the magnitude of pressure variations in the aorta for a normal human of 120 over 80mmHg, or an abnormal pressure of 180 over 120 mmHg. The dynamics of the model are a function of the model parameters such as elastance and resistance. Thus, creating a model to match a specific patient involves adjusting the parameters until the model dynamics match the dynamics measured from a patient. This task is well suited to structured optimisation.

The complex interaction between the parameters means that it is impossible to manually adjust the model to produce target outputs. Instead, optimisation techniques are used to numerically adjust the parameters to meet target performance outputs. Before using the CVS model in conjunction with the optimisation routine, the implementation of the CVS model must be adjusted to suit the optimisation routine. Target performance dynamics must be identified and the model parameters to be adjusted by the optimisation routine must be defined in a numerically robust fashion, similar to non-dimensionalising variables, to avoid computational error.

This chapter first explains the optimisation routine used in this research. The target CVS model performance metrics are identified and suitable optimisation parameters are chosen. The modifications required to enable an optimisation routine to be used are discussed. In particular, a method of accelerating the model to a steady state solution, satisfying predefined convergence criteria, is outlined. Accelerating the model will significantly enhance the computation speed of the optimisation approach. Finally, the steps used to find a steady state

solution to the CVS model as quickly as possible, while maintaining robustness, are described.

6.1 The Optimisation Routine

A particular feature of this optimisation problem is that the optimisation routine must be able to deal with imprecise function evaluations. Although the CVS model will converge to only one unique solution for a particular set of parameters, finding this solution to a high level of accuracy can take considerable time for some parameter and IC combinations. However, it is not desirable to use excessive computational time to find an accurate CVS model solution and less accurate results must be used. The optimisation routine must therefore be capable of dealing with the imprecise values that result from error in the CVS model solutions.

Inaccurate solutions will be particularly important as the optimisation routine converges to a steady state solution. Initially, the optimisation routine will make large steps which will cause significant changes in model dynamics. However, as the routine converges the amount the model parameters are adjusted, and the resulting variations in CVS model dynamics, will significantly decrease. Eventually, inaccuracies in the CVS model solutions will become significant compared to the magnitude of variations in the model outputs at each optimisation step. At this point the optimisation routine will be unable to converge further.

It was found that the standard MATLAB nonlinear least squares optimisation routine performed badly when optimising the CVS model parameters. The reason for this poor performance is unclear, but a combination of noisy function values and a lack of direct control over step size appeared to contribute. The optimisation routine used is a derivative-free, trust-region, Gauss-Newton method for nonlinear least squares problems. This optimisation routine is specifically designed for imprecise function evaluations, using a trust-region method of constraining the step size of each iteration [Conn et al., 2000]. The optimisation routine was designed and written by Dr Ian Coope from the mathematics department at the University of Canterbury.

Table 6.1 lists the optimisation parameters used in this research. Note that although a target precision of 1 would achieve an acceptable error of 1%, a target precision of 10^{-3} is used. This target precision is set significantly higher than required in order to test the capabilities of the optimisation routine.

Optimisation Parameter	Value
Target precision	10^{-3}
Initial finite difference step size	5×10^{-2}
Maximum number of iterations	22
Initial trust-region size	0.1

Table 6.1 Values of optimisation routine parameters.

The optimisation routine treats the CVS model as a black box, with no specific adaptations for this model. The basic function of the routine is to adjust an array of positive optimisation variables ($\underline{v}$) to minimise the sum of all the terms in an array of squared objective functions ($\underline{F}$).

$$\min \quad \underline{F}(\underline{v}) = \min \quad \sum_{k=1}^{n} F_k^2(\underline{v}) \quad \text{subject to} \quad \underline{v} > 0 \tag{6.1}$$

where k corresponds to a particular objective function and n is the number of objective functions to be optimised. The optimisation variables can correspond to any of the model parameters such as elastances, resistances and/or contractilities. The objective function array represents a selection of model outputs such as volumes, pressures and flow rates to be matched to patient data. This section discusses the choice of model parameters and objective functions used in the optimisation routine to create patient specific models.

Figure 6.1 schematically shows the optimisation routine solution process as a flow chart where i represents the optimisation sample step number. Model parameters ($\underline{p}$) are calculated from optimisation variables ($\underline{v}$) and passed to the CVS model. The CVS model is then simulated to a steady state solution and model function values ($\underline{M}$) calculated. From these model function values an objective function array ($\underline{F}$) is created. The objective function array is passed to the optimisation routine which determines new optimisation variables ($\underline{v}$). If the optimisation routine has converged, then final model parameters are output ($\underline{p}(f)$). This section covers each of these steps in detail outlining how the optimisation routine is used to find model parameters enabling the CVS model to achieve target performance dynamics.

6.1.1 Optimisation Variables

The optimisation variable array ($\underline{v}$) is an array of multiplying factors corresponding to an array of model parameters ($\underline{p}$) that the optimisation routine adjusts to

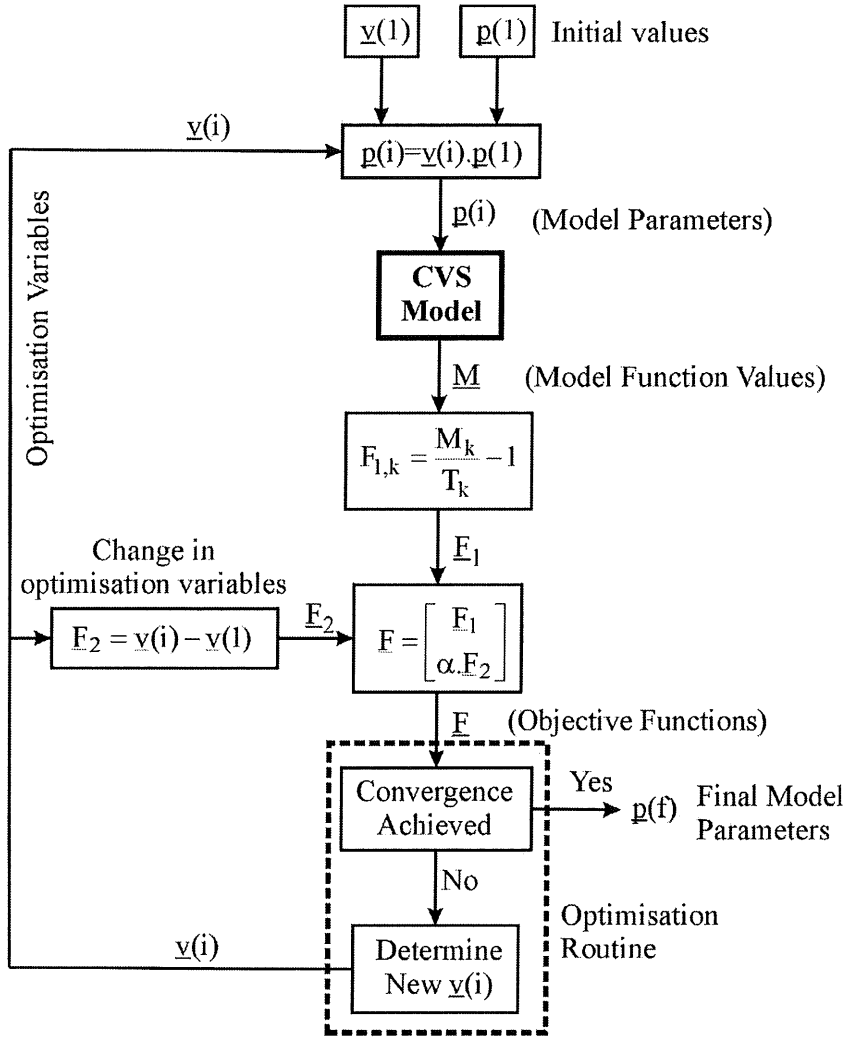

Figure 6.1 Flow chart showing the sequential steps of the optimisation routine.

minimise the objective function ($\underline{F}$). More specifically, the parameter values ($\underline{p}$) are not adjusted directly, but through a multiplying factor ($\underline{v}$) that scales them. Although any of the CVS model parameters can be used, selecting appropriate parameters is important. If too few parameters are chosen, the optimisation may not be able to minimise the entire objective function array, or the results may not be meaningful. Conversely, selecting too many parameters will mean unnecessarily large computational times for the optimisation routine and potentially conflicting non-unique solutions.

Table 6.2 lists the 12 model parameters used for this research. Therefore, the model parameters array is defined:

$$\underline{p} = [E_{vc},\ P_{0,lvf},\ E_{pa},\ E_{pu},\ P_{0,rvf},\ E_{ao},\ R_{tc},\ R_{pv},\ R_{pul},\ R_{mt},\ldots \\ R_{av},\ R_{sys},\ E_{es,lvf},\ E_{es,rvf}]^T \tag{6.2}$$

The base values of the model parameters ($\underline{p}(1)$) are manually determined as the non-dimensional form of those defined in Tables 5.1 and 5.2. All of the initial optimisation variables ($\underline{v}(1)$) are set to one. As Figure 6.1 shows, at each step of the optimisation routine, the CVS model parameters are redefined as the product of the optimisation variables and the base model parameters.

$$\underline{p}(i) = \underline{p}(1).\underline{v}(i) \tag{6.3}$$

where i corresponds to the optimisation solution step number and $\underline{p}(i)$ defines the CVS model parameters used at step i. This approach ensures that the optimisation variables have similar magnitudes, for computational and numerical simplicity. These model parameters are then passed to the CVS model.

Description	Symbol
Elastance of Vena-cava	E_{vc}
Elastance of Left Ventricle	$P_{0,lvf}$
Elastance of Pulmonary Artery	E_{pa}
Elastance of Pulmonary Vein	E_{pu}
Elastance of Right Ventricle	$P_{0,rvf}$
Elastance of Aorta	E_{ao}
Resistance of Tricuspid Valve	R_{tc}
Resistance of Pulmonary Valve	R_{pv}
Resistance of Pulmonary Circulation	R_{pul}
Resistance of Mitral Valve	R_{mt}
Resistance of Aortic Valve	R_{av}
Resistance of Systemic Circulation	R_{sys}
Contractility of Left Ventricle	$E_{es,lvf}$
Contractility of Right Ventricle	$E_{es,rvf}$

Table 6.2 Model Parameters to be optimised.

6.1.2 The Objective Function Array

The objective function array ($\underline{F}$) is a vector of function values to be minimised. It consists of two parts, an array of functions for target performance ($\underline{F}_1$) and

an array corresponding to the amount that the optimisation variables have been adjusted ($\underline{F}_2$). The second array ($\underline{F}_2$) is used to constrain the model parameters to their initial values unless it is necessary to adjust them. This ensures that all of the optimisation variables are constrained, even if they don't affect the target performance values. Figure 6.1 shows how the $\underline{F}_1$ and $\underline{F}_2$ matrices are combined to create an array of objective functions $\underline{F}$.

The Target Performance Metrics

Each function value in the $\underline{F}_1$ array corresponds to a target performance metric determined from the CVS model. Examples of possible performance metrics include the maximum, minimum, average or amplitude of variation of measurements such as pressure and volume over one heartbeat cycle. When the model achieves a steady state solution, the required performance metrics are calculated and returned to the optimisation routine as an array of model function values ($\underline{M}$). The objective function array is then calculated as the relative difference between the target function values ($\underline{T}$) and the corresponding model function values.

$$F_{1,k} = \frac{M_k}{T_k} - 1 \qquad \text{for all } k=1 \rightarrow n \tag{6.4}$$

where k is the position of the function value in the function array and n is the number of function values in the function array. Using Equation (6.4), the relative ratio of each model function value to it's corresponding target function value is determined.

As an example, suppose the target function values include the maximum pressure in the aorta of 120mmHg and the minimum pressure of 80mmHg. Suppose that for a given set of model parameters ($\underline{p}$) the model function values for the pressure in the aorta are a maximum of 180mmHg and a minimum of 110mmHg. The model parameters must be adjusted so that the model function values match the target function values. For this example, there are 2 function values (n=2) where $\underline{T}=[120,80]^T$ and $\underline{M}=[180,110]^T$. Using Equation (6.4) the objective function array is then calculated:

$$\underline{\mathbf{F_1}} = \begin{bmatrix} (180/120) - 1 \\ (110/80) - 1 \end{bmatrix} = \begin{bmatrix} 0.5 \\ 0.375 \end{bmatrix} \tag{6.5}$$

Note that the relative ratio and not the absolute difference is used, normalising the objective function matrix and giving each term equal weighting. Normalising the objective function matrix is important as the matrix contains both pressures and volumes which will be of very different magnitude.

The following data for an average human is taken from Guyton (1991). The pressure entering the left ventricle through the pulmonary vein is typically about 2mmHg. The left ventricle pumps blood into the aorta where the pressure cycles between a maximum value of 120mmHg during systole and a minimum value of 80mmHg during diastole. Blood returning from the systemic circulation drops to approximately 0mmHg in the vena-cava just before entering the right atrium. However, this pressure is measured inside the thoracic cavity, where there is an average pressure of -4mmHg. The location of the vena-cava chamber in the presented model is outside the thoracic cavity meaning the target pressure for the model vena-cava is set to 2mmHg. The right ventricle pumps the blood into the pulmonary artery where the pressure cycles between 25mmHg at systole and 8mmHg at diastole. Finally, on average, both ventricle volumes cycle between a maximum value of 115ml and a minimum value of 45ml. Hence, there are a total of ten maximum, minimum and average target pressure and volume metrics, as listed in Table 6.3.

Variable	**Target Output (max/min or avg)**
Aortic Pressure	P_{ao}=120/80mmHg
Pulmonary Artery Pressure	P_{pa}=25/8mmHg
Pulmonary Vein Pressure	P_{pu}= 2mmHg
Vena-cava Pressure	P_{vc}= 2mmHg
Left Ventricle Volume	V_{lv}= 115/45ml
Right Ventricle Volume	V_{rv}= 115/45ml

Table 6.3 Target Model Outputs from Guyton 1991.

The maximum and minimum values of the target model outputs can be used as the target performance metrics as shown in the previous example. However, manual testing of individual CVS model parameters reveals a more suitable relationship between model parameters and the average and amplitude of the model output dynamics. More specifically, the amplitude of the pressure in the aorta was found to be significantly dependent on the elastance of the aorta (E_{ao}), and the average aortic pressure is dependent on the systemic resistance (R_{sys}). Table 6.4 shows the ten target performance metrics used in the optimisation that correspond to the maximum and minimum values for a healthy human in Table 6.3.

Variable	Average	Amplitude
Aortic Pressure	Avg P_{ao}=100mmHg	Amp P_{ao}=40mmHg
Pulmonary Artery Pressure	Avg P_{pa}=16.5mmHg	Amp P_{pa}=17mmHg
Pulmonary Vein Pressure	Avg P_{pu}=2mmHg	
Vena-cava Pressure	Avg P_{vc}=2mmHg	
Left Ventricle Volume	Avg V_{lv}=80ml	Amp V_{lv}=70ml
Right Ventricle Volume	Avg V_{rv}=80ml	Amp V_{rv}=70ml

Table 6.4 Target Model Outputs as averages and amplitudes from Guyton 1991.

The model outputs listed in Table 6.4 are calculated after a steady state CVS model solution is found and grouped into a model function values array ($\underline{M}$):

$$\begin{aligned}\underline{M} = [&\text{Amp } P_{ao}, \text{ Avg } P_{ao}, \text{ Amp } P_{pa}, \text{ Avg } P_{pa}, \text{ Amp } V_{lv}, \ldots \\ &\text{Avg } V_{lv}, \text{ Amp } V_{rv}, \text{ Avg } V_{rv}, \text{ Avg } P_{pu}, \text{ Avg } P_{vc}]^T\end{aligned} \tag{6.6}$$

These values represent the performance of the steady state CVS model after transients from the initial conditions have damped out. Using Equation (6.4) and the target function values defined in Table 6.4, the objective function $\underline{F}_1$ is defined:

$$\underline{\mathbf{F}}_1 = \begin{bmatrix} (\text{Amp } P_{ao}/40) - 1 \\ (\text{Avg } P_{ao}/100) - 1 \\ (\text{Amp } P_{pa}/16.5) - 1 \\ (\text{Avg } P_{pa}/17) - 1 \\ (\text{Amp } V_{lv}/70) - 1 \\ (\text{Avg } V_{lv}/80) - 1 \\ (\text{Amp } V_{rv}/70) - 1 \\ (\text{Avg } V_{rv}/80) - 1 \\ (\text{Avg } P_{pu}/2) - 1 \\ (\text{Avg } P_{vc}/2) - 1 \end{bmatrix} \tag{6.7}$$

Therefore, the goal of the optimisation routine is to drive Equation (6.7) to zero.

The array of objective functions in Equation (6.7) can be adjusted in size depending on what patient specific information is available. However, this combination of model parameters from Equation (6.2) and objective functions from Equation (6.7) do not guarantee a unique solution. Some of the model parame-

ters may not affect any of the chosen objective functions and may be able to take any value. This will result in unnecessarily extended computational time and non-unique solutions. To avoid this problem, additional criteria must be added to the objective function array to fully constrain the model.

Minimising Parameter Adjustment

The number of objective functions available when attempting to create a patient specific model depends on the amount of patient specific information available. Often there is only limited information available as some CVS performance metrics are difficult, expensive or time consuming to measure. The result of not having enough objective functions will be an under-determined system where the number of objective functions is less than the number of optimisation variables. To ensure a more tractable, over-defined problem, an additional array ($\underline{F}_2$) is added to the objective function array representing the amount that the optimisation variables have been adjusted. As shown in Figure 6.1, this additional array of objective function values is calculated from the optimisation variables.

$$\underline{F}_2(i) = \underline{v}(i) - \underline{v}(1) \tag{6.8}$$

where i represents the optimisation solution step number and $\underline{v}(1)$ represents the initial optimisation variable values, which in this case are all unity. Setting these values to unity means the initial model parameters used in the optimisation are the base model parameters ($\underline{p}(1)$).

The $\underline{F}_2$ array is combined with the $\underline{F}_1$ array to form an augmented objective function array:

$$\underline{\mathbf{F}} = \begin{bmatrix} \underline{F}_1 \\ \alpha.\underline{F}_2 \end{bmatrix} \tag{6.9}$$

where α is a positive weighting factor determining the relative weighting of the $\underline{F}_2$ array in the objective function. With this definition of the objective function array, all the optimisation variables are now constrained regardless of which objective functions are chosen.

This weighting factor (α) is set to 10^{-3} giving more weighting to matching target performance metrics than minimising the amount that optimisation variables are adjusted. However, this magnitude of α is large enough to ensure that

only model parameters that significantly influence the target performance metrics will be adjusted. Hence, even if a large number of parameters are available for the optimisation routine to adjust, the parameters that most significantly affect the target performance metrics will be emphasised. Note that the value of α can be varied to obtain different results depending on how much the optimisation variables need to be adjusted.

This optimisation approach can be compared with the original aim of developing patient specific models to assist medical staff in patient diagnosis. By determining patient specific model parameters, the optimisation routine will highlight areas of the CVS that could contribute to any noted abnormalities. For example, suppose the optimisation routine significantly decreases the ventricle contractility of the left ventricle ($E_{es,lvf}$) in order to match a specific patient CVS function. This result would indicate to medical staff that the patient could potentially be suffering from a "floppy" heart. Thus, the optimisation presented can be used as a tool for assisting medical staff in analysing large amounts of patient data and pinpointing the source of dysfunction.

6.2 Restructuring the CVS Model for Optimisation

Modifications to the CVS model are required so that the optimisation routine can be effectively implemented. The computational time taken for the CVS model to find a steady state solution becomes an important factor in optimisation that must be minimised. In addition, solution errors must not stop the optimisation routine from converging, but instead discourage it from using a particular combination of parameters that produce erroneous results. Errors in CVS simulations resulting from inadequate parameters must be captured without compromising the optimisation routine.

For each iteration of the optimisation routine, the gradient of the objective function is first determined with respect to each of the optimisation variables to construct a Jacobian matrix. The Jacobian matrix is then used to determine a suitable iteration step size, adjusting all of the optimisation variables. Every parametric solution made by the optimisation routine requires the model to run to a steady state solution. Therefore, the time taken to find a steady state solution contributes significantly to the overall time required for the optimisation routine to find a solution.

The simplest method of finding a steady state solution is to run the CVS

model until predefined convergence conditions are satisfied and is referred to as the continuous simulation method. Typically, the model takes on the order of 20-50 heart beats to reach a steady state solution using this method. The number of heart beats required depends on the accuracy of the initial conditions, parameter values, and other factors. However, some sets of parameters can take more than 100 heart beats to reach a steady state solution, taking roughly 10 minutes of computational time. Given that the optimisation routine can take on the order of 50-300 CVS model simulations to reach a solution, a 10 minute computation time per solution is unacceptable, for a near real-time application. Note that these computation times are for un-optimised Matlab code and would be significantly shorter with optimised code.

This section investigates modifications made to the CVS model to adapt it for optimisation with fast solution times and minimal errors. A gradient estimation method is proposed that converges much more quickly to a steady state solution than the continuous simulation method of simply running the model to a steady state solution. The convergence criteria are specified, defining the requirements for a steady state solution. Error checking methods are outlined to identify erroneous results before they influence the overall optimisation routine. Finally, the steps taken to reach a steady state CVS model solution are laid out, combining gradient estimation with continuous simulation and error checking.

6.2.1 Gradient Estimation

As explained previously, the time taken to find a solution becomes very important when the model is simulated repeatedly using an optimisation routine. The model can take up to 10 minutes to find a solution using the continuous simulation method, particularly if one of the elastances is significantly lower than the others, a condition that would be desirable to identify. For this reason, a gradient estimation technique is employed. The gradient estimation technique involves running the model for a small number of heart beats and determining a linear approximation of the volume profile. Using a combination of linear approximations from different initial conditions, an estimation of the steady state solution can be found in significantly fewer cycles than required for continuous simulation.

Linear Approximations

Linear approximations give a straight line through the cycles in chamber volumes, estimating the gradient of the average volume over a series of cycles. A linear approximation requires the gradient and volume at time zero to be determined yielding a straight line representing the average chamber volume as a function of time. To obtain a linear approximation, the gradient of a given number of cycles is estimated.

Figure 6.2 shows a linear approximation example where the gradient of the last 3 heart beats of a 10 heart beat run is measured. The plot shows a series of lines connecting points on the last cycle and the equivalent points 3 heart beats back in time. Each of these lines is averaged to give an approximation of the gradient and volume at time zero for the last 3 heart beats. Using the combination of the gradient and the volume at time zero, a linear approximation can be constructed, as shown in Figure 6.2 (dashed line).

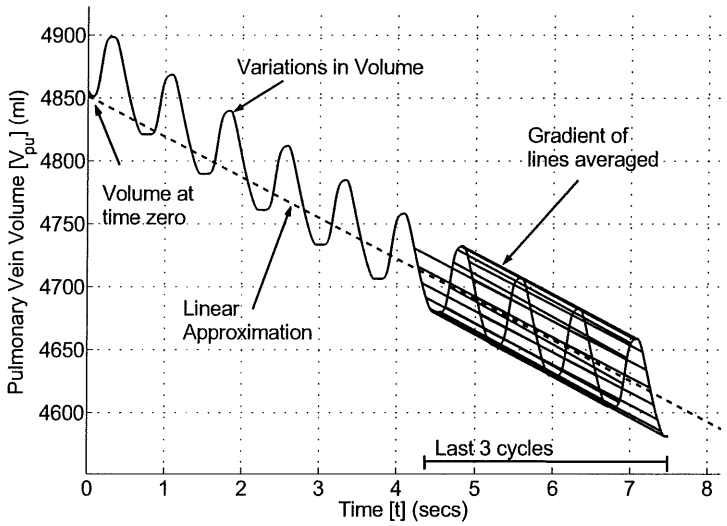

Figure 6.2 Diagram showing technique for making a linear approximation of the gradient of the pulmonary vein volume.

Steps to Gradient Estimation

Figure 6.3 is used to illustrate the gradient estimation method with the steady state solution for one volume variable in the state vector. Gradient estimation is carried out simultaneously for all of the volumes in the state vector. The initial condition used by the gradient estimation method is labelled $x_0(1)$. Using this

initial condition, the gradient estimation technique involves running the following steps until predefined convergence criteria are satisfied in step 2.

1. The simulation is run for 10 cycles to allow fluctuations from the initial conditions to settle out. A linear approximation of the last 3 heart beats of the 10 heart beat run is then determined, labelled x_0(1a) on Figure 6.3, for each volume in the state vector.

2. The gradient of this linear approximation is used to test if results satisfy predefined convergence criteria. If convergence has occurred, then gradient estimation is stopped, otherwise the following steps are carried out.

3. Using the linear approximation, the volume after 100 seconds is determined, labelled the reflection point on Figure 6.3.

4. A new set of initial conditions are determined that are reflected around the value at 100 seconds, labelled x_0(1b) on Figure 6.3. However, since the total volume of the system must remain constant, all volumes are scaled so that the total volume is maintained at 1500ml.

5. From this new set of initial conditions the model is run again for 10 seconds and another linear approximation is determined, labelled x_0(1c) on Figure 6.3.

6. The intercept of the two linear approximations, labeled x_0(1d) on Figure 6.3, is used as an estimate of the steady state solution for each volume. Once again the value of x_0(1d) is scaled for all volumes so that the total model volume equals 1500ml. Scaling produces a new set of initial conditions that are hopefully much closer to the steady state solutions for each volume. The new initial condition for this volume is labelled x_0(2) on Figure 6.3.

Gradient estimation fails if, after 2 gradient estimation steps, the gradient is diverging. Typically gradient estimation will find a solution within 3 gradient estimation steps, so if no solution is found after 5 steps the gradient estimation is assumed to have failed.

6.2.2 Convergence

Convergence criteria define the conditions the CVS model must satisfy before convergence is assumed to have been achieved and results can be fed back to the

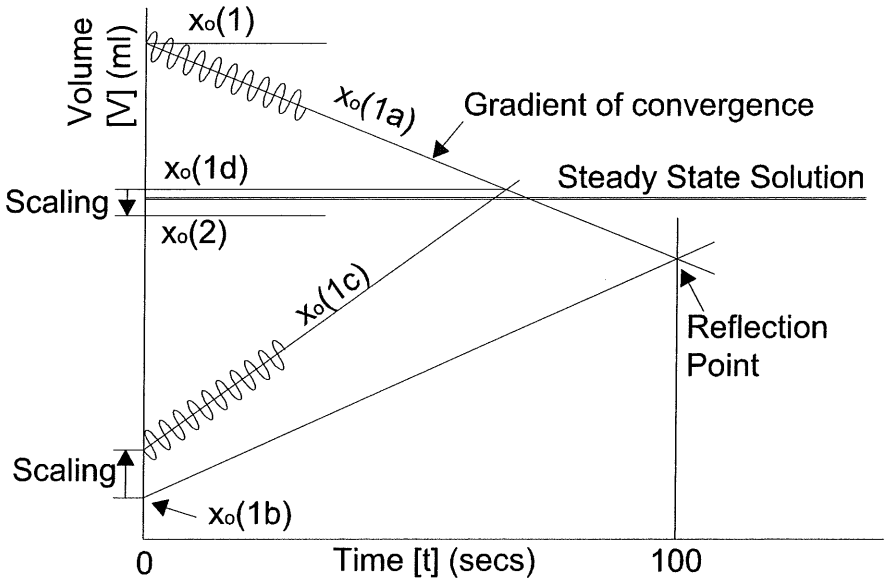

Figure 6.3 Diagram illustrating on iteration of the gradient estimation method.

optimisation routine. The convergence criteria used are based on the gradient of convergence of each volume in the state vector. The gradient of each separate volume is determined using the linear approximation method presented, and as illustrated in Figure 6.3. The model is assumed to have converged when the maximum gradient of convergence of all the volumes is less than 0.01. This value was chosen because, while gradient estimation converged quickly, it could not achieve a gradient of much less than 0.01. At this lower limit the linear approximation method of determining the gradient is too inaccurate, limiting the capability of the gradient estimation method. The approximate limit of the gradient estimation method occurs for each volume when the difference between the projected average value after 100 seconds and the initial condition is less than the amplitude of oscillation of the variable.

The gradient of convergence is calculated for each volume profile using the linear approximation method, as shown in Figure 6.2. If the convergence gradient is too high, subsequent simulations with very similar parameters may produce significantly different results. Effectively, the solution will be too inaccurate, which will cause problems for the optimisation routine, as discussed previously. Setting the convergence gradient threshold too low means the model will require considerably longer to converge. It was found that while gradient estimation converged quickly, it could not achieve a gradient of much less than 0.01. Therefore, in order to achieve more accurate solutions, the model would have to switch to continuous

simulation, which adds to the computational time.

6.2.3 Checking for Corrupt Results

In some cases, the model is unable to find a solution for a set of parameters, implying that the function values are erroneous. After each simulation using the ODE solver, the model checks for erroneous results. Erroneous results occur when either the ODE solver generates an error, or the heart does not start pumping after a period of simulation.

Errors in the ODE solver can potentially stop the entire optimisation routine. To avoid this result, the software checks Matlab's list of previous errors to see if any occurred during the solving process after the completion of each ODE solution. If errors have occurred, then the results are assumed to be erroneous. Erroneous results can also occur if the heart is not pumping blood, but the convergence criteria are satisfied. To avoid this result, if the stroke volume in any of the chambers is zero after an ODE solution, then the solution is assumed erroneous. The response of the model, if erroneous results are found, depends on what stage of the solving process is being attempted.

6.2.4 Finding a Steady State CVS Model Solution

Each time the CVS model is simulated the model first attempts to find a solution using initial conditions determined from the final state vector of the previous model simulation. The flow chart in Figure 6.4 is used to explain the steps made in the CVS model to find a solution. This flow chart is contained within the CVS model box in Figure 6.1. The following steps are tried consecutively until any one of the steps achieves convergence.

1. The gradient estimation method is used, starting with the loaded initial conditions, to attempt to find a steady state solution.

2. If gradient estimation fails with loaded initial conditions, then new initial conditions are calculated as explained in Chapter 4 and gradient estimation is re-attempted.

3. If gradient estimation fails with new initial conditions, then continuous simulation is attempted for up to 100 seconds of heart beats.

4. If continuous simulation fails to find a solution, but testing shows that the heart is beating and that no errors have occurred, then the results after 100 seconds of heart beats are fed back to the optimisation routine.

These steps are carried out at each solution step of the optimisation routine. Failure at any one of these steps can be due to lack of convergence, or erroneous results. If results of the final continuous simulation test are found to be erroneous the solution of the ODE solver is ignored. Instead, all the function values in the function array are set to 10^4. By setting the function values to this large number, the optimisation routine is discouraged from searching for a solution near the parameters in question. Therefore, optimisation can be continued even when errors in the model occur, resulting in a very robust routine. The significant majority of simulations were found to achieve convergence after step 1.

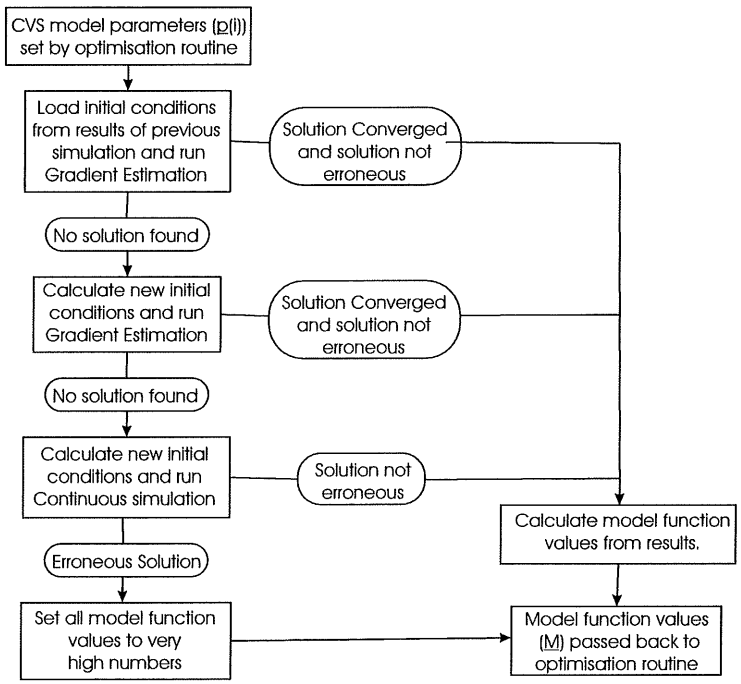

Figure 6.4 Steps taken by CVS model to find steady state solution.

6.3 Summary

This chapter introduced an optimisation process for producing patient specific models. Modifications to the implementation of the CVS model were required

to produce accurate steady state simulations of the model dynamics in minimal time. The continuous simulation technique is the most robust method of finding a steady state solution, however it takes the most computational time. An alternative method is proposed for estimating the steady state solution based on linear approximations of very short simulations. A method for capturing erroneous CVS model results before they influence the optimisation is explained. Finally, the steps taken to find a steady state CVS model solution as quickly as possible are outlined.

The selection of target performance metrics for the optimisation routine to adjust are outlined. Any parameters in the CVS model can be used, as the optimisation routine will only adjust parameters that are required to meet the target performance metrics. Any number of target performance metrics can be used depending on what patient data is available. However, the more target performance metrics that are available, the more accurately the optimisation routine will be able to create a patient specific model. The optimisation routine in this form will create patient specific models to assist medical staff in interpreting a wide range of patient data. The next chapter examines the results of using this optimisation approach.

Chapter 7

Optimisation Results

This chapter investigates the results of the optimisation routine presented in Chapter 6. The relative performance of the gradient estimation method compared with the continuous simulation method is investigated. Results from applying the optimisation routine to the CVS model are then presented. The results of this chapter indicate the potential of the optimisation routine combined with the CVS model in achieving the specified aims of this research. Specifically, to create a patient specific model capable of producing results to assist medical staff in diagnosis and therapy selection in "clinical real time".

7.1 Convergence

For the majority of simulations, the CVS model converges in about 30 seconds, although a worst case of up to 10 minutes can occur occasionally, as discussed in Chapter 6. Thus, the computational time taken by the optimisation routine per sample step is approximately 30 seconds. Figure 7.1 plots the variation in volume of the 4 peripheral chambers for a continuous simulation run until results satisfied the defined convergence criteria. Each different volume variable converges to its own steady state solution in typically less than 10-30 heart beats. For these short solution times, the gradient estimation method takes roughly the same computational time as the continuous simulation method. However, some simulations can take much longer to converge to a steady state solution and the modified approach is required.

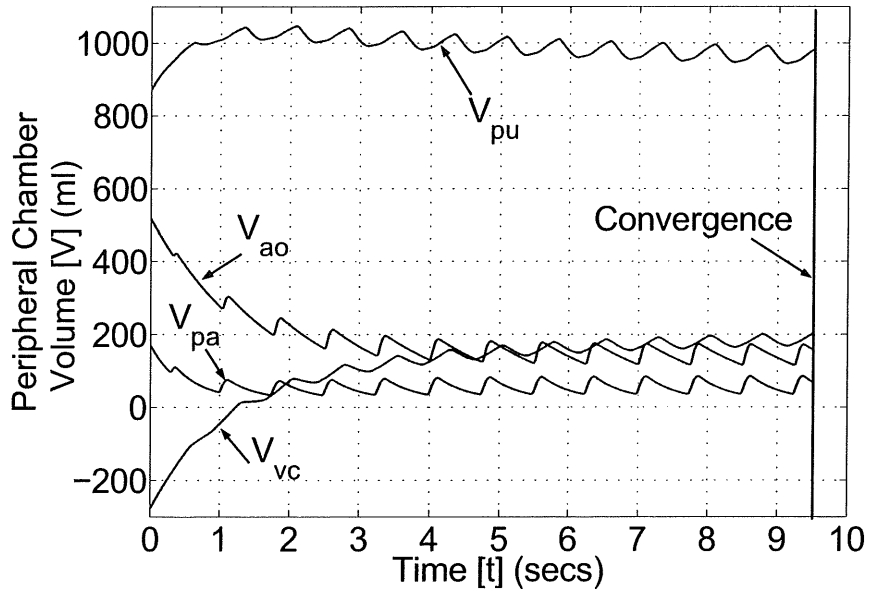

Figure 7.1 Peripheral chamber volume profiles resulting from continuous simulation to convergence.

7.1.1 Continuous Simulation

Figure 7.2 illustrates the variation in pulmonary vein volume, which is 1 of the 4 volumes plotted in Figure 7.1. Two continuous simulations are run for 150 seconds of heart beats at 80 beats per minute. The CVS model parameters used to create this simulation were a special case requiring long computational time to settle to a steady state solution. The rate of convergence of the case shown in Figure 7.2 is seen to be much slower than that shown in Figure 7.1. These special cases occur sporadically during optimisation and can considerably slow the optimisation routine. Table 7.1 shows that the simulation requires at least 80 heart beats before convergence is achieved, requiring 6 times the computational effort of the majority of solutions.

7.1.2 Gradient Estimation

Figure 7.3 shows results using the same model parameters and initial conditions used to generate Figure 7.2, but using gradient estimation instead of continuous simulation. The results are overlaid on the continuous simulation of Figure 7.2, plotted in light gray for comparison. The linear approximation lines explained in Figure 6.3 are illustrated in the simulation results of Figure 7.3. Graphically, it can be seen that one iteration of gradient estimation produces initial conditions

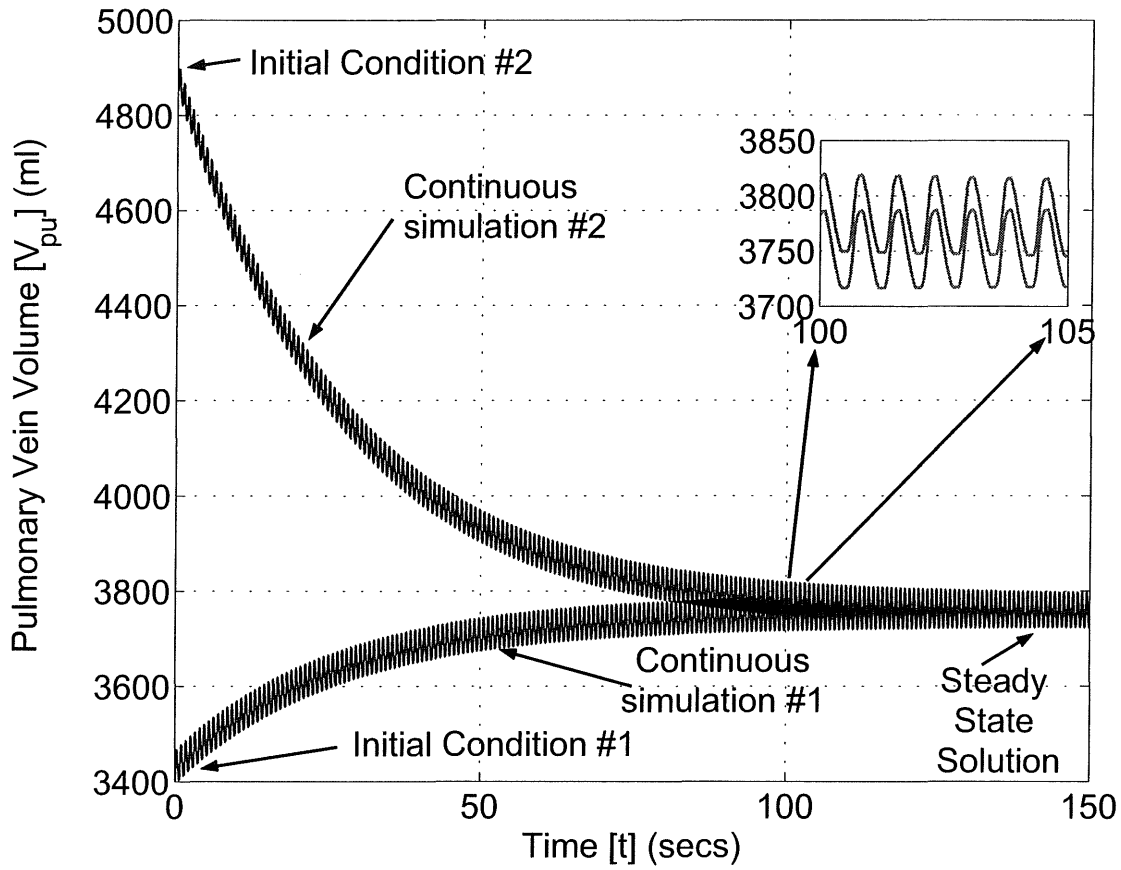

Figure 7.2 Plot of pulmonary volume converging to steady state solution from different initial conditions.

that are much closer to the steady state solution.

A steady state solution was found using gradient estimation after 2 iterations of the gradient estimation technique, requiring 50 heart beats. Table 7.1 compares the performance of the continuous convergence method against the gradient estimation method simulated from two different initial conditions. Both the computational time taken to find a steady state solution and the number of heart beats simulated are listed. In general, the computational time is dependent on a number of factors such as how often the gradient of convergence is determined. The number of heart beats to solution is a more accurate method of comparing the performance of the two methods as it is independent of these factors. For the special case shown in Table 7.1, the gradient estimation method typically requires 50-55% of the heart beats used for continuous simulation to find a steady state solution.

Thus, it is shown that in some cases significant decreases in computational

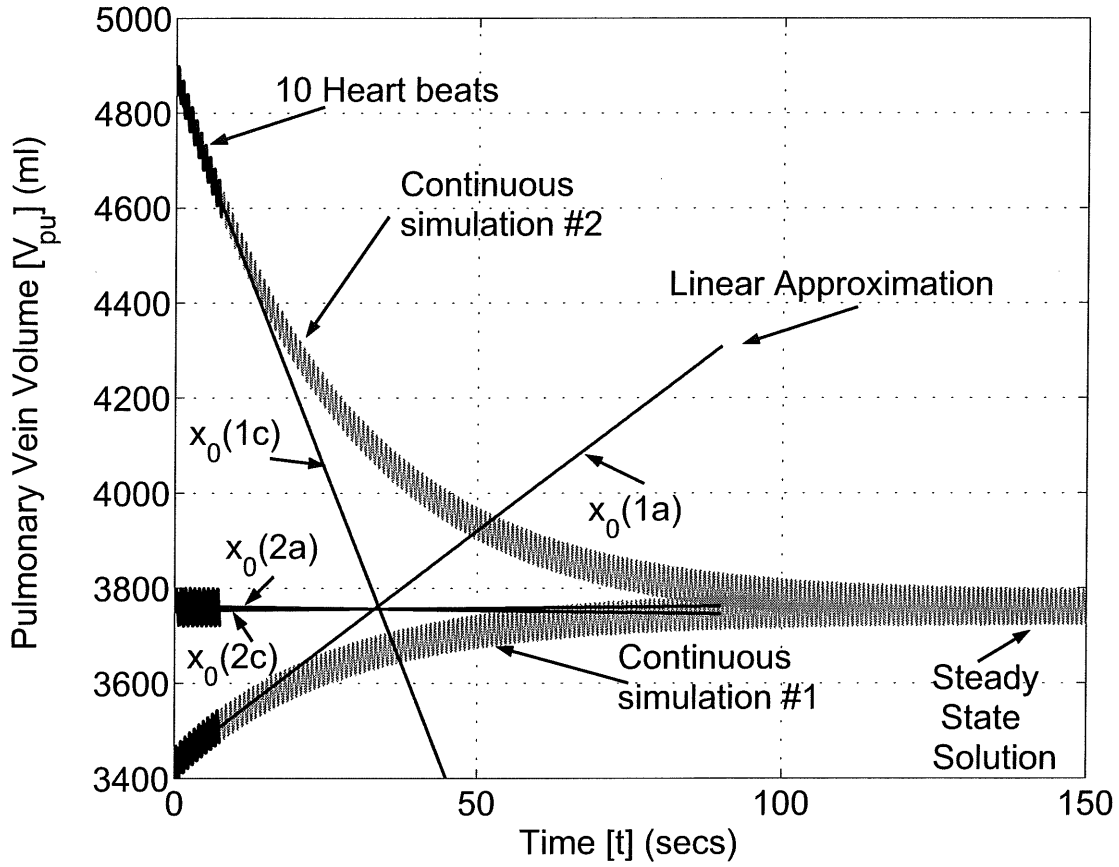

Figure 7.3 Gradient estimation plots overlaid on continuous simulation.

time can be achieved using the gradient estimation method. For simulations that are fast to converge, there is no significant benefit to using either the gradient estimation method or the continuous convergence method. These results reinforce the importance of attempting gradient estimation first to find a steady state solution as outlined in Chapter 6.

7.2 Optimisation

Figure 7.4 plots the optimisation variables (top) and the objective functions (bottom) after 20 optimisation sample steps using the optimisation routine described in Chapter 6. At the first sample step, all of the optimisation variables are set to one and the CVS model is run to gain a base point for optimisation. Then 14 optimisation sample steps are carried out to determine the Jacobian of the system at the base point. The optimisation variables are seen to form a saw

Initial conditions	Continuous Simulation ♯1	♯2	Gradient Estimation ♯1	♯2
Number of heart beats to convergence	80	110	40	60
Computational time to convergence (secs)	100	180	17	26

Table 7.1 Data comparing the rate of convergence of continuous simulation versus gradient estimation.

tooth pattern as the gradient with respect to each variable is sampled individually. As an example, the dashed line shows the variation in the value of the optimisation variable associated with the resistance in the tricuspid valve (R_{tc}). The first spike in the R_{tc} signal at sample step number 3 shows the optimisation routine sampling this variable and determining the response of the optimisation variables.

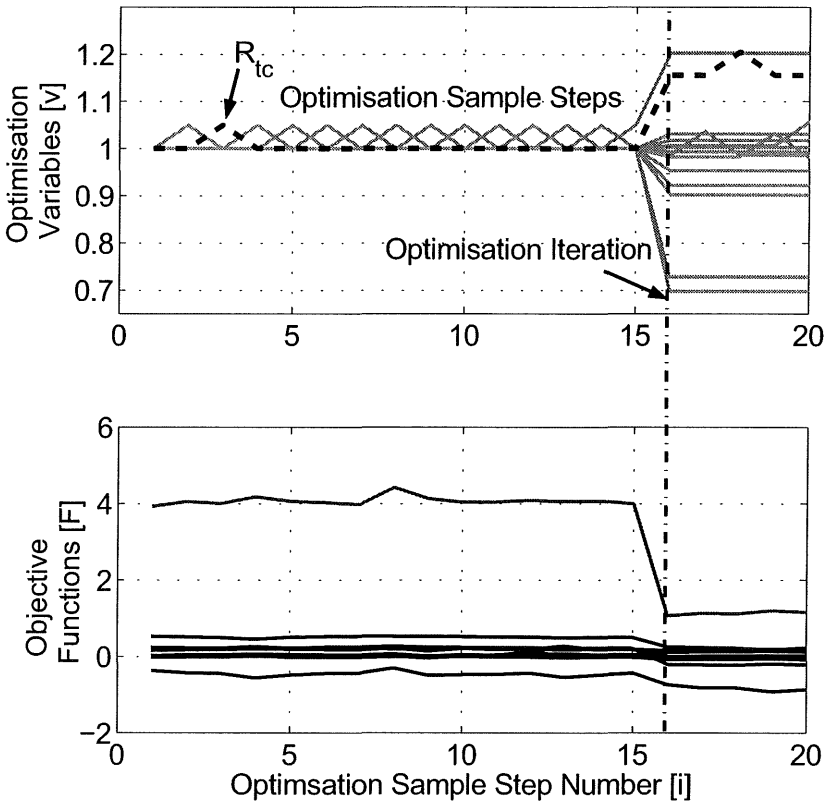

Figure 7.4 Profiles of the optimisation variables and objective functions for the first 20 sample steps.

After 14 iterations the Jacobian matrix has been constructed and the optimisation routine makes an iteration step to a new base point, as shown in Figure 7.4 at step number 16. Following this iteration step, the optimisation routine resumes sampling the gradient in each direction to form a new Jacobian matrix at the new base point. The bottom plot of Figure 7.4 plots the small variations in the objective function values as the optimisation variables are adjusted to find the Jacobian. Larger variations in the objective functions occur when the optimisation routine makes an iteration step such as at sample step number 16. At each optimisation iteration, the objective function values should move closer to the goal value of zero.

The optimisation routine took 16 iteration steps and 58 minutes of computational time to find a solution, although optimised code could reduce the computational time by 10-100 times. Figure 7.5 plots each of the 16 optimisation iteration steps taken to reach a solution. For clarity, only the optimisation iteration steps, and not the sample steps used to form the Jacobian are shown on this plot. Some of the optimisation variables and objective functions are labelled showing the manner in which they vary. The sub-figure in the bottom frame of Figure 7.5 shows a scaled view of the last 8 iterations of the optimisation routine. Table 7.2 lists the final parameter values after optimisation, which can be compared with the pre-optimisation values in Tables 5.1 and 5.2.

Description	**Symbol**
Elastance of Vena-cava	$E_{vc}= 1.29 \times 10^6$ N/m^5
Elastance of Left Ventricle	$P_{0,lvf} = 9.07$ N/m^2
Elastance of Pulmonary Artery	$E_{pa}= 44.5 \times 10^6$ N/m^5
Elastance of Pulmonary Vein	$E_{pu}= 0.85 \times 10^6$ N/m^5
Elastance of Right Ventricle	$P_{0,rvf} = 20.7$ N/m^2
Elastance of Aorta	$E_{ao}= 98 \times 10^6$ N/m^5
Resistance of Tricuspid Valve	$R_{tc}= 3.3 \times 10^6$ Ns^2/m^5
Resistance of Pulmonary Valve	$R_{pv}= 1 \times 10^6$ Ns^2/m^5
Resistance of Pulmonary Circulation	$R_{pul}= 19.3 \times 10^6$ Ns^2/m^5
Resistance of Mitral Valve	$R_{mt}= 2.33 \times 10^6$ Ns^2/m^5
Resistance of Aortic Valve	$R_{av}= 5.33 \times 10^6$ Ns^2/m^5
Resistance of Systemic Circulation	$R_{sys}= 139.6 \times 10^6$ Ns^2/m^5
Contractility of Left Ventricle	$E_{es,lvf}= 377 \times 10^6$ N/m^5
Contractility of Right Ventricle	$E_{es,rvf}= 87.8 \times 10^6$ N/m^5

Table 7.2 Model Parameter values after optimisation.

Table 7.3 lists the values of the 10 CVS model target performance metrics

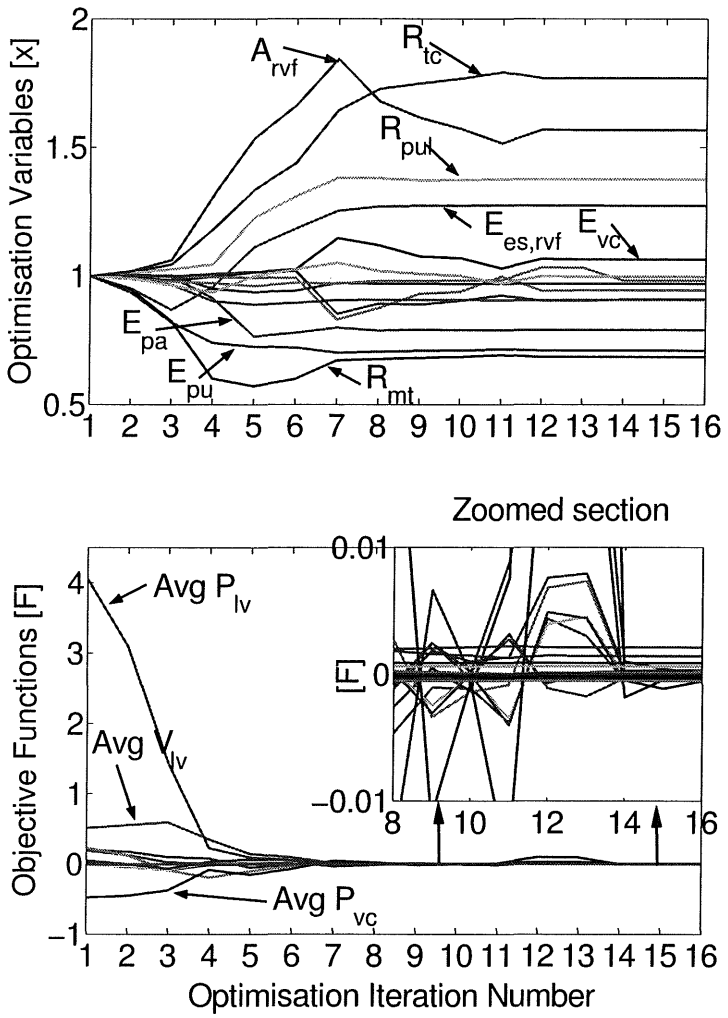

Figure 7.5 Variations in optimisation variables and objective function values over an optimisation run plotting only iterations.

before and after optimisation. The results after optimisation show that the optimisation routine was able to match target performance metrics to less than 0.1% error. Given that errors of up to 1% would be acceptable, this precision is more than enough to accurately simulate a specific patients CVS function. Figure 7.6 shows the results of a CVS model simulation using the model parameters determined by optimisation. These optimised CVS model outputs can be compared with the initial CVS model results plotted in Figure 5.9. These results not only validate this optimisation routine for finding model parameters, but also that the model is capable of simulating the dynamics specified by the target performance values.

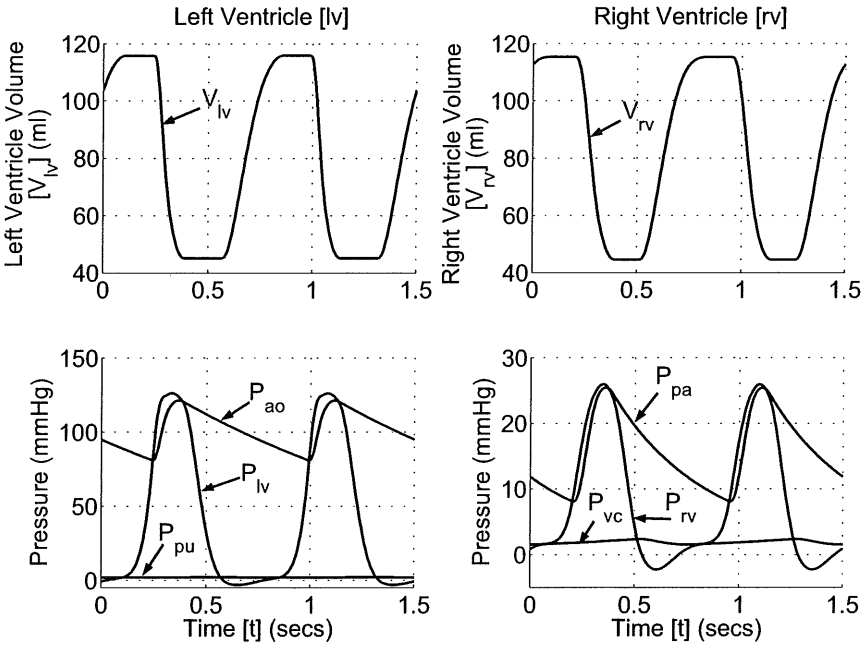

Figure 7.6 The CVS model outputs run using the model parameters determined by optimisation.

7.2.1 Sensitivity Analysis

The optimisation routine produces a Jacobian matrix at the final solution point. The values in this matrix can be plotted to identify the sensitivity of specific final model outputs to variations in model parameters. Figure 7.7 plots the objective functions as a function of the optimisation variables. This plot highlights which objective functions are most significantly effected by variations in particular optimisation variables for the final optimisation solution.

Some model parameters in Figure 7.7 have a relatively direct relationship with only a single model performance metric. For example, the elastance of the aorta (E_{ao}) significantly affects only the amplitude of variation of the pressure in the aorta (Amp P_{ao}). Other parameters have more complex effects. Figure 7.7 shows that variations in the systemic resistance (R_{sys}) significantly affect the average pressure in the aorta (Avg P_{ao}), as well as the average pressure in the vena-cava (Avg P_{vc}). Figure 7.7 can also be used to highlight parameters that have little effect on any of the performance metrics. It can be seen that the resistances in the pulmonary valve (R_{pv}) and the aortic valve (R_{av}) do not significantly affect any of the selected performance metrics. This result means that the variables R_{pu} or R_{av} are relatively unconstrained in the optimisation and could be left out

Model Variable	Target Value	Before Optimisation		After Optimisation	
		Value	% Error	Value	% Error
Pressure in Aorta					
Amp Pao	40mmHg	41.407	3.5%	39.992	-0.021%
Avg Pao	100mmHg	119.168	19.2%	99.971	-0.029%
Pressure in Pulmonary Artery					
Amp Ppa	17mmHg	20.414	20.1%	17.004	0.022%
Avg Ppa	16.5mmHg	20.314	23.1%	16.498	-0.010%
Volume in Left Ventricle					
Amp Vlv	70ml	69.508	-0.7%	70.003	0.004%
Avg Vlv	80ml	84.042	5.1%	79.998	-0.002%
Volume in Right Ventricle					
Amp Vrv	70ml	69.569	-0.6%	69.993	-0.011%
Avg Vrv	80ml	121.185	51.5%	79.991	-0.011%
Pressure in Pulmonary Vein					
Avg Ppu	2mmHg	10.112	405.6%	2.001	0.040%
Pressure in Vena-cava					
Avg Pvc	2mmHg	1.050	-47.5%	2.000	-0.025%

Table 7.3 Objective Function Values.

for this particular set of performance metrics.

An alternative to Figure 7.7 using the same Jacobian data is shown in Figure 7.8, where the optimisation variables are instead plotted as a function of the objective functions. This plot shows much of the same data, such as the dependence of the pressure in the aorta (P_{ao}) on the elastance of the aorta (E_{ao}). However, the alternative layout in Figure 7.8 can be a more useful means of finding which parameters must be adjusted to alter specific performance metrics. For example, the difficultly in adjusting the amplitude of variation of the right ventricle volume (Amp V_{rv}) is clearly highlighted in Figure 7.8 where no variable has a particularly large affect on this value.

It should be noted that Figure 7.7 plots the Jacobian at the final solution point of the optimisation routine. The magnitudes of the individual components of the Jacobian matrix may change and different components may be more significant at different stages in the optimisation process. However, assuming the optimisation routine has found a solution matching a specific patients CVS dynamics, the final Jacobian will be the most useful for that particular patient. It can also shed light on how best to treat any abnormality found in the parameters of the patient

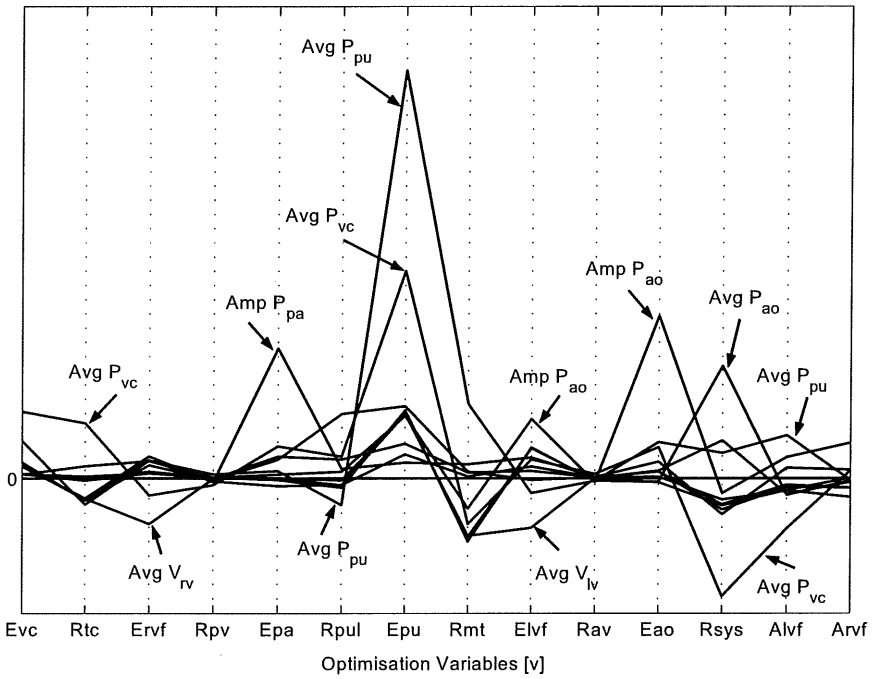

Figure 7.7 Plot of Jacobian matrix showing the sensitivity of each optimisation variable.

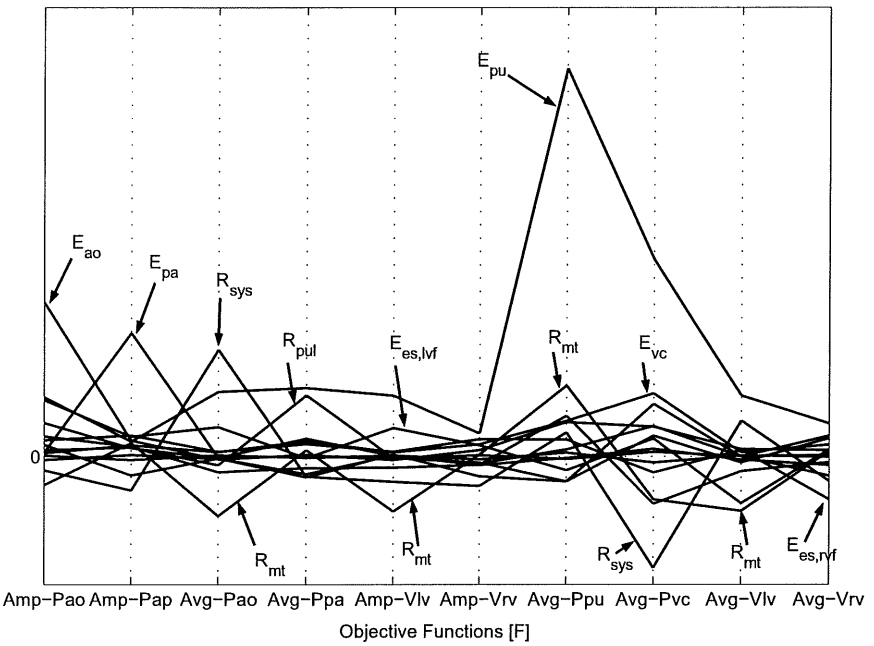

Figure 7.8 Plot of Jacobian matrix showing which optimisation variables significantly affect each objective function.

specific model.

7.3 Summary

Tests using the gradient estimation method show it converges to a steady state solution in roughly the same computational time as the continuous simulation method. However, some special case simulations were found that take significantly longer to converge. For these special case solutions, gradient estimation found a steady state solution in almost half the time of continuous simulation. These tests justify using gradient estimation first, followed by continuous simulation if convergence is not achieved, when optimising the CVS model parameters.

The results of the optimisation routine carried out on the CVS model show the significant potential of this method. The optimisation routine was found to meet target performance metrics to within 0.1% error. This considerable level of precision shows not only the potential of the optimisation, but also the capability of the CVS model to meet target CVS performance specifications. Loosening this tolerance would significantly ease computational time.

The optimisation routine required on the order of one hour to converge to a solution offering a proof of concept for the optimisation approach. However, with modifications to the simulation software, considerable computational time reductions could be achieved, easily reducing the time to solution to a matter of a few minutes. A further reduction in computational time could be achieved by running the algorithm in a lower level programming environment, such as C++. Additionally, developments in the numerical implementation, such as relaxing the optimisation target precision, could potentially halve the number of optimisation parameters required to reach a solution. A solution time of 2-5 minutes should be readily achievable on a C++ platform and target error tolerances of greater than 0.1%.

The initial aim of this research is to create a patient specific model for real time feedback to assist medical staff in diagnosis and treatment. The results of this chapter show the capability of the presented approach to create patient specific models. It is also shown that modifications to the routine could reduce the computational time to the matter of minutes necessary for real time, clinical feedback. Thus, these results offer a proof of concept for the presented method in achieving the specified goals.

Chapter 8

Dynamic Response Verification

The minimal CVS model presented has been shown to simulate the static response of the cardiovascular system to changes in state, but the transient dynamic response of the model to these changes has not yet been verified. Tests were carried out in Chapter 5 verifying the change in steady state solution of the system with variations in resistance and thoracic pressure. These tests show that the static response, or the change in steady state solution, of the model to changes in state matches known physiological response. This chapter investigates the dynamic response of the CVS system to changes in state, such as arterial constrictions and changes in thoracic pressure due to respiration.

This dynamic response verification focuses on ventricular interactions and cardiopulmonary interactions, which are important CVS interactions that contribute significantly to CVS dynamics. A review article by Weber et.al. (1981) justifies the intensive research into cardiopulmonary interaction by stating: *An understanding of the physiological behaviour of the cardiopulmonary unit will provide critical insight into the clinical recognition and management of the patient with respiratory failure.* The same justification applies to ventricular interaction, as gaining more understanding of the physiological interactions will improve the capability of medical staff to diagnose and treat CVS dysfunction.

This chapter is divided into two sections, the first focusing on ventricular interaction and the second investigating cardiopulmonary interaction. Each section contains a brief overview of the research carried out to date in measuring and modelling each interaction. The CVS model is then verified by simulating experimental studies in the literature and comparing the results.

8.1 Ventricular Interaction

There are two types of ventricular interaction, direct and series. Direct interaction occurs as a result of the septum and the pericardium. The deflection of the septum depends on the relative difference in pressures between the ventricles, while the pericardium essentially constrains the maximum total volume of the ventricles. Thus, if the volume of one ventricle increases, the other ventricle will become compressed. Series interactions occur when the dynamics of one ventricle propagate through the peripheral circulation system and into the other ventricle. The relative contributions of each type of interaction are difficult to measure [Beyar et al., 1987; Slinker and Glantz, 1986; Scharf and Cassidy, 1989].

There is extensive literature on the subject of ventricular interactions, discussing the mechanisms and magnitudes of how each ventricle affects the function of the other. Experimentally determining the contribution of ventricular interaction to human heart function poses many problems due to the difficulty in taking accurate measurements. Accurately measuring pressures, volumes and flow rates in and around the heart often requires invasive procedures which may affect the dynamics of the CVS, which is what is intended to be measured. For example, the pericardium is often removed to insert probes into the heart, significantly affecting the dynamics of the heart itself.

This section summarizes research that has been carried out to measure both the static and dynamic response of the CVS due to ventricular interaction. The capability of the minimal CVS model presented to capture the dynamics of ventricular interaction is verified against experimental results in the literature. The model can then be used to delineate the relative contributions of direct and series interaction to the CVS dynamics as well as the impact of the specific physiological elements modelled.

8.1.1 Static Ventricular Interaction

Measuring Static Ventricular Interaction

Experiments are most often carried out on anaesthetized dogs and usually involve surgically removing the heart from the circulation system and carrying out static tests [Maughan et al., 1987; Weber et al., 1981; Glantz and Parmley, 1978; Santamore and Dell'Italia, 1998]. Static tests involve disconnecting the heart from

the circulation system, isolating it from series interactions. A known quantity of blood is then injected into one ventricle of the isovolumetrically beating heart, while measuring the pressure changes in both ventricles. These tests quantify the amount of static interaction that occurs between the ventricles. However, they do not measure the transient ventricular interaction dynamics that occur when the operating conditions of one ventricle are altered.

For example, when a person breathes in, the pressure in the pulmonary circulation drops and significantly affects the function of both ventricles, but in different ways. The flow rate through the right ventricle will be initially higher than the flow rate through the left ventricle. However, this transient effect is only temporary before the CVS settles to a new steady state. Static tests will determine the change in steady state volume of the system, but give no indication of the transient response of the system. It is during this transient response that ventricular interaction may make a considerable contribution to CVS dynamics. The minimal model must be able to capture these dynamics and match the trends in experimental results.

A summary of experiments to quantify ventricular interaction begins with a review article by Glantz and Parmley (1978) summarising the understanding to that date. The article references a wide variety of publications outlining experimental tests, mostly carried out on dogs. The septum and the pericardium are identified as making significant contributions to the beat-to-beat changes in ventricle dynamics.

Weber et.al. (1982) published a review article on their well referenced work in ventricular interaction, including a summary of their extensive experimental work with isolated canine hearts [Janicki and Weber, 1980; Weber et al., 1981]. This work clearly quantifies static ventricular interaction during isovolumetric contraction of an isolated heart. Their work involves removing the heart from the circulation system of an anaesthetized dog and holding one ventricle volume constant while measuring the volume of the other. This arrangement means series interactions are removed and only direct interactions are measured.

The results of this work showed that increasing the volume of one ventricle will decrease the volume of the other ventricle due to direct interaction. As the volume of one ventricle is increased, because the ventricles are contained within the pericardium, the other ventricle will be compressed and the septum will deflect away from the inflated ventricle. The work of Weber et.al. (1982) made an important contribution to understanding of the static properties of ventricle in-

teraction and quantified the impact of one ventricle volume on the other ventricle. However, the experimental method did not give any indication of the transient response of ventricular interaction.

Simulating Static Ventricular Interaction

There are many examples in the literature of models designed to simulate ventricular interaction [Chung et al., 1997; Santamore and Burkhoff, 1991; Beyar et al., 1987; Olansen et al., 2000]. If the ventricular interaction function of these models is verified against experimental data, it is against the static data from research such as that carried out by Weber and Janicki [Weber et al., 1981]. However, the author was unable to find any models that were verified to simulate the transient dynamics of ventricular interaction.

The model of Beyar et.al. (1987) includes the effect of ventricular interaction, but contains minimal verification of its function. The septal interaction in the model of Chung et.al. (1997) is verified against the static interaction experiments in the literature of Bove and Santamore (1981). Santamore et.al. (1991) verify the performance of their model against experiments carried out within their group and by other groups such as Weber et.al. (1981). All of the experimental literature referenced in these articles contains only the static response of the CVS due to ventricular interaction.

8.1.2 Dynamic Ventricular Interaction

Slinker and Glantz (1986) extended earlier studies on ventricular interaction by analysing the transient effects of both direct and series ventricular interaction on CVS dynamics. This research was also carried out on anaesthetized dogs, but the heart remained connected to the circulation system, thus including series interaction between ventricles. This approach takes advantage of the time lag between direct and series interaction when investigating the effect of changing right ventricle state on left ventricle function. Direct interaction, through the septum and pericardium, will cause an immediate response in the left ventricle if the volume of the right ventricle is changed. The changes in left ventricle function due to series interaction will be delayed as the dynamics propagate around the pulmonary circulation. This delay was used to delineate and quantify the relative contributions of series and ventricle interaction to CVS function. However, using

the minimal model developed it is possible to directly separate each type of interaction.

Measuring Dynamic Ventricular Interaction

The experiment carried out by Slinker and Glantz (1986) involved sequentially constricting and releasing the pulmonary artery and vena-cava, as labelled on Figure 8.1. Pulmonary artery constriction (PAC) causes an increase in resistance downstream of the right ventricle, increasing the afterload against which the right ventricle must pump. Applying vena-cava constriction (VCC) decreases the pressure upstream of the right ventricle, decreasing the right ventricle preload as a result of reduced filling pressure. When the constrictions are subsequently released the CVS responds again, settling to its original state. These constrictions and their subsequent releases significantly impact the function of the right ventricle. Volumes, pressures and flow rates around both the right and left ventricles were measured to determine the response of the CVS to these changes in state.

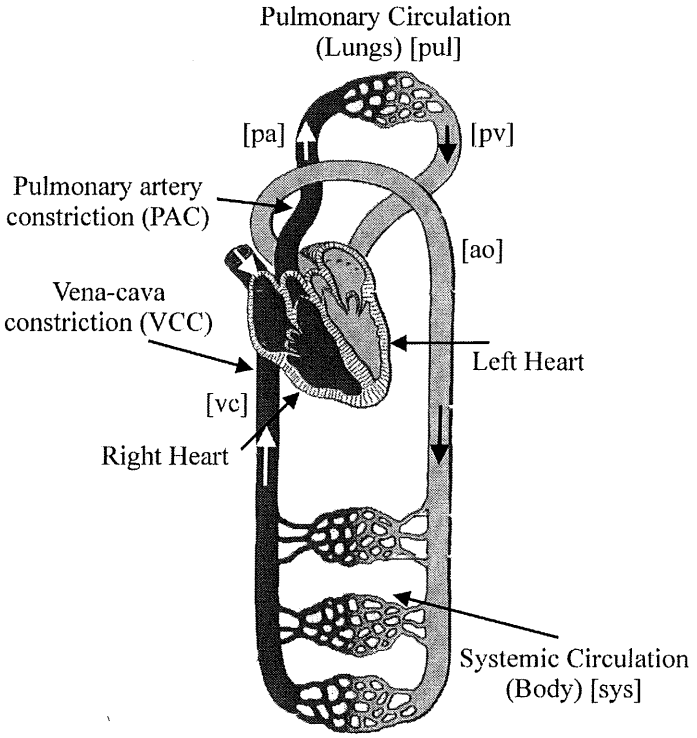

Figure 8.1 Diagram of the circulation system showing the location of the constrictions.

Pressure transducers were used to measure ventricle and arterial pressures,

and arterial flows were measured using electro-magnetic flow probes. The ventricle volumes are assumed to be proportional to the cross-sectional area of the ventricle. The cross-sectional area is estimated using a sonomicrometer and 5MHz hemispherical piezoelectric crystals placed at the anterior and posterior of the left ventricle, and in the middle of the septal, left and right ventricle free walls [Slinker and Glantz, 1986]. Figure 8.2 shows the location of the marker crystals on a cross-sectional illustration of the heart.

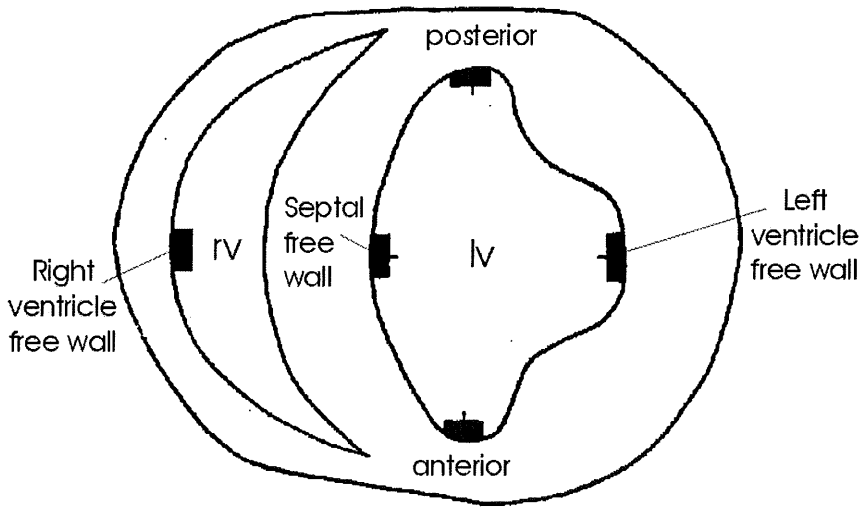

Figure 8.2 Sectioned heart view showing crystal locations.

Three ventricle dimensions are obtained using the marker crystals to estimate the ventricle volumes. The distance from the posterior to the anterior crystals is assumed to be proportional to the left ventricle free wall volume (V_{lvf}). The distance from the left ventricle free wall to the septum crystal represents the deflection of the septum (V_{spt}). Using these two measurements, the left ventricle volume (V_{lv}) is estimated as the product of the V_{lvf} and V_{spt}. Finally, the separation of the right ventricle free wall and the septal crystals is a measure of the right ventricle volume (V_{rv}).

Very little information about the mechanical properties of the canine hearts studied can be gained from the publication [Slinker and Glantz, 1986]. It is known that the heart rate was maintained at roughly 130 beats per minute, there is no respiration, and the data was taken with the pericardium removed. To verify that the minimal model captures the experimental dynamics, in spite of the lack of specific information, the generic model parameters outlined in Chapter 5 for the static trend verification are used. The heart rate is changed to 130 beats

per minute and the pericardium effects are removed by setting the elastance to a negligible value ($P_{0,pcd} = 10^{-6}$). The pulmonary artery constriction is simulated by increasing the pulmonary valve resistance (R_{pv}) by a factor of 20. Similarly, the vena-cava constriction is simulated by increasing the tricuspid valve resistance (R_{tc}) by a factor of 4. These factors for varying the resistances were found by trial and error to approximately match the performance magnitudes of the data in Slinker and Glantz (1986).

Primary Experiment and Results

Figure 8.3 shows the main results obtained by Slinker and Glantz (1986). The experiment shown involved constricting the pulmonary artery after about 4 seconds (PAC) followed by vena-cava constriction after about 12 seconds (VCC). At 20 seconds the constriction on the pulmonary artery is released and after about 27 seconds the vena-cava constriction is released. Figure 8.3 plots the experimentally determined variations in pressures, volumes and flow rates around both ventricles during these constrictions and releases.

Figure 8.4 plots the results of a simulation carried out on the CVS model to simulate the experimental results in Figure 8.3. Comparing these plots highlights the ability of the CVS model to capture all of the trends measured experimentally by Slinker and Glantz (1986). Note that the magnitudes of each variable do not match the experimental results due to the lack of detailed information available and the use of generic human parameters. However, by capturing these trends the model is shown to accurately capture the dynamics of ventricular interaction in the CVS. Most importantly, the model captures the trends in the deflection of the septum, verifying the method developed for modelling and simulating septal deflection. The author was unable to find any other model that was verified to capture these transient dynamic trends.

Figure 8.5(a) plots the variation in left ventricle end-diastolic area, which is assumed to be proportional to left ventricle end-diastolic volume during the experiment. The black dots are experimental data. The solid and dashed lines plot the results of a statistical analysis by Slinker and Glantz (1986) to capture the changes, and are not experimental data. Figure 8.5(b) plots the variation in simulated left ventricle volume (V_{lv}) using the CVS minimal model. The dark line along the top of the graph marks the variation in end-diastolic volume. The model results in Figure 8.5(b) are seen to contain all the major trends and

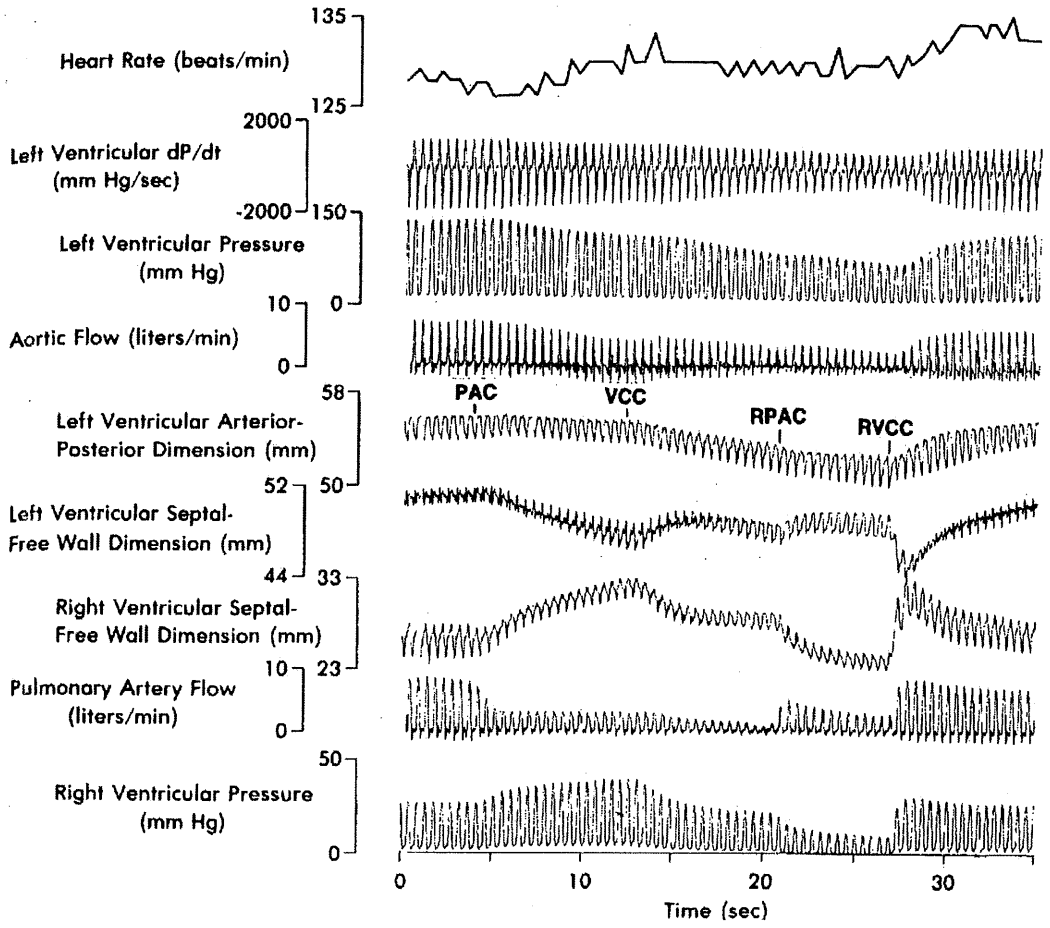

Figure 8.3 Haemodynamic CVS responses to sequential constrictions and releases of the pulmonary artery and vena-cava [Slinker and Glantz, 1986].

transient dynamics in the experimental results of Figure 8.5(a).

Second Experiment and Results

A second experiment by Slinker and Glantz (1986) involved applying a different combination of the same constrictions. The pulmonary artery constriction is again applied after 4 seconds, but released after about 23 seconds. At about 37 seconds a subsequent vena-cava constriction is applied until the end of the experiment. The experimentally measured variations in left ventricle end-diastolic area are plotted in Figure 8.6(a). This experiment was also simulated using the minimal model, and the trends shown in Figure 8.6(b) are seen to accurately match experimental results.

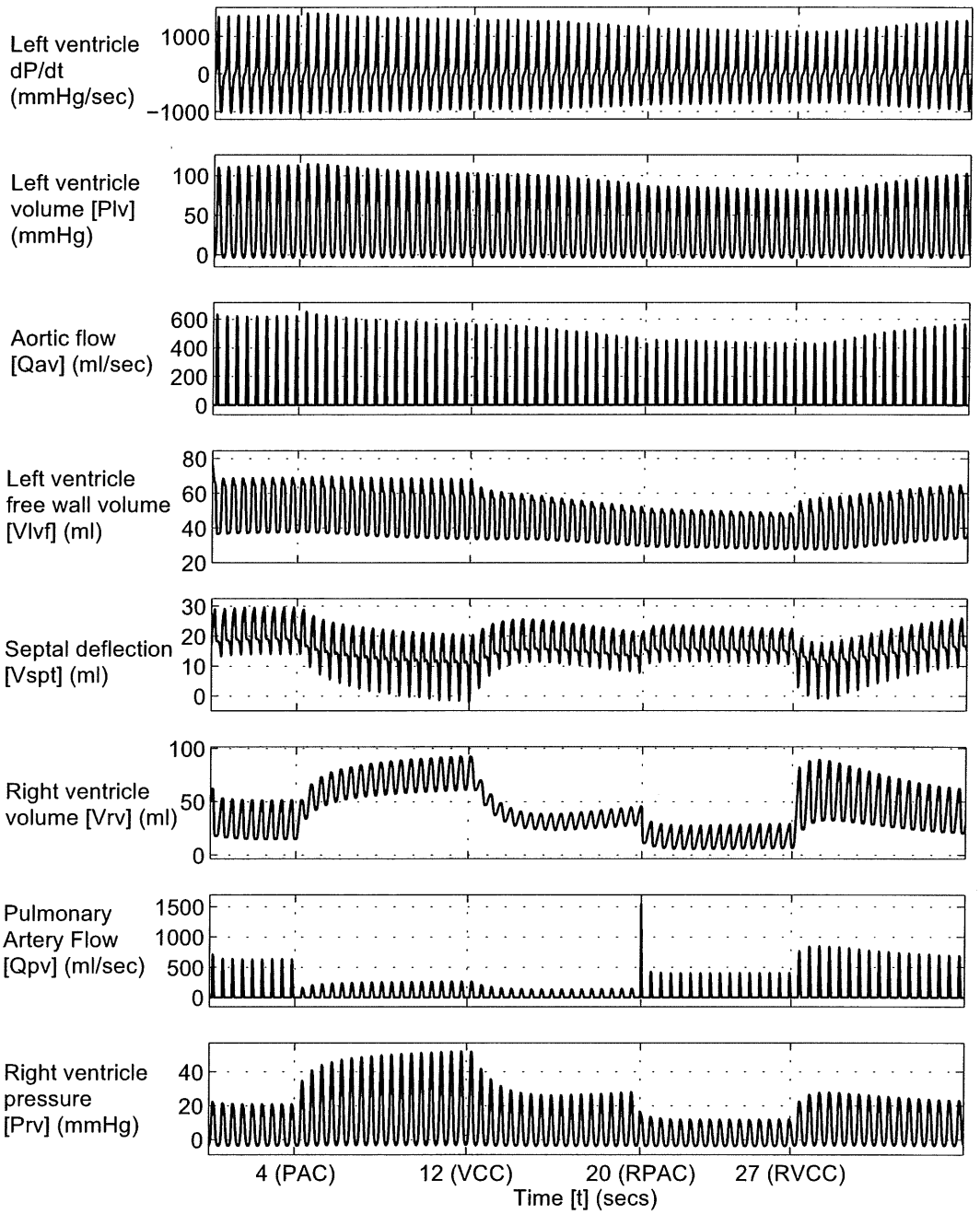

Figure 8.4 Haemodynamic CVS responses simulated using the presented model.

Left Ventricle Volume Response

As discussed, the experimental research carried out by Slinker and Glantz (1986) investigates the relative contributions of direct and series interaction on CVS dynamics. However, it is very difficult to experimentally separate and isolate

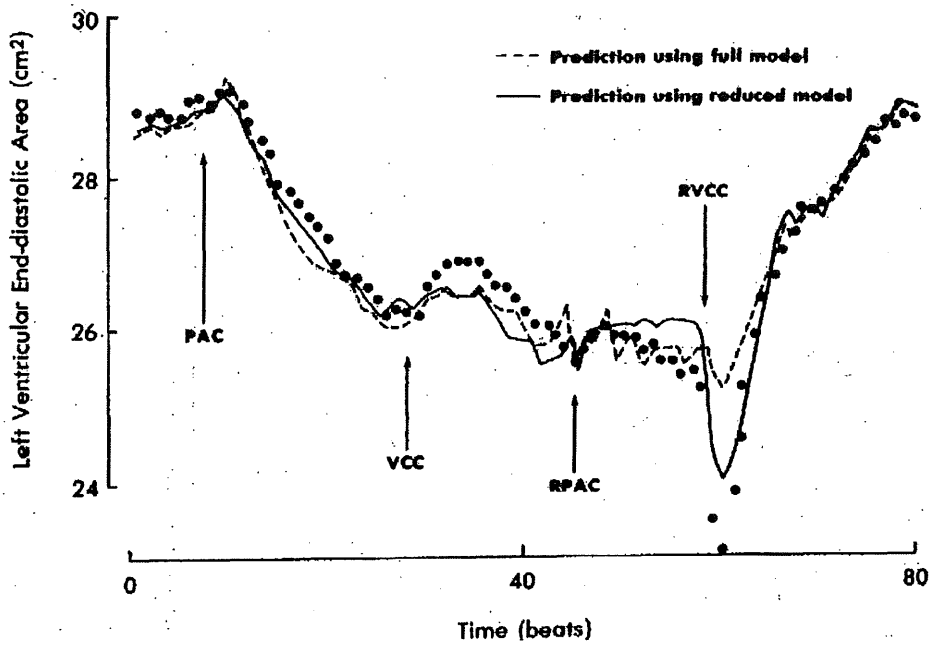

(a) Experimentally determined change in left ventricle end-diastolic area [Slinker and Glantz, 1986].

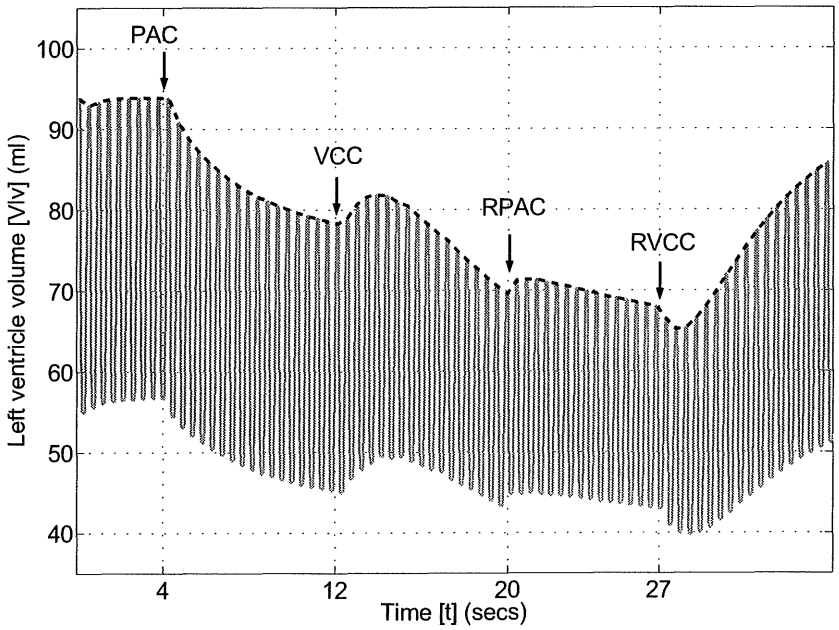

(b) Simulated variations in left ventricle volume (light grey) and end-diastolic volume (dark dashed line)

Figure 8.5 Comparing experimental and simulated changes for primary experiment.

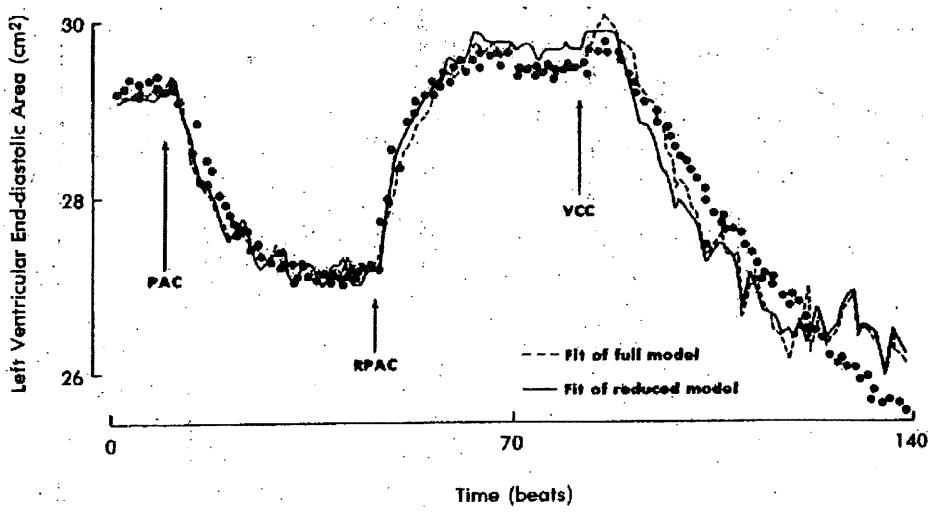

(a) Experimentally determined change in left ventricle end-diastolic area [Slinker and Glantz, 1986].

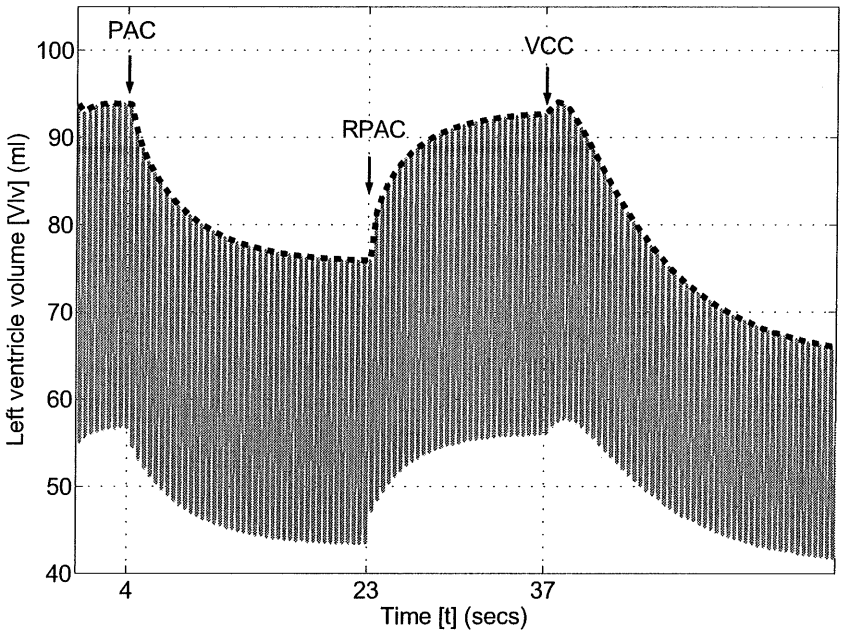

(b) Simulated variations in left ventricle volume (light grey) and end-diastolic volume (dark dashed line)

Figure 8.6 Comparing experimental and simulated changes for secondary experiment.

the different contributions of each interaction mechanism, and determine how they affect CVS dynamics. The CVS minimal model presented is capable of analysing these effects by simply excluding certain interactions without changing the remainder of the system.

The top panel of Figure 8.7 plots the variations in left ventricle volume determined by simulation of the primary experiment. The individual contributions of direct and series interaction can be seen in the middle and bottom panels respectively. The direct interaction plot is created by removing series interactions from the simulation by setting constant pressure boundary conditions around the ventricles. The series interaction plot is created by setting the elastance of the septum to a high number ($P_{0,spt}= 10^6$), making it effectively rigid to eliminate direct interaction through the septum.

Both the pulmonary artery constriction and the vena-cava constriction impact directly on the function of the right ventricle. For this reason, the variations in left ventricle volume are investigated as this offers the best representation of the effects of ventricular interaction. Increases in right ventricle volume will cause decreases in left ventricle volume, and vice-versa, due to direct interaction.

The direct interaction only response of the system, shown in the centre panel of Figure 8.7, highlights the immediate impact of right ventricle parameter adjustments on left ventricle function. The left ventricle volume is seen to respond to direct interaction and settle to a steady state solution within 5 heart beats in each case. Conversely, the series interaction only results show a delayed response to the parameter changes around the right ventricle. Series interactions occur due to the changes in cardiac output and ventricle preloads as resistances are increased and decreased.

Figure 8.4 shows that increasing the pulmonary valve resistance to simulate PAC causes an increase in right ventricle afterload and results in a build-up of right ventricle volume and pressure. This build-up causes an immediate drop in left ventricle volume, which the middle panel of Figure 8.7 shows is due to direct interaction, as the septum deflects into the left ventricle. The continued long term drop in left ventricle volume is then attributed to series interactions. The increase in resistance in the pulmonary artery decreases left ventricular preload, and reduces cardiac output and left ventricular volume.

Subsequently constricting the vena-cava (VCC) causes a transient sudden by small rise in left ventricle volume, followed by a gradual continued reduction. The middle panel of Figure 8.7 shows that this initial transient is attributed to direct interaction. Constricting the vena-cava causes a reduction in right ventricle preload and the right ventricle volume decreases causing the septum to deflect towards the right ventricle. This septal deflection causes a sudden rise in the volume of the left ventricle. The continued long term reduction in left ventricle

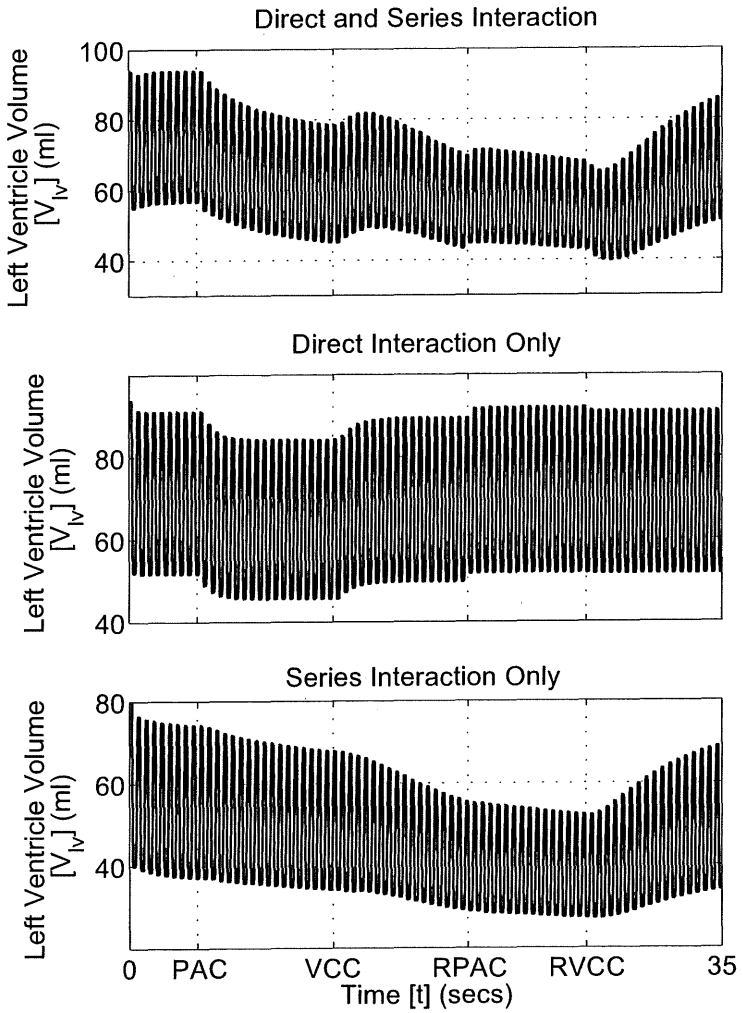

Figure 8.7 Left ventricle volume variations with both series and direct interaction (top), with direct interaction only (middle) and series interaction only (bottom).

volume is due to the delayed, but long term, response due to series interaction. Constricting the vena-cava further constrains the flow of blood in the CVS causing a reduction in cardiac output and preload of both left and right ventricles.

Releasing the pulmonary artery (RPAC) decreases the afterload on the right ventricle and results in a further septal shift towards the right ventricle due to the resulting drop in right ventricle pressure as seen in Figure 8.3. The left ventricle volume in Figure 8.7 is seen to continue decreasing as the system has not had time to reach a steady state solution after the vena-cava constriction. Finally, the vena-cava constriction is released (RVCC), which results in a sharp rise in right ventricle pressure and volume, temporarily pushing the septum into the left ventricle. However, as the cardiac output builds up due to the decrease

in resistance, the left ventricle volume increases and the septum returns to its steady-state position.

Thus, Figure 8.7 shows how the CVS minimal model developed can separate the relative contributions of series and direct interaction. The model allows detailed analysis of the relative contributions of each interaction type by simply deactivating a particular CVS function without affecting other parts of the CVS. This capability offers a considerable advantage over current, heavily invasive, surgical techniques of measuring ventricular interaction.

8.1.3 Ventricular Interaction Summary

The different experimental results that attempt to quantify ventricular interaction are reviewed. In particular, results that measure the transient response of the CVS due to ventricular interactions are outlined. The minimal CVS model presented is verified to accurately capture the major trends in experimentally measured CVS dynamics. These results verify that the model is capable of capturing the transient dynamic response of the CVS due to both direct and series ventricular interaction. No other model found in the literature was verified to capture these transient responses in CVS dynamics due to ventricular interaction.

Following this verification, the model is used to delineate the relative contributions of the different contributing factors of ventricular interaction. Results are shown that show both the immediate response of the system due to direct interaction and the delayed response due to series interaction. The minimal model enables much more detailed analysis, such as that presented, without needing to resort to experimental methods, and allows the individual contributions and dynamics to be fully studied.

8.2 Cardiopulmonary Interaction

As discussed in Chapter 1, the location of the heart between the lungs in the thoracic cavity means that its function is significantly influenced by pressure variations in the lungs and lung movement during respiration. As the pressure in the lungs changes during respiration, the pressure around the heart and pulmonary circulation varies, influencing cardiac function. This section investigates the ability of the minimal CVS model to simulate experimentally reported haemodynamic trends due to cardiopulmonary interactions.

8.2.1 Respiratory Function

Different types of respiration can have different effects on CVS haemodynamics depending on the amount of change in thoracic pressure. Spontaneous respiration typically involves thoracic pressure variations from a maximum of about -4mmHg during expiration to a minimum of about -8mmHg during inspiration [Guyton, 1991]. During positive pressure ventilation of normal individuals, the average thoracic pressure rises and typically may vary from a maximum of 3mmHg at end inspiration to a minimum of -3mmHg at end expiration [Scharf et al., 1980]. More severe pressure variations can occur in ventilated patients with lung injury or disease.

Respiratory manoeuvres such as the Mueller and the Valsalva manoeuvre can be used by medical staff to evaluate cardiopulmonary function. During a Mueller manoeuvre the patient attempts to forcibly inspire against a blocked airway which results in a drop in thoracic pressure on the order of -70mmHg [Schwartz et al., 1999]. The Valsalva manoeuvre involves forcibly attempting to exhale with the airway blocked, and results in significantly elevated thoracic pressures on the order of 10-40mmHg [Lu et al., 2001].

Spontaneous respiration typically has only a minimal impact on CVS haemodynamics due to the minimal variations in thoracic cavity pressure [Scharf and Cassidy, 1989]. Positive pressure respiration results in an increase in the average pressure in the thoracic cavity, placing a higher pressure on the heart and results in decreased cardiac output. However, the transient changes in haemodynamics during the respiratory cycle are dependent on the amplitude of variation in pressure. The large variations in pressure caused by the Mueller and Valsalva manoeuvres, and used to investigate cardiopulmonary interactions, have a significant impact upon CVS haemodynamics. The changes in CVS function

during these manoeuvres are large enough to be easily detected using commonly available medical equipment. For this reason these manoeuvres are also used by medical staff to evaluate cardiopulmonary function, such as diagnosing heart failure [Braunwald, 1997].

The body will often react quickly to the catastrophic impact of the Mueller and Valsalva manoeuvres on CVS function by activating reflex responses. For example, during the Valsalva manoeuvre the considerable positive pressure acting on the heart causes a significant drop in cardiac output. The body will respond by activating the baroreceptor reflex that, amongst other things, increases the heart rate to improve cardiac output [Lu et al., 2001]. The minimal model developed does not include the autonomous activation of baroreceptor reflexes. However, the impact of the body's reflex response on haemodynamics is less significant during lesser variations in thoracic cavity pressure. Thus, both the spontaneous and positive pressure respiration cases are simulated, as they involve only small thoracic pressure variations, to further validate the dynamic response of the minimal model.

Mechanisms for Cardiopulmonary Interaction

Variations in thoracic pressure lead directly to immediate changes to the boundary pressures acting on the heart. For example, if thoracic pressure drops, such as during spontaneous inspiration, it reduces the pressure acting on all of the chambers within the thoracic cavity in Figure 2.1. The pressures in the pulmonary artery, pulmonary vein and in the heart will therefore decrease. Equations (2.12-2.14), (2.19) and (2.20) show how the minimal model incorporates the thoracic pressure in determining chamber pressures.

During inspiration in spontaneous breathing, the pressures in the heart and pulmonary circulation drop relative to the pressure outside the body. However, the pressures in the systemic circulation, outside the thoracic cavity, are not affected. Thus, the right ventricle preload, or the pressure in the vena-cava relative to the right ventricle pressure, increases. In the same way, the left ventricle afterload, or the pressure in the aorta relative to the left ventricle, increases. The overall result of these changes is an increase in stroke volume and output of the right ventricle, and a decrease in stroke volume of the left ventricle. Therefore, these changes in pressure mean the blood is redistributed from the systemic circulation to the pulmonary circulation.

The result of this redistribution of blood is a net blood volume increase in the pulmonary circulatory system until a new steady state equilibrium is reached. The opposite effect occurs during spontaneous expiration when the pressure in the thoracic cavity increases, resulting in a net increase in blood volume in the systemic circulation. It is shown in Chapter 5 that the model captures these static variations in cardiac output as a result of changes in thoracic cavity pressure. However, a more important test is the ability of the model to capture these same trends in the transient haemodynamic response of the CVS during respiration.

Cyclic variations in thoracic pressure during respiration cause transient fluctuations in the haemodynamics that must be captured in a dynamic simulation. This section first summarises the experimental research carried out to measure the impact of respiration on haemodynamic function. A brief summary of previous attempts to simulate cardiopulmonary interactions is then outlined. Published experimental data is used to test the ability of the presented CVS model to capture the transient haemodynamic response of the CVS due to variations in thoracic cavity pressure. Both spontaneous and positive pressure respiration case studies are used in this dynamic model verification. It is shown that the model can be used to identify the contributions of particular cardiopulmonary functions that are currently impossible to isolate experimentally.

8.2.2 Measuring Effects on CVS

As with ventricular interaction, there have been many major contributors to research on cardiopulmonary interactions. Buda et.al. (1979) reviewed previous publications that discussed the effect of respiration and respiratory manoeuvres on cardiac function. They emphasised the "controversy" surrounding the mechanisms by which left ventricle function is depressed during respiratory dysfunction. Scharf and Cassidy (1989) published a comprehensive review of cardiopulmonary interactions in both healthy and diseased patients. This review covers many of the main contributors to the field including experimental research carried out by themselves.

The minimal model is verified against results measured by Scharf et.al. (1979; 1980) on cardiopulmonary interaction during both spontaneous and positive pressure respiration. Many similar experiments have been carried out that also plot the dynamic response of the CVS during respiration, including more recent research by Denault et.al. (1999; 2001). However, other work does not contain the detailed measurements of pressures and flow rates taken by Scharf et.al. (1979;

1980). The intention here is to verify the ability of the model to simulate the transient dynamic response of the CVS due to variations in pulmonary resistance. The measurements taken by Scharf et.al. (1979; 1980) are ideal for this task.

8.2.3 Other Models

Few of the closed loop CVS models investigated include the effects of thoracic pressure changes. Beyar et.al. (1987) and Chung et.al. (1997) include thoracic pressure in their model descriptions, but investigate only static response of the models due to thoracic pressure changes. Others have taken a more detailed approach, attempting to simulate the dramatic effect of the valsalva manoeuvre on CVS dynamics [Sun et al., 1997; Lu et al., 2001].

Sun et.al. (1997) simply adds the thoracic cavity pressure to their very complex CVS model, shown in Figure 1.10, in a similar way to the method used in the model presented in this thesis. The thoracic cavity pressure is added to the pressure of the pulmonary circulation. The model also claims to include baroreflex effects. The effects of normal respiration and valsalva manoeuvre on aortic pressure (P_{ao}) are simulated. However, the results are not directly compared with experimental results and do not delineate the contribution of the baroreceptor reflexes [Lu et al., 2001].

Lu et.al. (2001) proposes a model which includes a detailed description of airway and lung function, and the effect of the baroreceptor control on heart rate. This model is built on the closed loop ventricular interaction model of Chung et.al. (1997) and Olansen et.al. (2000). The resulting impact of the Valsalva manoeuvre on aortic pressure and heart rate are measured. Their results are shown to match experimental trends. However, only the dynamic response of the aortic pressure is reported, the variations in pulmonary artery pressure and blood flow through the pulmonary circulation are absent.

8.2.4 Simulation of Cardiopulmonary Interaction

All model verification of cardiopulmonary dynamics is tested against the experimental work by Scharf et.al. (1979; 1980). As with simulations of ventricular interaction, there is only minimal information available on the mechanical properties of the canine cardiovascular systems employed. For this reason, the generic human parameters used in the static verification in Chapter 5 are used.

A significant contributor to cardiopulmonary interaction is the time varying nature of the pulmonary vascular resistance. This resistance is represented in the model by the pulmonary resistance (R_{pul}), as shown in Figure 2.1. During mechanical ventilation pulmonary vascular resistance increases as lung volume increases due to stretching of the lung walls and the resulting effect on the intra-alveolar vessels [Scharf and Cassidy, 1989]. However, the exact relationship between pulmonary vascular resistance and lung volume is non-linear [West, 1985; Lu et al., 2001]. To maintain simplicity in the model while obtaining the basic trends for verification, a linear relationship between time varying pulmonary resistance ($R_{pul}(t)$) and lung volume (V_{lungs}) is assumed for mechanical ventilation.

$$R_{pul}(t) \propto V_{lungs}(t) \tag{8.1}$$

During mechanical ventilation the thoracic pressure can be assumed to be proportional to the lung volume, for normal changes in volume [West, 1985].

$$V_{lungs}(t) \propto P_{th}(t) \tag{8.2}$$

Therefore, by combining Equations (8.1) and (8.2), a linear relationship between $R_{pul}(t)$ and the thoracic cavity pressure (P_{th}) is assumed.

The following definition is used to approximate the pulmonary vascular resistance ($R_{pul}(t)$) as a function of P_{th}.

$$R_{pul}(t) = R_{pul}(\text{relaxed}) \left[1 + \left\{R_{pul}(\text{multi}) - 1\right\}\left\{\frac{P_{th} - P_{th}(\text{relaxed})}{\Delta P_{th}}\right\}\right] \tag{8.3}$$

where $R_{pul}(\text{relaxed})$ and $P_{th}(\text{relaxed})$ is the pulmonary vascular resistance and thoracic cavity pressure when the lungs are relaxed at end-expiration, $R_{pul}(\text{multi})$ is a factor representing the maximum variation in resistance and ΔP_{th} is the maximum variation in thoracic cavity pressure. The factor $R_{pul}(\text{multi})$ defines the maximum amount that the base resistance will be multiplied by at end inspiration. Figure 8.8 shows an example of variations in P_{th} and $R_{pul}(t)$ during positive pressure respiration. For these examples, the base value of R_{pul} is set to 1, defining the pulmonary vascular resistance when the lungs are relaxed.

The value of $R_{pul}(\text{multi})$ is set to 2.5 for positive pressure respiration, indicating the proportional changes in resistance modelled. This value was found by adjusting the value of R_{pul} until the percentage changes in the simulated out-

puts approximately matched the experimental results. This result shows how the model can be used to estimate the magnitude of changes of physiological parameters, such as the pulmonary resistance during ventilation.

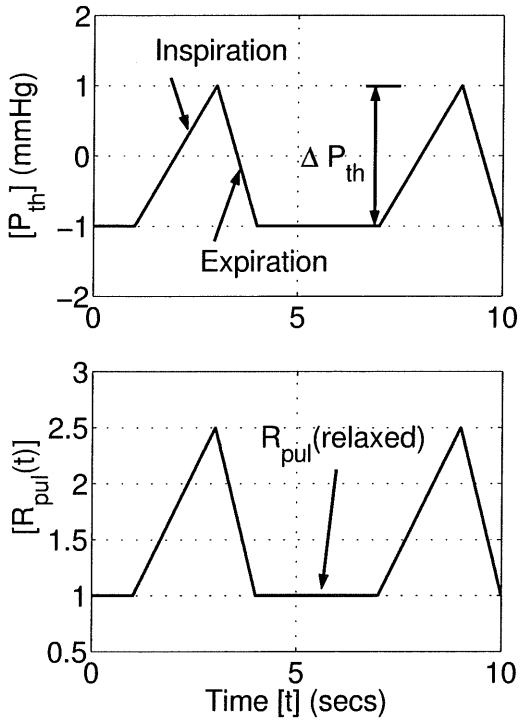

Figure 8.8 Changes in thoracic cavity pressure (P_{th}) and pulmonary vascular resistance ($R_{pul}(t)$) during positive pressure respiration.

Experiments by Scharf et.al. (1979; 1980) measured variations in arterial flow rates and pressures, and the pleural pressure during ventilation. Table 8.1 outlines which model variables are used to represent each experimental variable. The pleural pressure (P_{PL}) is represented in the model as the thoracic cavity pressure (P_{th}). The experimentally measured variation in pulmonary artery pressure (P_{pa}) correlates to the pulmonary artery pressure in the model (P_{pa}). The measured systemic artery pressure (P_{art}) is simulated in the model as the pressure in the aorta (P_{ao}). The blood flow rates through the pulmonary artery ($\dot{Q}_{pa}$) and the aorta ($\dot{Q}_{ao}$) are simulated in the model as flow through the pulmonary valve (Q_{pv}) and the aortic valve (Q_{av}) respectively. The right and left atrial pressures (P_{ra} and P_{la}) are not included in the basic minimal model.

Description	Scharf et.al. (1979; 1980)	Model Equivalent
Thoracic cavity pressure	P_{PL}	P_{th}
Pulmonary artery pressure	P_{pa}	P_{pa}
Pressure in aorta	P_{art} or P_{ao}	P_{ao}
Pulmonary artery flow	Q_{pa} or $\dot{Q}_{pa}$	Q_{pv}
Flow through aorta	Q_{ao} or $\dot{Q}_{ao}$	Q_{av}
Atrial pressures	P_{ra} and P_{la}	Not simulated

Table 8.1 Correlation between model variables and the experimental measurements taken by Scharf et.al. (1979; 1980).

Positive Pressure Respiration

Research carried out by Scharf et.al. (1980) on positive pressure ventilation in anaesthetized dogs was investigated first. Various arterial pressures and flow rates were measured on anaesthetized dogs during positive pressure ventilation. During spontaneous respiration, air flows into the lungs as the pressure in the lungs drops below atmospheric pressure. However, during positive pressure respiration air is forced into the lungs and inspiration is marked by an increase in thoracic cavity pressure above atmospheric.

System parameters for the CVS model for these experiments include a respiratory rate of 10 breaths per minute, and a heart rate of roughly 160 beats per minute [Scharf et al., 1980]. Time varying pulmonary resistance is set proportional to the thoracic cavity pressure. The thoracic cavity pressure varies between -1mmHg at end-expiration and 1mmHg at end-inspiration. R_{pul}(multi) is set to 2.5 meaning the pulmonary resistance increases by a factor of 2.5 as the pressure increases from -1mmHg to 1mmHg.

Figure 8.9 reproduces experimental results from Scharf et.al. (1980). These results can be compared with the results from simulation of positive pressure respiration shown in Figure 8.10. Note that the model captures all of the major trends in the transient response of the CVS during positive pressure respiration.

The main trends reported by Scharf et.al. (1980) include the immediate drop in Q_{pv} and rise in P_{pa} with inspiration, and the immediate opposite response with expiration. The initial, temporary rise in P_{ao} followed by a significant drop during inspiration is also reported. The minimal model results in Figure 8.10 capture all of these trends. Of particular note is the delayed drop of Q_{av} experimentally measured to be about 0.75 seconds after the drop of Q_{pv}. Figure 8.11 plots the variations in Q_{pv} and Q_{av} from Figure 8.10, which are scaled to highlight the

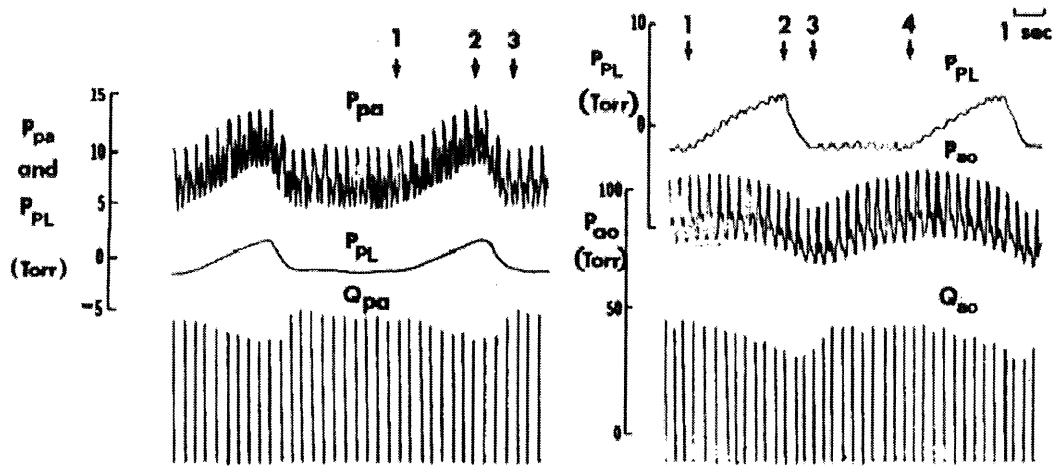

Figure 8.9 Experimental data measured during positive pressure respiration [Scharf et al., 1980].

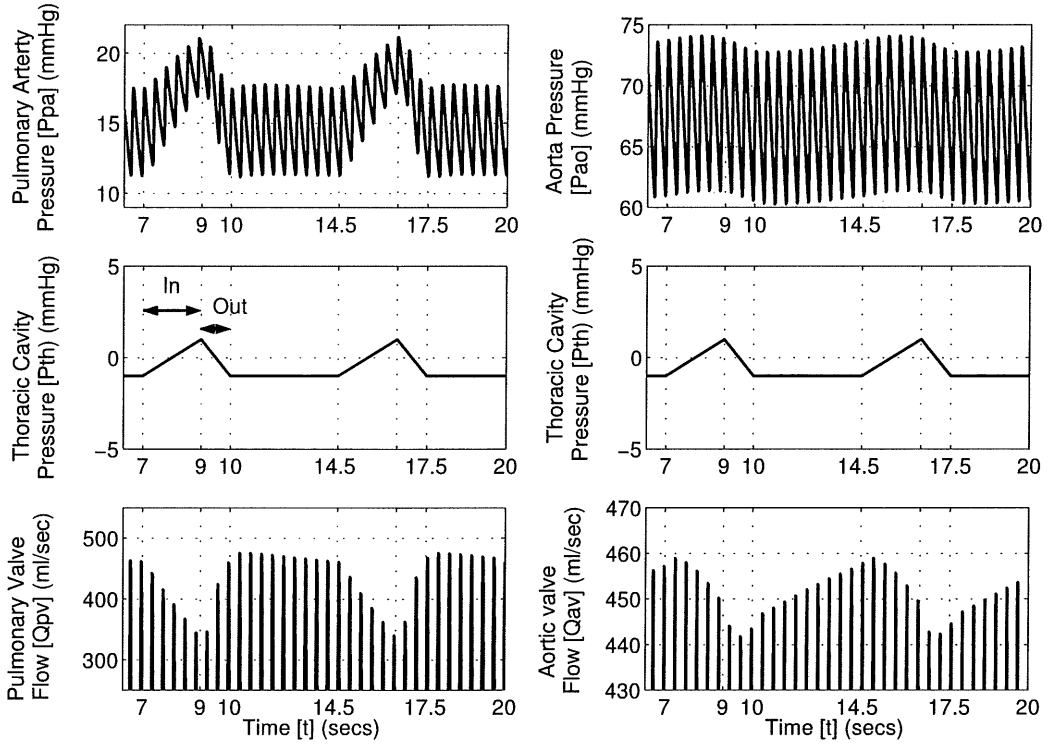

Figure 8.10 Simulated changes in CVS dynamics during positive pressure respiration with time varying pulmonary resistance (In=inspiration, Out=expiration).

lag of Q_{av} behind Q_{pv}. A lag of approximately 0.5 seconds in the initial drop and about 0.75 seconds in the minimum values is evident in the minimal model simulation results.

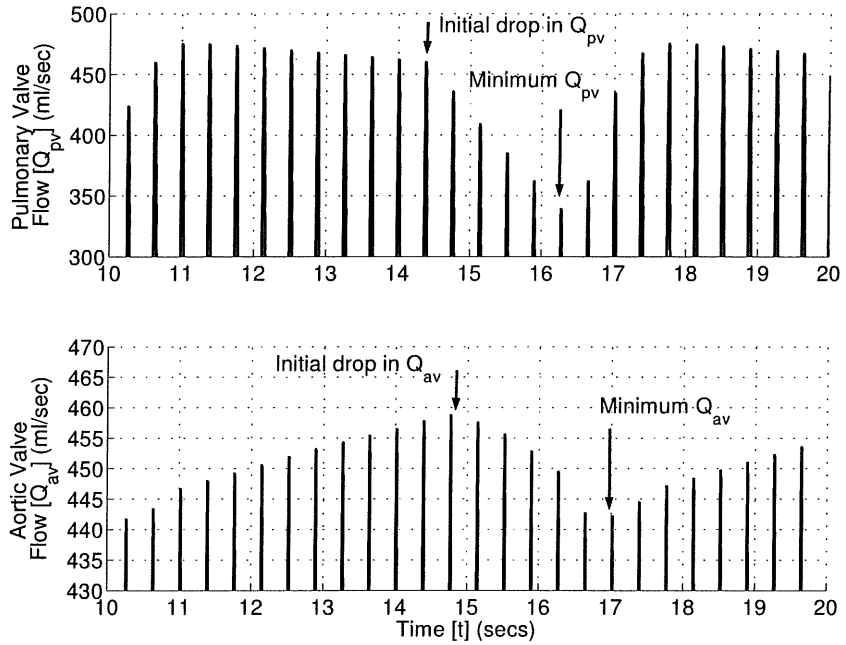

Figure 8.11 Scaled view the Q_{pv} and Q_{av} plots from Figure 8.10 showing Q_{av} lags Q_{pv} by approximately 0.75 seconds.

During positive pressure inspiration the pressure in the thoracic cavity rises, which results in a drop in right ventricle filling pressure. This decreased filling pressure means the stroke volume of the right ventricle drops, as evidenced by the drop in pulmonary artery flow (Q_{pv}). The increase in P_{th} also causes a drop in left ventricle afterload, causing a short term increase in flow through the aorta. The short term increase in Q_{av} causes a temporary rise in P_{ao} before flow rate decreases due to the increase in thoracic cavity pressure, causing a drop in cardiac output.

As with ventricular interaction, a key advantage of using computer simulations of cardiopulmonary function, instead of experimental work, is the ability to easily include or remove various physiological functions. As an example, Figure 8.12 shows the model outputs with constant pulmonary resistance. Comparing Figure 8.10 with Figure 8.12 shows that the constant resistance model is able to capture all of the changes except the pulmonary artery pressure (P_{pa}). Minimal attention is focused on the variations in P_{pa} as it is simply thought to be varying with the thoracic pressure. However, these graphs show that without time varying pulmonary resistance the response of P_{pa} is significantly different.

Figure 8.12 shows that without time varying pulmonary resistance, the pul-

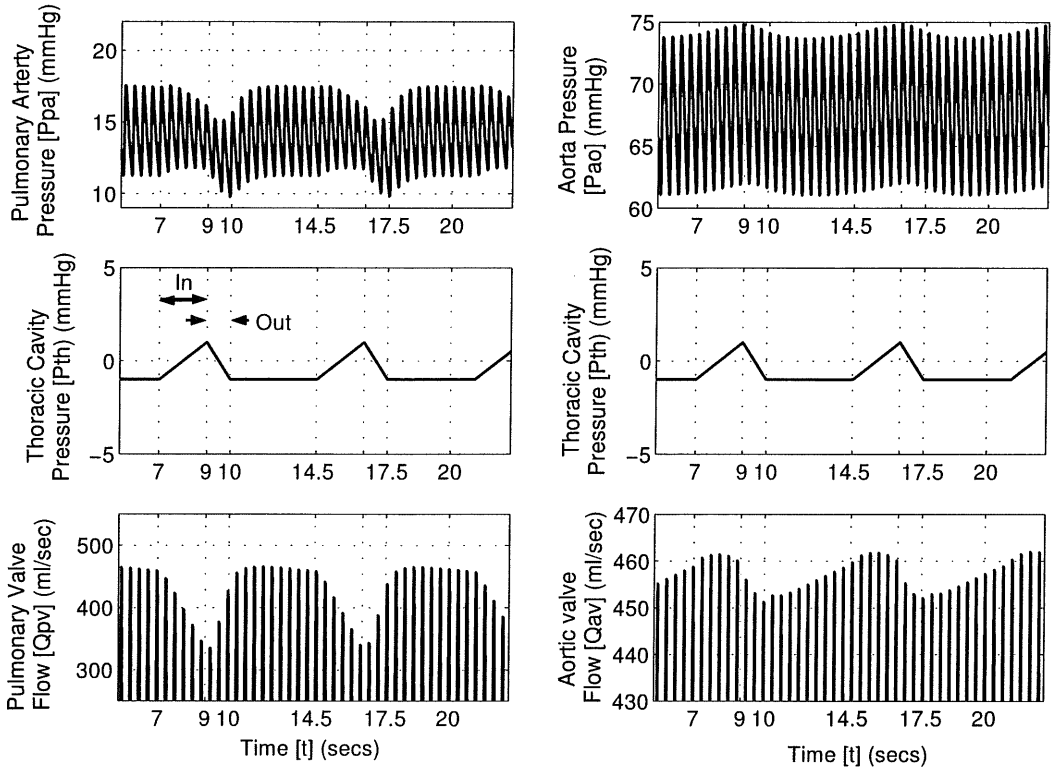

Figure 8.12 Simulated changes in CVS dynamics during positive pressure respiration with constant pulmonary resistance (In=inspiration, Out=expiration).

monary artery pressure does not respond in a physiologically accurate manner. With constant R_{pul} the rise in thoracic pressure causes a drop in pulmonary artery pressure due to the drop in cardiac output of the right ventricle, as evidenced by the drop in Q_{pv}. This drop continues through inspiration and rises again during expiration to the original value. The inclusion of time varying pulmonary resistance ($R_{pul}(t)$) causes the pulmonary resistance to rise during positive pressure inspiration. Figure 8.10 shows that this rise results in a rise in P_{pa} as the increased resistance further restricts flow through the pulmonary circulation system, and blood builds up in the pulmonary artery. Thus, it is shown that the pressure in the pulmonary artery is not simply caused by the increase in thoracic pressure, but more likely by the increase in pulmonary resistance.

Spontaneous Respiration

A second verification of model function is a simulation of experimental results measured by Scharf et.al. (1979) on spontaneous respiration in anaesthetized

dogs. The experimental procedure involved carrying out a bilateral cervical vagotomy on the dogs, which involves removing the effect of the vagal reflex on the heartrate. This procedure produces conditions that more accurately match the model, which does not directly simulate the activation of these reflex responses. The airway is restricted, resulting in laboured breathing and slightly higher thoracic pressure changes from a minimum of -8mmHg to a maximum of 0mmHg. The respiration rate was set to 10 breaths per minute and the heart rate is set to 150 beats per minute to match the experimental conditions.

During spontaneous respiration air is sucked into the lungs and lung volume is now assumed to be inversely proportional to thoracic pressure.

$$V_{lungs}(t) \propto \frac{1}{P_{th}(t)} \tag{8.4}$$

It is expected that pulmonary vascular resistance (R_{pul}) will still be proportional to lung volume, as defined in Equation (8.1), due to lung wall stretching. However, in order to match experimental results, it was found that R_{pul}(multi) must be reduced to 0.4 for spontaneous respiration. Interestingly, setting R_{pul}(multi) to a value of less than 1 simulated a decrease in pulmonary vascular resistance during spontaneous inspiration as the lung volume is increasing. This implies that during spontaneous respiration, there is an inverse relationship between lung volume and the value of R_{pul}.

During positive pressure ventilation the pulmonary vascular resistance increases when air is forced into the lungs during inspiration causing axial stretching or compression of alveolar capillaries [West, 1985; Lu et al., 2001]. This implies that pulmonary vascular resistance is proportional to lung volume during mechanical ventilation. However, it is unclear from the literature how R_{pul} varies during spontaneous ventilation where air is sucked into the lungs. To match experimental data, it is found that R_{pul} must be decreased during spontaneous ventilation. A potential explanation for the inverse relationship between lung volume and R_{pul} is that during spontaneous ventilation the alveolar vessels are not compressed because lung expansion is driven by expansion of the surrounding cavity. In addition, there may be radial stretching of extra-alveolar causing an increase in vessel diameter, and a corresponding decrease in R_{pul}.

The experimental data measured by Scharf et.al. (1979) is reproduced in Figure 8.13. Figure 8.14 plots the simulated response of the CVS due to equivalent changes in thoracic cavity pressure. By comparing Figure 8.13 with Figure 8.14

it can be seen that the simulated results capture all of the major trends in the experimental results.

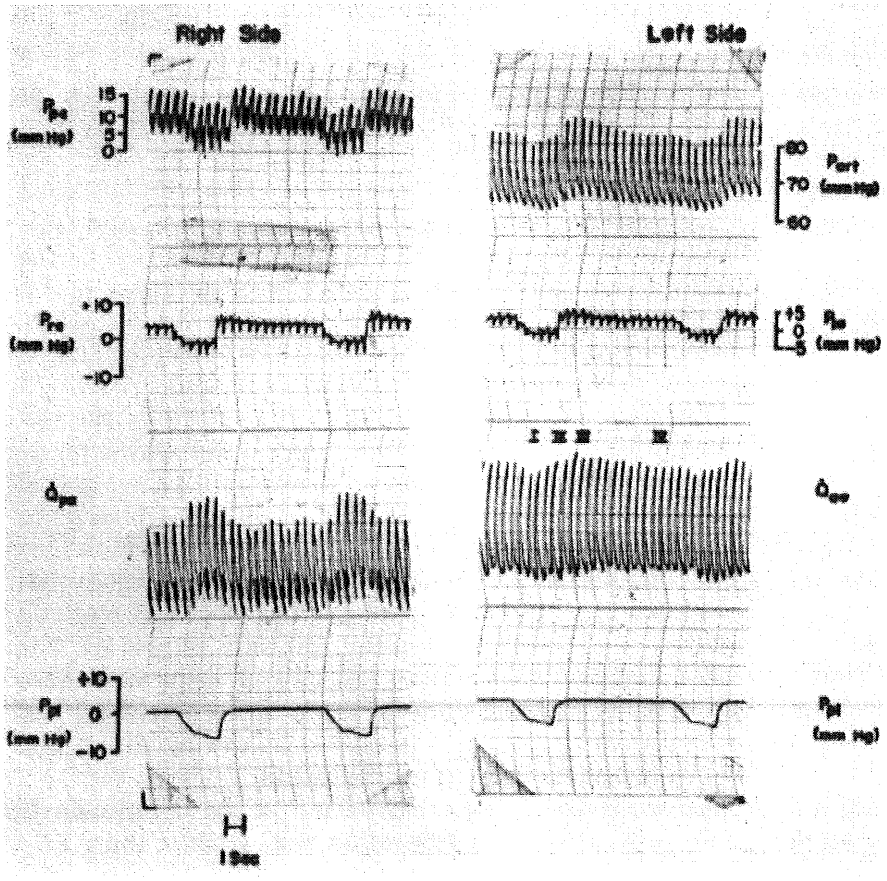

Figure 8.13 Experimental data measured during laboured spontaneous respiration [Scharf et al., 1979].

Scharf et.al. (1979) divides the changes in aortic pressure into four stages during the respiratory cycle. Stage I occurs at the onset of inspiration and is characterised by a temporary decrease in flow rate through the aorta. Stage II labels the subsequent rise in aortic flow rate. Stage III occurs at the beginning of expiration and involves a temporary rise in aortic flow rate. Finally, stage IV labels the return of the aortic flow to a steady state value. The model results in Figure 8.14 are seen to capture all of these stages, as labelled in the graph of Q_{av}.

During early inspiration the thoracic cavity pressure drops significantly, causing an increase in right ventricle filling pressure. This increase in filling pressure results in an increase in right ventricle stroke volume, which is shown by the increase in flow rate through the pulmonary artery (Q_{pv}) in Figure 8.14. The drop in thoracic pressure also means the left ventricle afterload increases and the

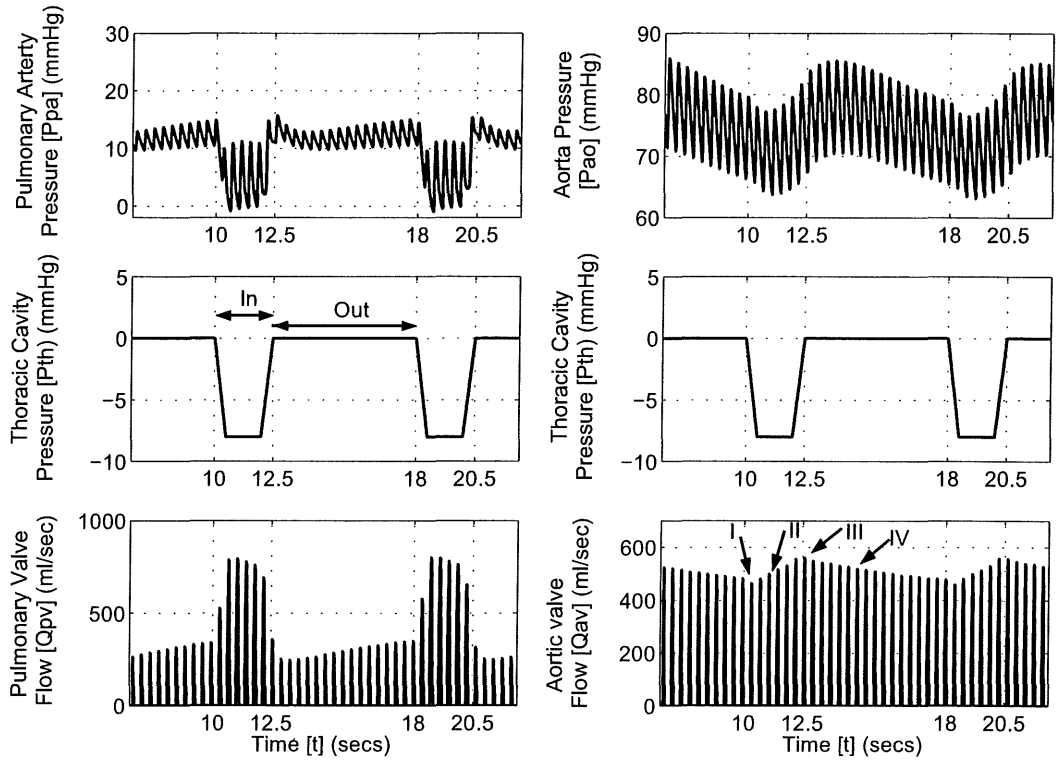

Figure 8.14 Simulated changes in CVS dynamics during laboured spontaneous respiration with time varying pulmonary resistance (In=inspiration, Out=expiration).

stroke volume of the left ventricle decreases, as shown by the short term drop in aortic flow rate (Q_{av}). A couple of heart beats after inspiration begins, the drop in left ventricle output causes the aortic pressure (P_{ao}) to begin to decrease. This change in aortic pressure decreases the left ventricle afterload and the aortic flow builds up again.

As the thoracic pressure rises again at the beginning of expiration the right ventricle filling pressure decreases and the pulmonary artery flow rate drops off. The flow through the aorta increases and overshoots slightly before dropping off and settling toward a steady state solution. The overshoot results from the sudden increase in thoracic pressure and the resulting drop in left ventricle afterload. However, after a couple of heart beats the drop in stroke volume of the right ventricle causes the left ventricle output to decrease as well.

Figure 8.15 plots the same response presented in Figure 8.14, but with a constant pulmonary vascular resistance (R_{pul}). Again, it can be seen that without time varying pulmonary resistance the pulmonary artery pressure does not respond in a physiologically accurate manner. As thoracic pressure drops during

early inspiration, Figure 8.15 shows that it causes an immediate drop in pulmonary artery pressure (P_{pa}). However, this drop is short lived and the eventual response is a significant rise in P_{pa}. The drop causes a sudden increase in blood flow into the pulmonary artery and pulmonary artery blood volume increases as a result of the increased pulmonary resistance (R_{pul}). With time varying pulmonary resistance, this resistance drops during inspiration and limits the build-up of blood in the pulmonary artery. Thus, the inclusion of time varying pulmonary resistance produces much more physiologically accurate results, matching the experimental results of Figure 8.13.

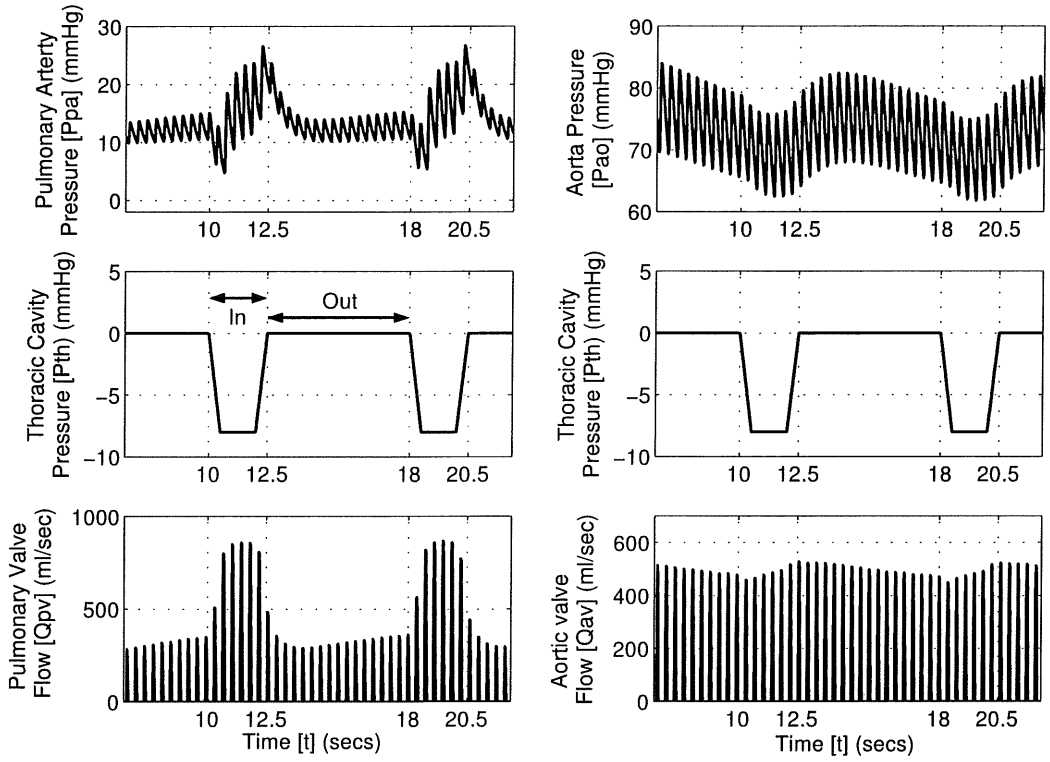

Figure 8.15 Simulated changes in CVS dynamics during laboured spontaneous respiration with constant pulmonary resistance (In=inspiration, Out=expiration) .

8.2.5 Cardiopulmonary Interactions Summary

The minimal model developed shows very good correlation with experimentally measured data investigating the haemodynamic effects of cardiopulmonary interactions. The model captures all of the major trends, but the limited availability of patient specific parameters restricts its ability to match the explicit magnitudes of changes. These two examples show the capability of the model to explicitly

delineate the contribution of time varying pulmonary resistance to CVS haemodynamics. It is found that the changes in pulmonary vascular resistance contributes significantly to the changes seen in experimentally measured pulmonary artery pressure, but only minimally to other areas of the CVS. Removal of time varying resistance in the pulmonary circulation from experimental measurements is impossible, but removing it from the CVS model is simple. These results explicitly defined the contributions and impact of pulmonary vascular resistance (R_{pul}).

8.3 Summary

The dynamic verification examples in this chapter have shown the capability of the minimal CVS model presented to capture significant and complex transient changes in CVS dynamics. The transient effects of both ventricular and cardiopulmonary interactions on CVS haemodynamics have been investigated and compared with experimental data. Most other full CVS models found in the literature are verified only against the static responses of the CVS and none capture the transient dynamics of ventricular interaction. The minimal model is the first known example of a full closed loop model that is robust enough to simulate the dynamics of many areas of the CVS. Therefore, these results represent a significant advance over previous models that focus on simulating the static responses of a particular CVS function. Now that the minimal model is verified to simulate both static and transient CVS function, the next step involves testing its ability to capture specific types of CVS dysfunction.

Chapter 9

Simulating Disease State

Studying the causes of heart disease and the resulting effects on CVS dynamics can be a complex task of differentiating mechanical interactions and adaptive reflex responses. Medical staff faced with measured patient data, such as pressures and cardiac output, must attempt to identify the cause of CVS dysfunction. However, measured patient data also includes the effect of various autonomic reflex actions that act to change CVS properties, such as peripheral resistances, heart rate and the stressed blood volume. If the minimal model can be used to simulate different types of CVS dysfunction, then it can also be used to gain a more detailed understanding of the relative contributions of different mechanical and reflex actions to CVS function.

This chapter investigates the ability of the model to simulate different types of CVS dysfunction commonly encountered in critically ill patients where quick, accurate diagnosis can be essential to patient survival. The first section focuses on dysfunction directly associated with the heart and how it can be simulated using the minimal model. In particular, myocardial dysfunction and valvular disorders are simulated, and compared with known physiological responses. The second section investigates shock states, their impact on CVS function, and the impact of different reflex actions. Each different dysfunction is simulated by adjusting the appropriate minimal model parameters, however the complex interactions prevent exact knowledge of the physiological changes. Therefore, these parameters are adjusted well beyond physiologically realistic limitations, to highlight the resulting impact on CVS haemodynamics and to clearly illustrate the trends in dynamic response.

9.1 Heart Failure

Heart failure can be caused by inadequate ventricle filling, classified as diastolic dysfunction, and/or inadequate ejection of blood, classified as systolic dysfunction. This section investigates myocardial and valvular disorders that are the most common causes of these two basic types of cardiac dysfunction. The focus is primarily on left ventricle failure, as it is more common than right heart failure and has a much more catastrophic impact on CVS function [Katz, 2002]. Minimal model function is compared with known CVS trends and schematic illustrations from medical references showing the effects of various types of heart dysfunction on ventricle pressures and volumes.

9.1.1 Myocardial Dysfunction

Myocardial dysfunction relates to abnormalities in the cardiac muscle that impact on the hearts ability to pump. Diastolic dysfunction caused by myocardial disorders, such as myocardial ischemia and hypertrophy, affect the elastance of the ventricle during diastole. Systolic dysfunction due to cardiac muscle disorders, such as acute myocardial infarction, primarily result in a drop in left ventricle contractility or the strength of contraction of the heart. In many cases myocardial dysfunction affects both systolic and diastolic function simultaneously, however this research investigates the independent contributions [Braunwald, 1997].

Diastolic Dysfunction

Diastolic dysfunction caused by myocardial disorders, such as ischemia or hypertrophy, limits the ability of the heart to relax so blood can enter the ventricle during diastole. Ischemia occurs when the myocardium is not supplied with enough oxygen, perhaps due to a blocked artery or some other cause of diminished cardiac output. Myocardial hypertrophy is an expansion of the ventricle walls, usually as a long term result of increased ventricle loading, such as in aortic stenosis where the aortic valve fails to open properly. Both myocardial ischemia and hypertrophy impede diastolic function by limiting the ability of the ventricle to expand during diastole. The effect of this dysfunction can be simulated by increasing the ventricle elastance at end-diastole, represented in the model by the parameter P_0 in Equation (2.2), and changing the EDPVR. A heart with a high diastolic elastance is often referred to as a "stiff" heart.

Figure 9.1(a) shows a PV diagram illustrating the impact of increased end-diastolic elastance on the cardiac cycle where the gradient of the ESPVR line has increased [Braunwald, 1997]. Increased end-diastolic elastance is simulated by significantly increasing $P_{0,lvf}$ by a factor of 10, as shown in Figure 9.1(b). Both figures show the cardiac cycle moving to the left on a PV diagram due to the modified ESPVR. Diastolic dysfunction is characterised by an increase in ventricle filling pressure, a decrease in ventricle volume, diminished cardiac output, and in the absence of reflex responses, a drop in end-systolic pressure. The minimal model results in Figure 9.1(b) show that the model captures all of these trends. Figure 9.1(a) is a schematic illustration specifically focused on end-diastolic function and does not show changes in end-systolic pressure.

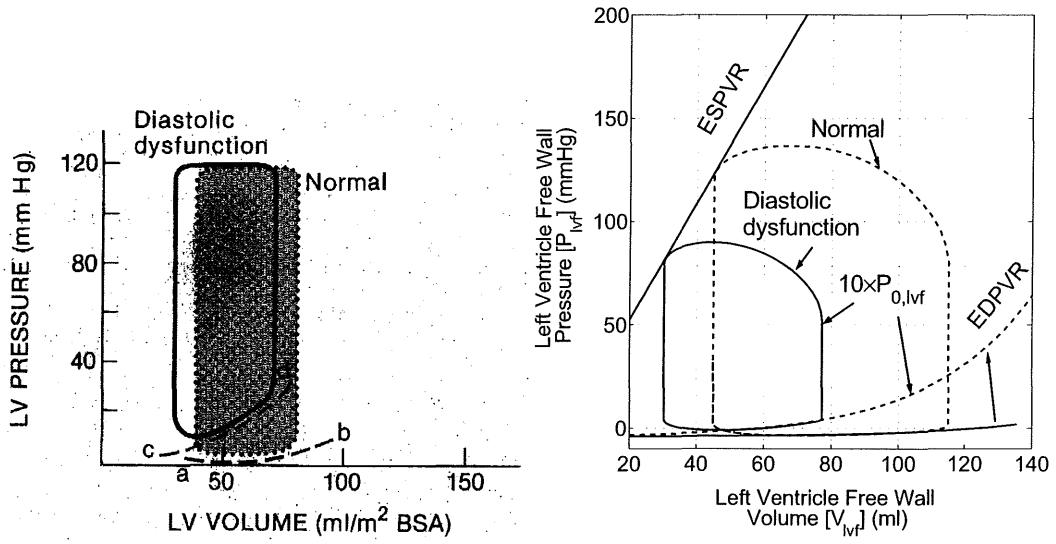

(a) Effect of diastolic dysfunction causing an increase in ventricle elastance on a PV diagram of the left ventricle [Braunwald, 1997].

(b) Minimal model simulated drop in left ventricle diastolic elastance.

Figure 9.1 Comparison of diastolic dysfunction schematic with simulated results.

Systolic Dysfunction

Myocardial infarction occurs where myocardium tissue has died due to lack of oxygen and can lead to catastrophic heart failure. The main impact of myocardial infarction is a drop in ventricle contractility because the weakened heart is no longer able to eject an adequate amount of blood. Decreased contractility is simulated in the minimal model by decreasing the parameter E_{es} in Equation (2.1),

which decreases the slope of the ESPVR. Characteristic haemodynamics of decreased contractility include increased ventricle preload, a rise in ventricle volume, a drop in stroke volume, and decreased systemic pressure [Kumar and Parrillo, 1995; Braunwald, 1997].

Figure 9.2(a) schematically shows the impact of decreased contractility due to systolic dysfunction on a PV diagram. This figure can be compared with the simulated response of halving the left ventricle contractility of the model ($0.5 \times E_{es,lvf}$), shown in Figure 9.2(b). The drop in contractility causes a shift in the cardiac cycle to the right, increasing the ventricle volume. This shift also causes a rise in the diastolic pressure resulting in an increase in ventricle preload. Figures 9.2(a) and 9.2(b) show the decrease in stroke volume, resulting in a drop in cardiac output, that matches known physiological trends. Figure 9.2(b) also shows how decreased contractility causes a drop in end-systolic pressure. The drop in end-systolic pressure is not evident in Figure 9.2(b), perhaps because this graph plots results after reflex actions such as vaso-constriction have been actuated to raise the arterial pressure.

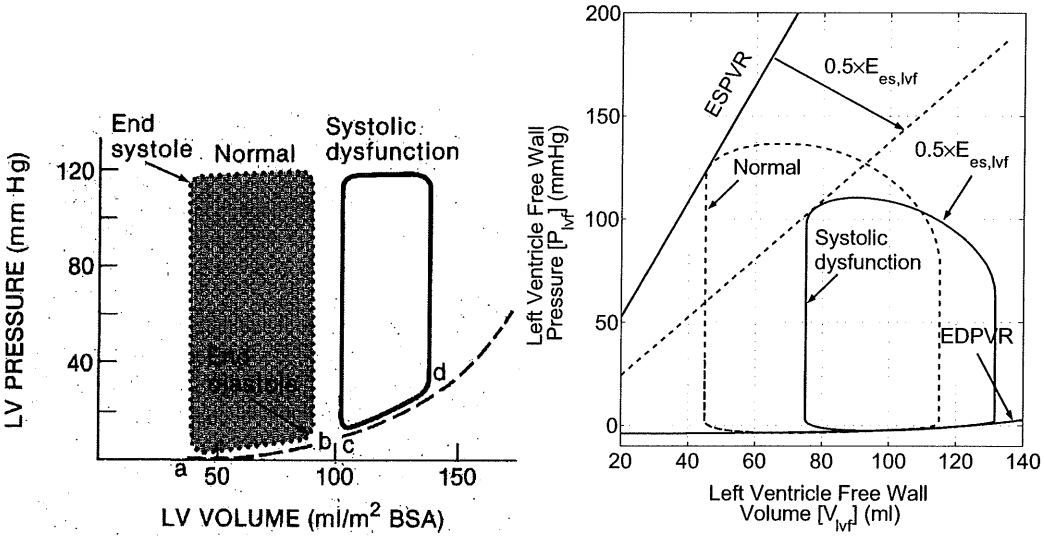

(a) Effect of systolic dysfunction causing a drop in contractility on a PV diagram of the left ventricle [Braunwald, 1997].

(b) Minimal model simulated decrease in left ventricle contractility.

Figure 9.2 Comparison of systolic dysfunction schematic with simulated results.

PV diagrams from the literature showing different types of myocardial dysfunction were found to differ significantly depending on the experimental techniques used. The PV diagram in Figure 9.3 shows the impact of reduced con-

tractility [Parrillo and Bone, 1995]. Where a patient is found to have symptoms of reduced contractility, a vasodilator is often administered to reduce peripheral resistance. This reduction causes a recovery in cardiac output, but at the expense of a drop in blood pressure. The hatched region in Figure 9.3 shows how administering the vasodilator causes an increase in stroke volume that is directly related to cardiac output and a drop in end-systolic pressure, which accompanies a drop in mean arterial pressure. Figure 9.4 repeats Figure 9.2(b) and shows the simulated minimal model response of the CVS due to decreased contractility, as well as results from halving the systemic resistance ($0.5 \times R_{sys}$) to model the effect of a vaso-dilator. The model is seen to capture the increase in stroke volume and decrease in end-systolic pressure that occurs as a result of vasodilator administration. This example highlights the ability of the model to assist medical staff in choosing suitable therapies for different types of cardiac dysfunction by simulating the known effect of a drug and identifying its impact on the CVS.

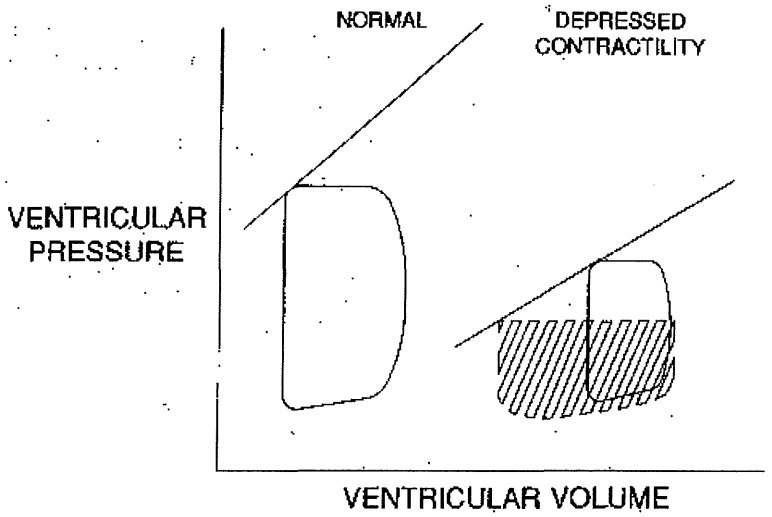

Figure 9.3 Effect of decreased contractility and administration of a vasodilator (hatched) [Parrillo and Bone, 1995].

9.1.2 Valvular Disorders

Heart valves play a critical role in the pumping function of the heart, so valvular disorders can often be life threatening. There are two main types of valvular disorders, valvular stenosis and valvular insufficiency. Valvular stenosis occurs when a heart valve doesn't open properly, causing a much higher resistance to blood flow passing through the valve and decreasing flow rate. Valvular insuffi-

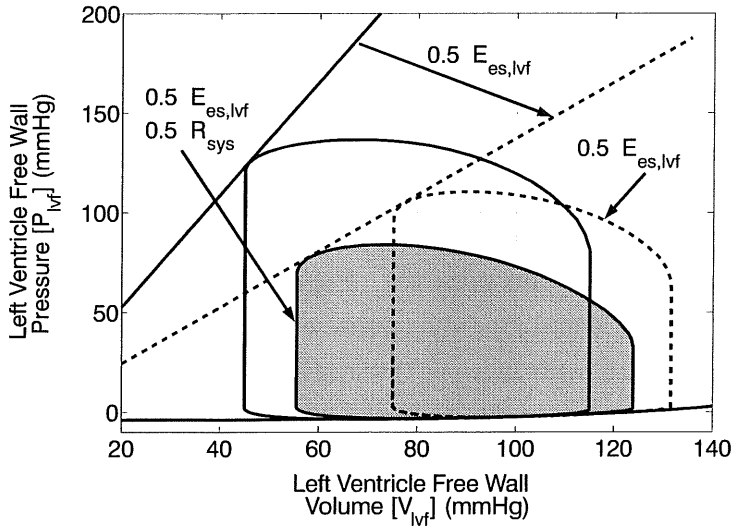

Figure 9.4 Minimal model simulated effect of decreased left ventricle contractility (dashed line) and decreased resistance simulating administration of a vasodilator (shaded area).

ciency, also known as valvular regurgitation, results from inadequate closure of a heart valve, causing blood to flow backwards through the valve when it should be closed. This results in a decrease in the pumping ability and stroke volume of the ventricle.

This section investigates both types of valvular dysfunction for the aortic and mitral valves. The trends in aortic valve dysfunction are compared with published illustrations of ventricular function, as well as the overall impact on CVS dynamics. However, the subtle dynamic variations in atrial pressures cannot be simulated by the model in its current form as it does not include atria. The author was also unable to find suitable graphical representations of mitral valve dysfunction in the literature. For these reasons, only the general effects of mitral valve disorders are investigated and results are not graphically compared with physiological results.

Valvular Stenosis

The most common cause of valvular stenosis, particularly in the elderly, is calcium deposition on the surface of the valve, which limits the valves ability to open properly. Characteristic haemodynamic consequences of aortic stenosis include increased left ventricle systolic pressure and decreased average aortic

pressure [Braunwald, 1997]. The middle panel in Figure 9.5 illustrates the impact of aortic stenosis resulting in an increase in the difference between the maximum left ventricle pressure and the maximum aortic pressure (max P_{lv}- max P_{ao}). This increased difference is caused by the larger pressure drop across the aortic valve as a result of the higher resistance.

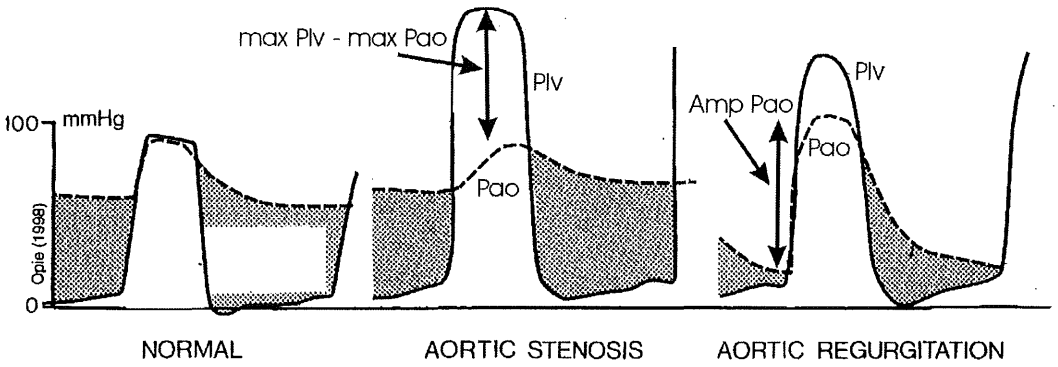

Figure 9.5 Left ventricle pressure (solid line) and aortic pressure (dashed line) schematic profiles for a normal heart, one with aortic stenosis, and one with aortic regurgitation [Opie, 1998].

Aortic stenosis is simulated in the model by increasing the aortic valve resistance (R_{av}) by a factor of 5. The middle panel of Figure 9.6 shows the simulated response from the minimal model, which is seen to capture the increase in pressure drop across the aorta. The maximum left ventricle pressure (P_{lv}) increases significantly along with a drop in the average pressure in the aorta.

The characteristic haemodynamic response during mitral stenosis is an increase in pulmonary venous pressure, and a decrease in left ventricle volume and stroke volume [Braunwald, 1997]. Mitral stenosis is simulated in the minimal model by multiplying the mitral valve resistance (R_{mt}) by 2. This produces a rise in pulmonary venous pressure from P_{pu}=2mmHg to P_{pu}= 4.2mmHg, a reduction in average left ventricle volume from 80ml to 66ml, and the stroke volume decreases from 70ml to 58ml. As discussed, the model is unable to exactly match measured physiological trends because the model does not include the atria.

Valvular Insufficiency

Aortic insufficiency is characterised by an increase in left ventricle volume and stroke volume, and reduced aortic diastolic pressure [Braunwald, 1997]. Although ventricle stroke volume increases, cardiac output decreases, as much of the

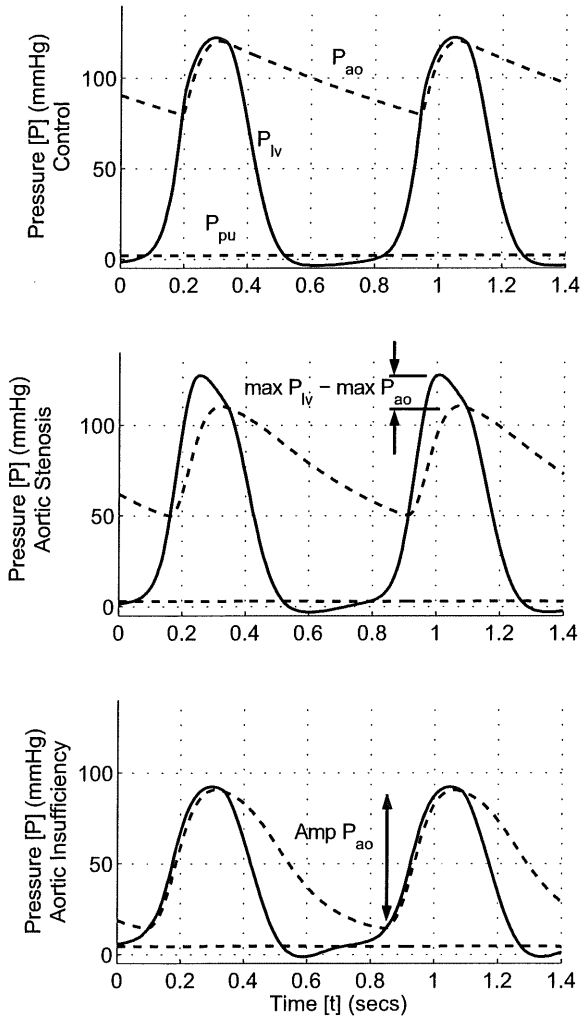

Figure 9.6 Minimal model simulations of left ventricle pressures for a healthy heart valve (top), aortic stenosis (middle) and aortic insufficiency (bottom).

blood pumped into the aorta during diastole can return to the ventricle during diastole. The panel on the right side of Figure 9.5 schematically illustrates the effect of aortic regurgitation on ventricle and aortic pressures. The main trend is a significant increase in the amplitude of variation of the aortic pressure (Amp P_{ao}) as the diastolic aortic pressure decreases.

Valvular insufficiency is simulated in the minimal model by modifying the way the model responds to a change in model state when valves open and close. As discussed in Chapter 4, when the flow rate becomes negative in a normally functioning heart, that flow rate variable is removed from the state vector. To simulate aortic insufficiency, the flow rate variable is not removed from the state vector. Instead, the resistance to the regurgitating flow through that valve is

significantly increased. Therefore, reversing flow has a much higher resistive force acting on it but blood can still return to the ventricle during diastole, which is a physiologically accurate method of simulating valvular insufficiency. When the flow rate becomes positive, the resistance is restored to it's original value.

Aortic insufficiency is simulated by increasing the aortic valve resistance by a factor of 20 when the valve would normally close. The simulated response, plotted on the bottom panel of Figure 9.6, captures most of the haemodynamic trends on the right side panel of Figure 9.5. The average left ventricle volume increased from 80ml to 94ml and the stroke volume increased from 70ml to 120ml. This latter result simulates the swelling of the left ventricle, characteristic of aortic insufficiency. The increase in stroke volume does not indicate an increase in net cardiac output as a significant amount of blood is regurgitating. Figure 9.6 also shows a drop in aortic pressure, matching known physiological response.

Mitral insufficiency is simulated by increasing the mitral valve resistance (R_{mt}) by a factor of 10 when the flow is reversing. The characteristic haemodynamic response due to mitral insufficiency is an increased pulmonary venous pressure (P_{pu}) and an increase in ventricle stroke volume [Braunwald, 1997]. During simulation of aortic insufficiency, P_{pu} increases from a base value of 2mmHg to 3.2mmHg. The stroke volume increases from 70ml to 120ml, although as with aortic insufficiency, this result does not represent a net increase in cardiac output. Once again these trends match known physiological function.

9.1.3 Summary of Heart Failure Simulation

The minimal CVS model presented is used to simulate a variety of different forms of heart disease and the results compared with known physiological trends. Examples include different types of ventricular and valvular dysfunction. The PV diagram is the most common method of investigating ventricular function during heart disease and the minimal model is clearly shown to capture most variations in CVS state that occur during dysfunction. The known effects of a vasodilator are also simulated and the results found to match known response, giving an example of the potential usefulness of the model in predicting CVS response to therapy. These specific cases focus primarily on the function of the heart. The next section investigates shock which, although it is still based heavily on heart function, is also dependent on the state of the peripheral vascular system.

9.2 Shock

Shock is a serious condition, often encountered in intensive care units (ICUs) that frequently leads to progressively worsening patient condition and eventually death. A general definition of shock is *tissue damage due to lack of oxygen and other nutrients*, which can be caused by low cardiac output. Cardiac muscle tissue damage, due to low blood flow, results in a further drop in cardiac output and continued, cyclic worsening of patient condition. For this reason the time taken to diagnose the cause of shock in a patient can be an important factor in patient survival.

Understanding the cause and effect of different types of shock can be difficult as powerful nervous reflex actions in the body are activated to maintain blood pressure and cardiac output [Guyton, 1991]. These reflex actions cause other significant variations in CVS haemodynamics making it difficult to determine the source of dysfunction. This section investigates the ability of the minimal CVS model to capture the haemodynamic trends that occur due to changes in CVS state that result in shock.

Simulations of shock using the minimal CVS model will only capture the CVS dynamics resulting from mechanical interactions, and do not simulate the autonomous activation of reflex actions. However, once the initial response of the CVS due to a particular dysfunction has been identified, the effects of different reflex actions can be manually simulated to determine their relative contribution to CVS response. For example, systolic dysfunction causes a drop in mean arterial pressure. The body typically responds by increasing systemic resistance through vasoconstriction which leads to a recovery in the blood pressure. Thus, reflex actions in the body may hide the effect of a particular dysfunction, confounding attempts to identify or diagnose it.

The shock states simulated are divided into four groups, hypovolemic shock, cardiogenic shock, extracardiac obstructive shock and distributive shock. Hypovolemic shock results from a decrease in circulating blood volume, such as during severe haemorrhage. Cardiogenic shock occurs due to failure of the heart as a pump, such as systolic or diastolic dysfunction. Extracardiac obstructive shock is caused by an obstruction to flow in the CVS. Finally, distributive shock is caused by inflammatory mediators in the blood stream.

Simulations of each different shock state are carried out using the minimal CVS model by changing model parameters to simulate the known causes of each

shock state. The resulting CVS model dynamics, including cardiac output and pressures in the arteries and veins, are then compared with published results [Parrillo and Bone, 1995]. If simulations of the shock state do not match physiologically known changes in CVS dynamics, then reflex changes in certain model parameters are simulated to identify likely reflex actions involved in the response.

The correlation between measured patient data from medical textbooks and the minimal model variables is outlined in Table 9.1. The pulmonary capillary wedge pressure (PCWP) gives a measure of the left ventricle filling pressure and correlates to the pulmonary vein pressure in the minimal CVS model (P_{pu}), as seen in Figure 2.1. The mean arterial pressure (MAP) quantifies the left ventricle afterload and correlates to the CVS model pressure in the aorta (P_{ao}). Similarly, vena-cava pressure from the model represents the central venous pressure (CVP) and indicates right ventricle filling pressure. Finally, the mean pulmonary arterial pressure (PAP) is simulated as the pressure in the pulmonary artery (P_{pa}) and indicates the right ventricle afterload.

Description	Measured Data	Model Variable	Ventricle Boundary Condition
Pulmonary capillary wedge pressure	PCWP	P_{pu}	LV filling pressure
Mean arterial pressure	MAP	P_{ao}	LV afterload
Central venous pressure	CVP	P_{vc}	RV filling pressure
Mean pulmonary arterial pressure	PAP	P_{pa}	RV afterload

Table 9.1 Correlation between measured physiological data and model variables.

For each type of shock simulated, the variations in the 4 peripheral chamber pressures are plotted and the cardiac output noted. The base set of parameters used in each simulation are taken from Table 7.2 in Chapter 7. The steady state pressure variations are labelled as a solid black line, labelled base, in each figure. The effects of shock are then simulated by adjusting parameters away from the base values. For example, the pulmonary resistance is multiplied by a factor of 2 to simulate a pulmonary embolism, where the pulmonary circulation is partially blocked. The resulting change in the steady state CVS solution, after parameters have been changed to simulate shock state, is plotted as a dashed line. Thus, the difference between the solid (base) line and the dashed (shock) line shows the effects of the associated changes as a direct result of the dysfunction,

ignoring reflex actions. Where necessary, some plots have a dotted line showing the effect of a simulated reflex response on the measured pressures. Table 9.2 shows the known physiological response of the cardiac outputs, key pressures and peripheral resistances during different types of shock. Single arrows indicate a mild to moderate change, double arrows ($\downarrow\downarrow$ or $\uparrow\uparrow$) indicate a moderate to severe change and horizontal arrows indicate minimal, if any, change. Note that only trends are shown as specific magnitude values are not available in the literature.

Measured Data	**CO**	**MAP**	**PAP**	**CVP**	**PCWP**	**SVR**	**PVR**
Model Variable	**CO**	P_{ao}	P_{pa}	P_{vc}	P_{pu}	R_{sys}	R_{pul}
Hypovolemic shock	$\downarrow\downarrow$	$\downarrow$	$\downarrow$	$\downarrow\downarrow$	$\downarrow\downarrow$	$\uparrow\uparrow$	$=$
Pericardial tamponade	$\downarrow\downarrow$	$\downarrow$	$\uparrow\uparrow$	$\uparrow\uparrow$	$\uparrow\uparrow$	$\uparrow\uparrow$	$\uparrow\uparrow$
Pulmonary embolism	$\downarrow\downarrow$	$\downarrow$	$\uparrow\uparrow$	$\uparrow\uparrow$	$\downarrow$	$\uparrow\uparrow$	$\uparrow\uparrow$
Septic shock	$\uparrow$	$\downarrow\downarrow$	$\rightarrow\uparrow$	$\downarrow\rightarrow\uparrow$	$\rightarrow\downarrow$	$\downarrow\downarrow$	$\rightarrow\uparrow$
Cardiogenic shock	$\downarrow\downarrow$	$\downarrow$	$\uparrow$	$\uparrow$	$\uparrow\uparrow$	$\uparrow\uparrow$	$\uparrow$
RV-infarction shock	$\downarrow\downarrow$	$\downarrow$	$=$	$\uparrow\uparrow$	$=$	$\uparrow\uparrow$	$\uparrow$

Table 9.2 Known physiological response of CVS variables during different shock states, reproduced from Parrillo and Bone (1995).

9.2.1 Reflex actions

The effect of the most common reflex responses on CVS dynamics are investigated to identify their individual contributions. Important reflex actions include a rise in systemic (R_{sys}) and/or pulmonary (R_{pul}) vascular resistances, increased stressed blood volume (V_{tot}) and increased heartrate (HR) [Guyton, 1991]. Figure 9.7 plots the changes in peripheral pressures for each of the common reflex actions, the effects of which are summarised in Table 9.3.

Model Parameter Adjustment	**CO**	P_{ao}	P_{pa}	P_{vc}	P_{pu}
$2 \times R_{sys}$	$\downarrow$	$\uparrow\uparrow$	$\downarrow$	$\downarrow\downarrow$	$\uparrow$
$4 \times R_{pul}$	$\downarrow$	$\downarrow$	$\uparrow\uparrow$	$\uparrow$	$\downarrow$
$1.5 \times V_{tot}$	$\uparrow$	$\uparrow$	$\uparrow$	$\uparrow\uparrow$	$\uparrow\uparrow$
$2 \times HR$	$\downarrow$	$\downarrow\downarrow$	$\downarrow$	$\downarrow\downarrow$	$\uparrow\uparrow$

Table 9.3 Summary of the CVS response to different common reflex actions, as plotted in Figure 9.7.

Increasing peripheral vascular resistance is a common reflex mechanism of the body to maintain arterial pressure. In almost all cases of shock, with the

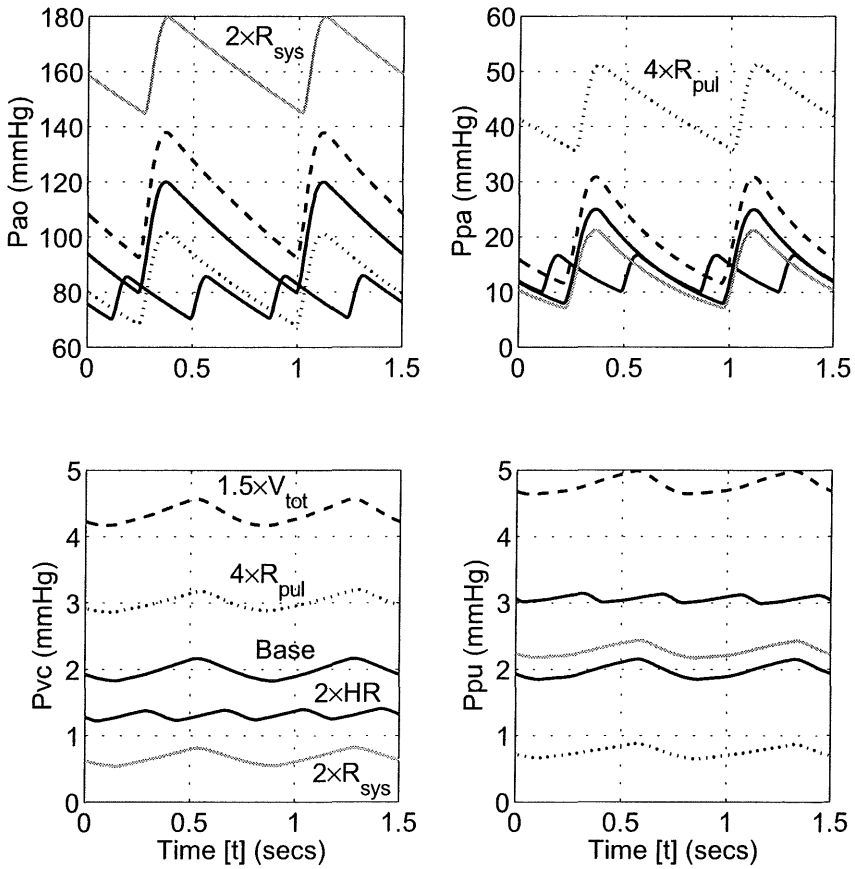

Figure 9.7 Minimal model simulated changes in peripheral pressures due to common reflex response changes in resistance, heartbeat and stressed blood volume.

exception of distributive shock, the body responds by raising peripheral vascular resistance. During shock, the focus of the body's reflex action is on maintaining mean arterial pressure, and the most common method is to raise systemic vascular resistance (R_{sys}). Table 9.3 shows that this increase causes a rise in pressures around the left ventricle (P_{pu} and P_{ao}), particularly in the aorta, but a drop in the remaining pressures and the cardiac output. Increasing pulmonary vascular resistance (R_{pul}) is also a common dynamic reflex response that increases pulmonary artery pressure (P_{pa}). Table 9.3 shows the result is a rise in pressures around the right ventricle, particularly the pulmonary artery, but a drop in all other pressures and the cardiac output.

The body often reacts to shock by increasing the stressed blood volume through venous constriction, where the large blood storage areas in the CVS, such as the veins, contract to push more blood into the stressed volume. Table 9.3 shows that increasing the stressed blood volume (V_{tot}) causes an increase

in cardiac output and all other pressures.

In most cases, the body will increase heartrate to increase cardiac output, however Table 9.3 shows a drop in cardiac output when the heartrate is doubled, in this case from 80 beats per minute to 160 beats per minute. Figure 9.8 plots the typical changes in cardiac output that occur with changes in heartrate during exercise, labelled Ex, and a relatively normal state, labelled SVT [Opie, 1998]. The plots show that the peak cardiac output typically occurs at about 160 beats/min, for the case labelled SVT.

The results in Figure 9.8 can be compared with the simulated changes in cardiac output at different heartrates from the minimal model shown in Figure 9.9. The line labelled Params A is plotted using the optimised parameters in Table 7.2. The peak cardiac output using Params A occurs at a heartrate of about 90 beats/min. The line labelled Params B is the result of the pre-optimisation generic parameters listed in Chapter 5 and reaches a maximum cardiac output at about 140 beats/min. This result shows that the combination of parameters used for the simulations in this chapter, Params A, will not show an increase in cardiac output with increased heartrate as is normally the case. However, the model more accurately simulates the curve shown in Figure 9.8 using an alternative combination of parameters (Params B).

The minimal model uses only a simple method of simulating heartrate that does not account for physiological changes that occur in the heart as the heartrate changes. For example, it is known that the shape of the driver function, shown in Figure 2.4, changes with different heartrates, but how it changes is not well understood [Olansen et al., 2000]. Alternatively, the continued rise in cardiac output could be attributed to the autonomous activation of reflex actions. For example, as heart rate increases the systemic vascular resistance may decrease to further increase cardiac output. Thus, it is difficult to account for large changes in heartrate without knowing the changes in driver function and reflex actions. The model could be used in an inverse fashion to determine these changes and the optimiser can also include such performance metrics as additional objective functions.

9.2.2 Hypovolemic Shock

Hypovolemic shock is the leading cause of death for trauma patients under the age of 45 years [Kumar and Parrillo, 1995]. Hypovolemic shock is caused by a

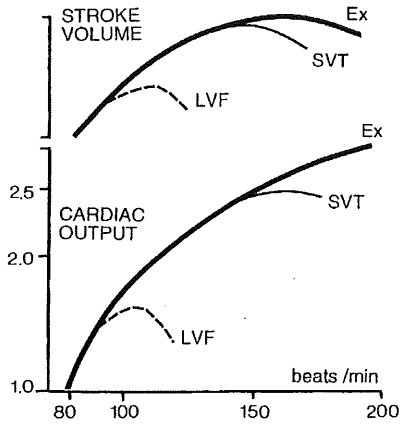

Figure 9.8 Variations in stroke volume and cardiac output with heartrate during exercise (Ex), supraventricular tachycardia (SVT) and left ventricle failure (LVF) [Opie, 1998].

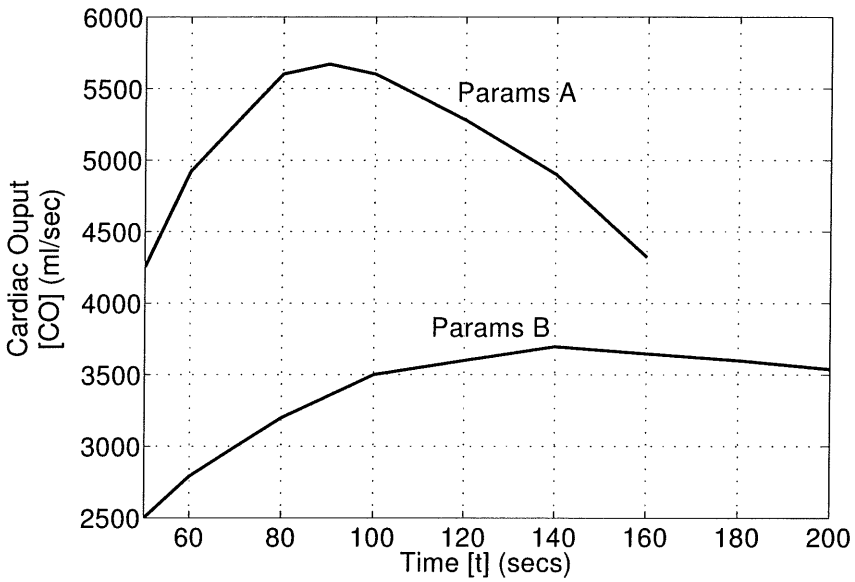

Figure 9.9 Variations in cardiac output versus heart rate for the minimal model with two different sets of parameters.

drop in blood volume, and primarily results in a drop in cardiac output and mean arterial pressure along with a decrease in ventricle filling pressures. To combat the drop in mean arterial pressure, arterioles in the systemic circulation constrict to increase systemic arterial pressure.

Hypovolemic shock is simulated by decreasing the total volume of blood in the minimal model, which represents only the stressed volume in the human CVS, as discussed in Chapter 5. However, the physiological response of the CVS to

a drop in blood volume is constriction of the venous system, which decreases the amount of unstressed blood volume and supplements the total stressed blood volume. After a significant level of blood loss the body will be unable to maintain adequate stressed blood volume and the CVS will fail.

Figure 9.10 plots the peripheral pressures determined by simulation of hypovolemic shock using the minimal CVS model. The dashed line plots the results after a 50% drop in stressed blood volume. All pressures are seen to drop, especially ventricle preload pressures (P_{vc} and P_{pu}), matching known physiological trends in Table 9.3 [Groeneveld and Thijs, 1995]. Cardiac output also drops from the base value of 5.6 L/min to 4.1 L/min. To restore systemic arterial pressure (P_{ao}), the systemic vascular resistance (R_{sys}) increases through arterial vasoconstriction activated by the sympathetic nervous system. This effect is simulated by doubling the systemic vascular resistance ($R_{sys} \times 2$). The dotted line in Figure 9.10 shows that the increase in peripheral resistance restores the mean arterial pressure (P_{ao}), but also results in a further drop in cardiac output to 3.7 L/min, matching the trends in Table 9.3. There is no change in P_{pu} when R_{sys} is doubled, and the plot of P_{pu} is overlaid on the dashed line in Figure 9.10.

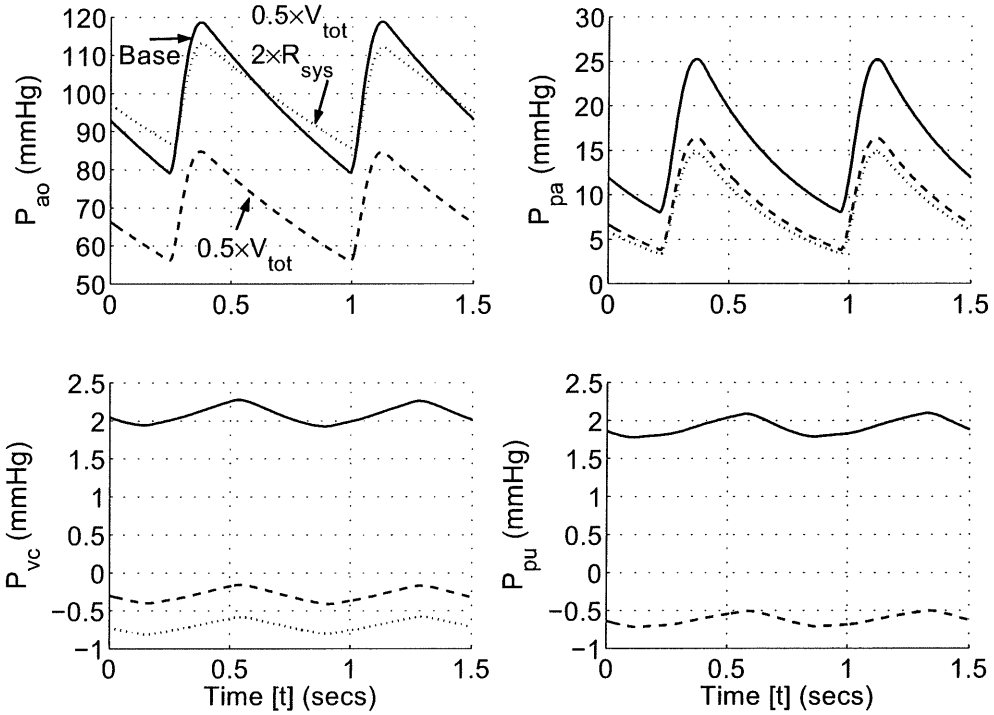

Figure 9.10 Simulation of hypovolemic shock, before blood loss (—), after blood loss (- - -), after blood loss and increased R_{sys} due to reflex action (· · ·) .

9.2.3 Distributive Shock

The mechanisms associated with distributive shock are not well known and it is one of the leading causes of death in intensive care units [Natanson et al., 1995]. Septic shock, alternatively referred to as blood poisoning, is a common type of distributive shock that is characterised by a drop in systemic vascular resistance. This drop is thought to occur due to a drop in vascular auto-regulatory control [Parrillo and Bone, 1995].

Septic shock is simulated in the minimal CVS model by halving the systemic resistance ($0.5 \times R_{sys}$). Figure 9.11 shows the resulting variation in pressures. Cardiac output increases from 5.6 L/min to 6.2 L/min with the drop in systemic resistance. Overall, the model captures the main published physiological responses during septic shock outlined in Table 9.2, including a drop in mean arterial pressure (P_{ao}) and a rise in cardiac output.

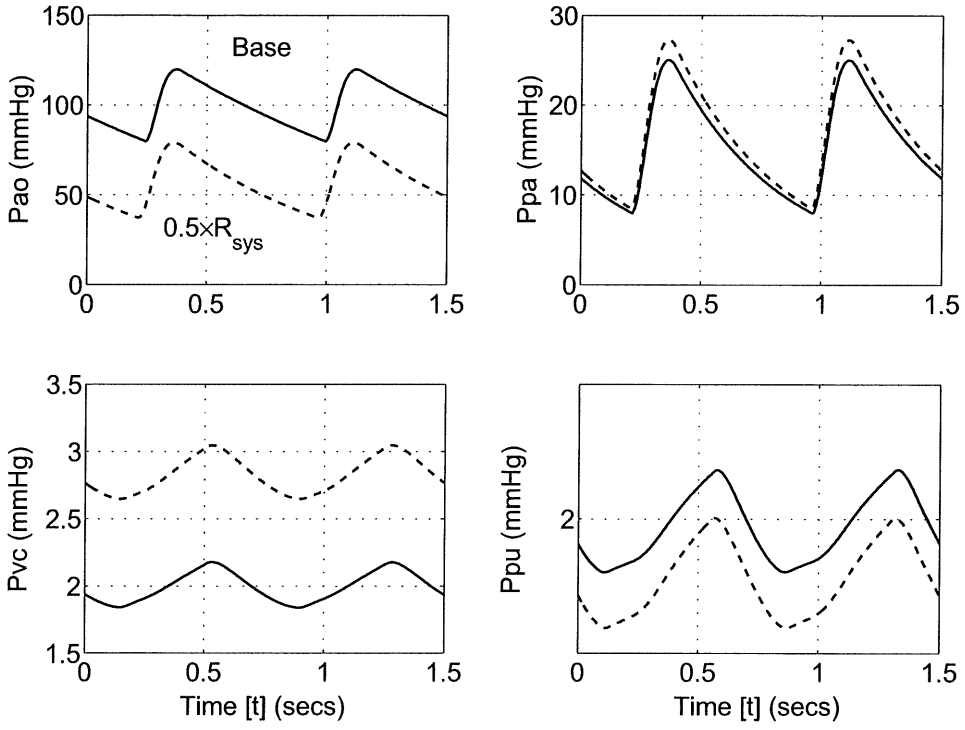

Figure 9.11 Simulation of distributive septic shock, before drop in systemic resistance (—) and after (- - -).

9.2.4 Cardiogenic Shock

Cardiogenic shock results from failure of the heart to pump an adequate amount of blood as a result of damage to the myocardium. Myocardial dysfunction usually results from an infarction, where part of the myocardium dies due to lack of oxygen. The main result of myocardial infarction is a drop in ventricle contractility, represented in the minimal model by the parameter E_{es}.

Cardiogenic shock is generally characterised by an increase in ventricle filling pressures and ventricle volumes, and reductions in both cardiac output and systemic arterial pressure. Hence, less blood is distributed to the tissues, including the myocardium. As a result, further myocardial damage can occur and if this sequence continues, death will rapidly ensue.

Left Ventricle Infarction

Figure 9.12 shows the simulated effects of reduced left ventricle contractility on the peripheral pressures. Contractility is reduced to only 50% of the base value ($0.5 \times E_{es,lvf}$) to emphasise the effects of left ventricle infarction on CVS dynamics. The key results are a drop in both systemic arterial pressure and cardiac output. The cardiac output drops from 5.6 l/min to 2.6 l/min and Figure 9.12 shows a drop in P_{ao}. The literature also refers to a rise in P_{pa}, P_{vc} and P_{pu} during left ventricle infarction [Parrillo and Bone, 1995]. The simulated results are shown to capture the rise in pulmonary venous pressure (P_{pu}), which raises the left ventricle filling pressure and causes the characteristic increase in left ventricle volume. However, the simulated pressures around the right ventricle (P_{vc} and P_{pa}) decrease.

A common reflex action to cardiogenic shock is a rise in both pulmonary and systemic vascular resistance (R_{pul} and R_{sys}). Increasing R_{sys} produces an increase in P_{ao} and P_{pu}, but causes a further drop in P_{vc} and P_{pa}. Increasing R_{pul} causes a recovery in both P_{pa} and P_{vc}. More specifically, P_{pa} increases to greater than the base value, matching published results, but the increase in P_{vc} is not enough to recover the base value. An alternative reflex action is venous constriction which increases the stressed volume of blood in the CVS. Figure 9.12 shows that increasing the stressed blood volume by a factor of 1.5 will cause all of the pressures, except P_{ao}, to increase above base values to match physiological response. Thus, a combination of these reflex actions would cause the simulated model to match the responses outlined in Table 9.2, and may all be involved in

the actual physiological response.

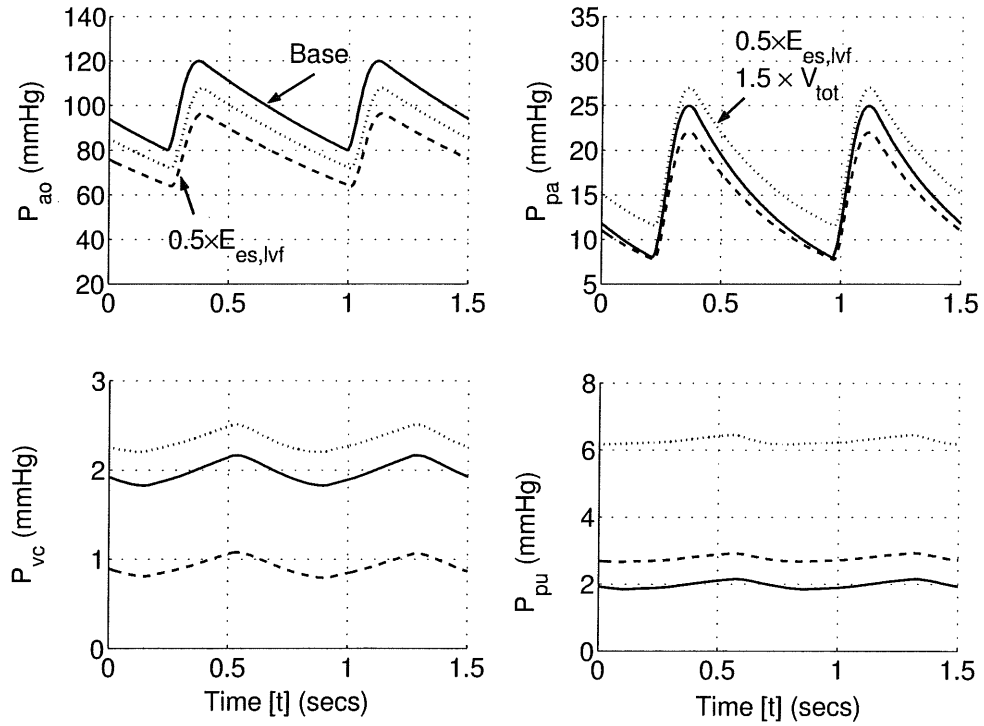

Figure 9.12 Minimal model simulation before (—) and after (- - -) left ventricle infarction, and after increased stressed blood volume (· · ·).

Right Ventricle Infarction

Right ventricle infarction is simulated by reducing the right ventricle contractility ($E_{es,rvf}$) to 50% of the base value ($0.5 \times E_{es,rvf}$). Once again, the model captures the main trends including a drop in mean arterial pressure (P_{ao}), as shown in Figure 9.13 and a drop in cardiac output from 5.6 l/min to 4.8 l/min. The central venous pressure (P_{vc}) increases, matching the response outlined in Table 9.2 of an increase in ventricle preload, and the consequent increase in right ventricle volume. However, the model shows a significant drop in pulmonary venous pressure (P_{pu}) where normal physiological response shows no significant variation in P_{pu} [Parrillo and Bone, 1995].

Figure 9.13 shows that increasing the stressed blood volume of the model (V_{tot}) by a factor of 1.2 causes an increase in P_{vc}, a recovery in P_{ao} and minimal change in the other pressures, matching the responses in Table 9.2. Therefore, it is likely that reflex changes that increase stressed blood volume are a major

contributing factor in the physiological response to right ventricle infarction.

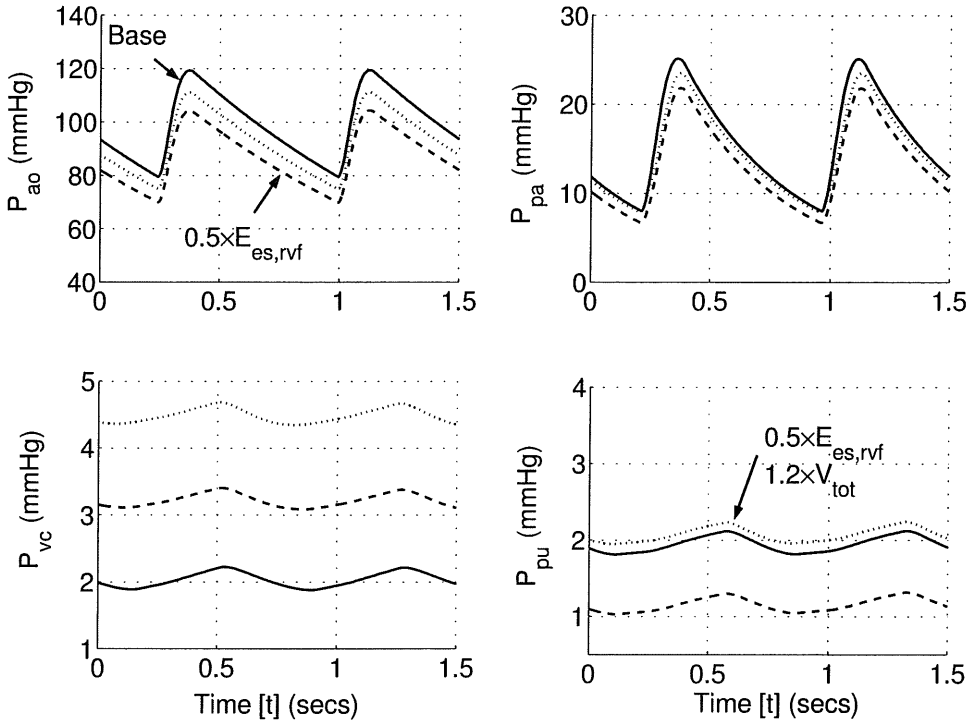

Figure 9.13 Minimal model simulation before (—) and after (- - -) right ventricle infarction, and after increased stressed blood volume (· · ·).

To summarise, the model is found to simulate the main trends characteristic of cardiogenic shock, including decreases in systemic arterial pressure and cardiac output. Simulation of known reflex changes in systemic and pulmonary vascular resistance and stressed blood volume produced model results that more closely match the physiological responses outlined in Table 9.2. Hence, the model may serve as a framework for determining the relative importance and contribution of different reflex actions in the body's response to cardiogenic shock.

9.2.5 Extracardiac Obstructive Shock

Extracardiac obstructive shock results from an obstruction to flow in the cardiovascular system. Examples of obstructions to flow include a pulmonary embolism or pericardial tamponade. Pulmonary embolism is most often caused by a blood clot that has broken free from the veins in the systemic circulation and become lodged in the pulmonary circulation. Pericardial tamponade occurs when blood fills the pericardial chamber and limits the expansion of the ventricles. Different

types of obstructive shock cause different haemodynamic responses including the usual drop in cardiac output and blood pressure.

Pulmonary Embolism

Pulmonary embolism is an obstruction to blood flow in the pulmonary circulation system, potentially due to a blood clot. In an otherwise healthy person more than 50% of the pulmonary vascular area must be blocked to cause a significant rise in pulmonary arterial pressure. This blockage increases the right ventricle afterload and impairs the ability of the right heart to pump blood for oxygenation in the pulmonary system.

Pulmonary embolism is simulated by significantly increasing the pulmonary vascular resistance (R_{pul}) by a factor of 4. This increase in resistance causes cardiac output to drop from the base value of 5.6 L/min to 4.5 L/min. Simulated variations in peripheral pressures during pulmonary embolism are shown in Figure 9.14. A blockage in the pulmonary circulation is generally characterised by an increase in pulmonary arterial pressure (P_{pa}) and central venous pressure (P_{vc}). As a result of the increased pulmonary resistance, the pressure in the pulmonary vein decreases, causing a drop in left ventricle preload and decreases in both systemic arterial pressure (P_{ao}) and cardiac output. The model is able to capture all of these trends without adding compensatory effects due to reflex actions, although an increase in systemic vascular resistance (R_{sys}) causes a recovery in systemic arterial pressure (P_{ao}).

Pericardial Tamponade

Pericardial tamponade occurs due to the accumulation of abnormal amounts of fluid between the inside wall of the pericardium and the outside of the ventricles. This fluid increases the pressure on the ventricles and limits their ability to fill with blood during diastole. The main characteristic of pericardial tamponade is a rise in central venous pressure as ventricle filling is restricted, and blood builds up in the venous system.

Pericardial tamponade is simulated by decreasing the total relaxed volume of the pericardium to half its base value ($0.5 \times V_{0,pcd}$). Figure 9.15 shows the simulated response, with an increase in ventricle filling pressures (P_{vc} and P_{pu}) and a drop in systemic arterial pressure (P_{ao}), matching known physiological

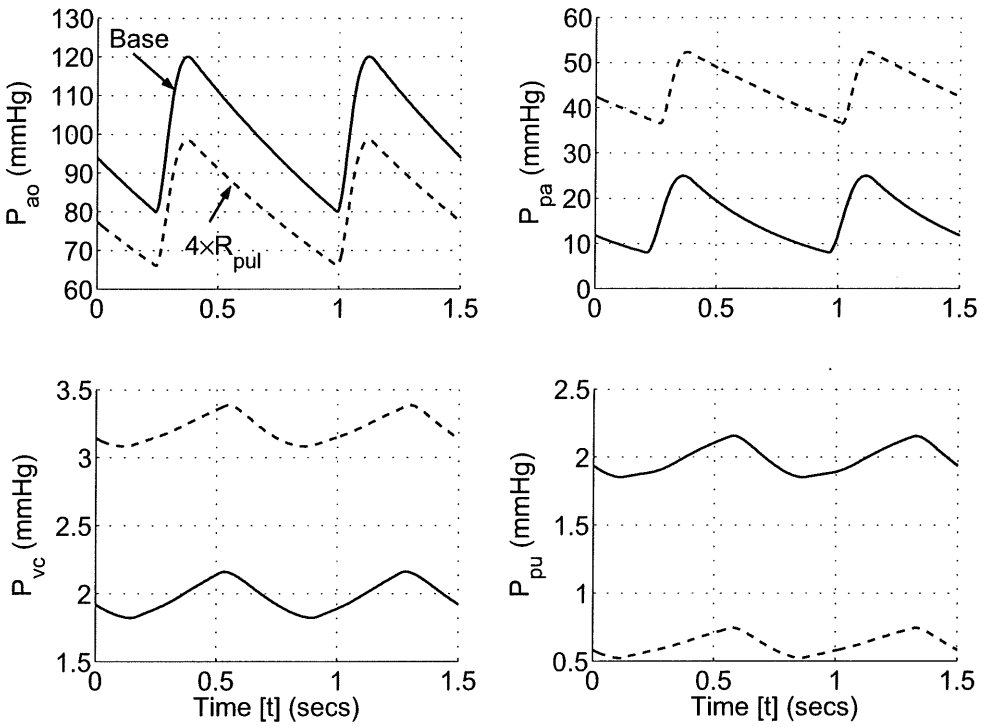

Figure 9.14 Simulation of pulmonary embolism, before (—) and after (- - -).

response in Table 9.2. However, P_{pa} decreased where Table 9.2 indicates the physiological response for the pulmonary artery pressure is to increase.

An explanation for increased P_{pa} is an increase in pulmonary resistance (R_{pul}), but this change is found to cause an undesirable drop in pulmonary venous pressure (P_{pu}) to below the base value. Alternatively, increasing the stressed blood volume caused further increases in P_{vc} and P_{pu}, but has little effect on the value of P_{pa}. However, increasing both pulmonary resistance and the stressed blood volume simultaneously produces results matching those in Table 9.2. The dotted line in Figure 9.15 shows the resulting effect of increasing R_{pul} by a factor of 2 and increasing V_{tot} by a factor of 1.2 to match the expected trend. This case highlights how a combination of reflex actions may be making significant contributions to CVS haemodynamics during shock.

9.2.6 Shock Discussion

The minimal model is shown to simulate all of the variations in pressures, volumes and cardiac output for different cases of shock. In many cases, such as hypovolemic shock, distributive shock and pulmonary embolism, the model is

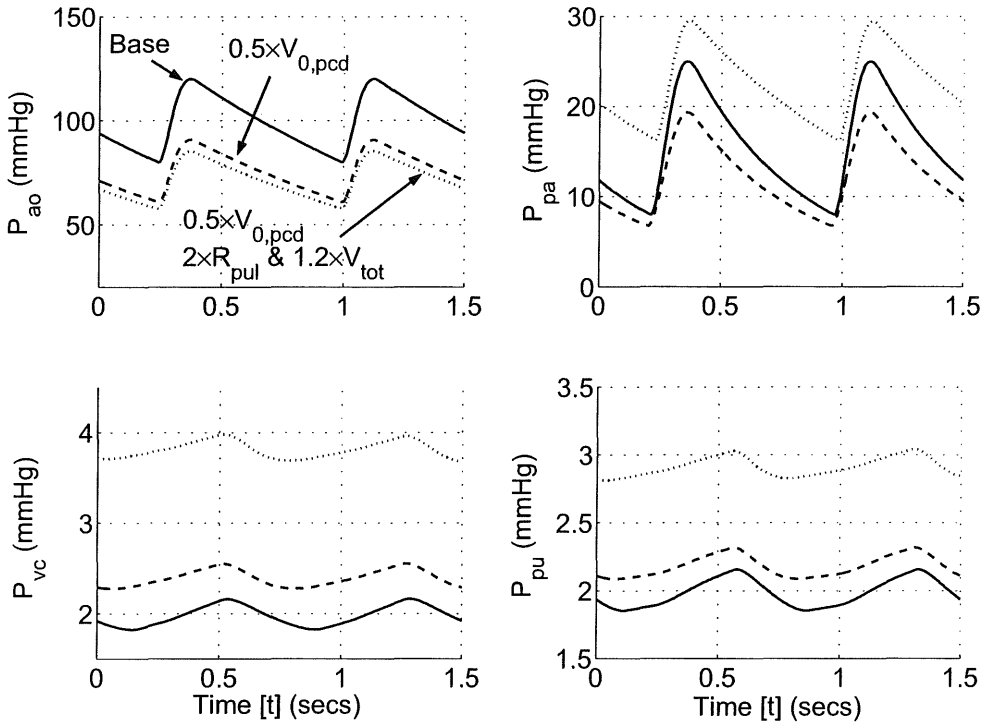

Figure 9.15 Minimal model simulation of pericardial tamponade before (—), after (- - -) and after potential reflex actions (· · ·) .

able to capture all of the published trends when simulating these different types of dysfunction. For the remaining shock states tested, including left and right ventricle cardiogenic shock and pericardial tamponade, the model is able to capture all published trends by simultaneously applying the known effects of one or more reflex actions. The main autonomous nervous reflexes, including increased peripheral resistances and increased stressed volume, were applied where necessary to produce model results matching published variations. Thus, the model enables investigation of the relative contributions of mechanical interactions and different reflex actions to CVS haemodynamics during shock. Given specific data the measurement of these relative contributions can be more exactly determined.

9.3 Summary

This chapter shows a wide range of different types of dysfunction, affecting both the heart and the wider circulation system, that have been simulated using the minimal model and compared with known physiological trends in steady state pressure and volume. It is shown that the model parameters can be modified

to simulate various types of CVS dysfunction and reflex actions. In many cases, the model accurately captures the changes in pressures, volumes and cardiac output in and around the heart during CVS dysfunction. During severe shock, the body's autonomic nervous system responds to decreased cardiac output and blood pressure by initiating powerful reflex actions that significantly affect CVS function. In these cases, it is necessary to include the effects of reflex action in model simulations to match reported physiological trends. Hence, the minimal model can be used to identify the relative contributions of CVS functions and reflex actions. This capability offers a powerful new tool that can be used in conjunction with experimental investigations into CVS function during health and disease.

Chapter 10

Conclusions

Cardiovascular system function involves a complex interaction of mechanical, hydraulic and autonomous reflex effects that can make diagnosis of CVS dysfunction difficult and time consuming. This thesis presents a model of the human CVS that can be used to assist medical staff in understanding, diagnosis and treatment selection for patients with CVS dysfunction. A model is developed using a minimal philosophy leading to a minimum number of parameters, variables and governing equations. The resulting model is both stable and simple to solve, with a simpler structure than most closed loop models in the literature.

The initial focus is on creating a physiologically and fluid dynamically accurate model that is numerically stable. Therefore, the individual function of the separate components including the active and passive elastic chambers, ventricular interaction and components simulating blood flow are developed first. A method of modelling the active cardiac chambers based on the PV diagram is outlined because PV diagrams are commonly used and understood by medical staff. Equations governing fluid flow are included along with a novel approach of tracking velocity profile variations that uses a mixed finite-element and lumped-parameter formulation, and includes time varying resistance and inertial effects. This approach is combined with a physiologically accurate method of simulating heart valve function.

The basic components, such as elastic chambers and elements simulating fluid flow, are verified separately before combining them to create the full closed loop model. The advantages in numerical stability, model robustness and uniqueness of solution of the minimal model approach to CVS modelling are presented. In contrast, other models in the literature were found to be overly complex, unstable, physiologically inaccurate, or too focused on specific aspects of the CVS.

Optimisation is used to achieve one of the key aims of this research, to create

patient specific models by matching specific patient CVS performance. A set of model parameters are adjusted using an optimisation routine until the minimal model output dynamics satisfy a set of objective functions. The optimisation technique presented can be used to make the minimal model match the general CVS function of any animal or human in reasonable time to within 0.1% of target values. Medical staff will be able to investigate irregularities in the optimised parameters to assist in identifying areas of dysfunction. The optimised model can also be used to simulate the known effects of different therapies to assist in choosing a suitable intervention. Thus, patient specific models created using the optimisation approach developed will directly assist medical staff in diagnosis and treatment selection.

Static and dynamic experiments investigating the response of the CVS due to ventricular and cardiopulmonary interactions are used to verify the function of the CVS model. Static responses are commonly used to verify the function of models in the literature, however few other closed loop models accurately simulate the transient dynamics of cardiopulmonary interactions and none simulate the transient dynamics of ventricular interaction. The minimal model is shown to capture the dynamics of both types of interactions accurately. Experimentally quantifying the relative effects of series and direct ventricular interactions is normally a difficult task, however it is shown to be easy using the presented model. In addition, the model also enables the relative importance of different physiological elements in these interactions to be investigated. For example, pulmonary resistance variations during respiration are found to be an important contributor to the dynamics of the pulmonary artery pressure.

The ability of the model to simulate dysfunction is also investigated. Particular cases of heart disease and shock are simulated to compare the minimal model outputs with the known physiological response of the human CVS to various types of dysfunction. Heart disease and shock can cause severe states of dysfunction in the CVS and the body responds with powerful reflex actions. It is shown how the model can be used to not only investigate the effects of dysfunction, but also investigate the most likely reflex responses that contribute to the characteristic CVS measurements. The increased systemic vascular resistance required to maintain mean arterial pressure is an example of a common reflex action that is simulated.

The case studies on ventricular and cardiopulmonary interaction, and cardiac dysfunction, highlight the model's capability to delineate the relative contribu-

tions of different interactions and/or dysfunction to particular CVS responses. Normally, isolating these individual contributions using experimental methods is difficult, if not impossible, however different contributions can be easily included or excluded using the minimal model developed. Thus, the minimal model offers a powerful tool that can be used as a teaching aid, in a research environment to improve understanding of experimentally measured CVS function.

The ability of the minimal model developed to simulate a wide range of CVS dynamics and dysfunction means it can be of direct use in teaching, research and clinical environments. As a teaching aid, the minimal model will help medical students learn more about CVS function through simulation. The minimal model would help researchers develop experimental methods and increase understanding of the results. Clinically, the minimal model can create patient specific models and simulate a variety of dysfunction to assist clinical staff in diagnosis and treatment selection.

The author believes the following areas summarize the novel and significant contribution to knowledge in the area of CVS modelling made in this thesis:

- The minimal model offers a stable, flexible model of the entire CVS that can be used to simulate a variety of dysfunctions. It uses significantly fewer state variables and an event driven solver to account for the changes in state as the valves open and close during the cardiac cycle.

- More physiologically realistic and numerically stable methods of simulating ventricular interaction and valve functions, including a reasonable valve law.

- A physiologically accurate method of simulating pulsatile flow through large arteries for use with lumped-parameter models.

- A novel method of determining initial conditions to improve the rate of convergence, which is particularly useful in parameter identification.

- A method of creating patient specific models using optimisation of model parameters.

- Model verification against experimentally measured transient changes in CVS dynamics due to ventricular and cardiopulmonary interaction. This verification shows the full capability of the model and is unique in the CVS modelling literature.

- Simulation of disease state and the delineation of the relative contributions of autonomous reflex actions on CVS dynamics.

Chapter 11

Future Work

The minimal model developed can simulate many of the major trends in CVS function due to interactions and disease. Further modifications could enable it to more accurately simulate more subtle variations in CVS pressures and volumes, and a wider range of CVS dysfunction. However, as mentioned earlier, care should be taken to only included additional complexity where it will make a significant, and necessary, contribution to the models performance and physiological accuracy.

This section investigates changes to the model structure that would enable it to more accurately simulate some aspects of CVS function, such as the addition of more elastic chambers. The cardiac driver function is also identified as a key area where further work would improve model functional. Potential modifications to the optimisation routine that would produce more accurate results are also discussed. Finally, further work is now needed to specifically investigate how the model can be best used in the clinical environment by medical staff.

11.1 Model Structure

The minimal model presented captures many of the major CVS haemodynamics, which was the initial intention of the model. Many modifications could be carried out using components already developed for the minimal model. This section investigates examples of adding complexity to capture specific dynamics that would improve function and accuracy.

Figure 11.1 shows a potential modification to the model structure where three additional elastic chambers have been added to simulate the left and right atria (la and ra) and divide the systemic artery into two elastic chambers (ao and ar). The addition of atria would enable the model to capture more subtle variations

in ventricle filling pressures, particularly during valvular dysfunction that affect the inlet valves, as discussed in Chapter 8. Dividing the aorta into two chambers would enable the model to simulate the dicrotic notch.

Active elastic chambers, with the same governing equations as the ventricles, could be used to simulate the function of the atria. These chambers would be enclosed in the pericardium and the thoracic cavity, and contribute to the total pericardium volume. The right atrium elastic chamber would not only simulate the right atrium, but also the section of vena-cava that is within the thoracic cavity. Thus, the addition of atria will create a more physiologically accurate representation of the CVS with a minimal addition of complexity.

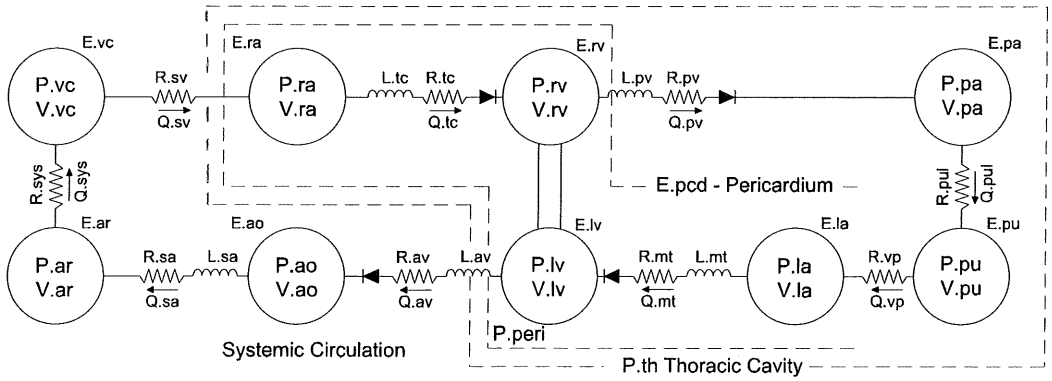

Figure 11.1 Potential model structure for capturing more subtle CVS dynamics.

Figure 11.2 illustrates the dicrotic notch, which is a common characteristic of the aortic pressure profile [Noble, 1968]. The dicrotic notch is a sudden dip in aortic pressure that occurs immediately after the aortic valve closes. It is commonly thought to occur due to inertial effects in the blood flow through the aorta [Fung, 1997; Hurst, 1966]. Immediately after aortic valve closure blood is still flowing through the systemic arteries due to inertial forces, even with a zero, or even positive, pressure gradient. Hence, the pressure in the aorta momentarily drops below the downstream pressure before the flow rate becomes zero and blood flows back into the aorta to equalise the pressures.

By modifying the structure of the minimal model to divide the systemic artery into two chambers separated by a resistance and an inductor, the model should capture the dicrotic notch. When the aortic valve closes, flow through the aortic valve (Q_{av}) is stopped, however blood will still be flowing through the systemic arteries (Q_{sa}) due to the inertial effects modelled by the inertance L_{sa}. This inertial flow will cause the pressure immediately downstream of the left ventricle,

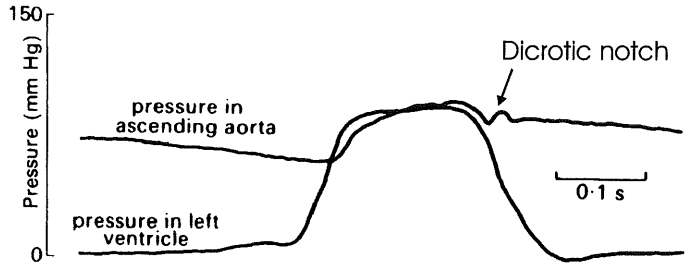

Figure 11.2 Left ventricle and ascending aorta pressures in a dog [Noble, 1968].

in the aorta (P_{ao}), to drop below the pressure in the arterioles (P_{ar}). However, once the Q_{sa} drops to zero, the lower P_{ao} will cause blood to flow back into the aorta. Thus, the pressure in the aorta will dip after valve closer before rising again as blood flows back into the aorta, simulating the dicrotic notch.

These examples of adding chambers to the minimal model illustrate how the structure of the model can be easily extended and modified to capture more subtle CVS dynamics. However, the addition of chambers adds complexity to the model and should only be done where it is necessary. For example, if the only benefit of splitting the systemic artery into two chambers is to capture the dicrotic notch, then this change should only be done when it is necessary to simulate this particular dynamic. The current structure of the minimal model has been shown to capture a wide range of major CVS dynamics in its current state and additional complexity should only be added where it is necessary.

11.2 Cardiac Driver Function

As discussed in Chapter 2, a simple cardiac driver function (e(t)) profile is used to leave the focus on the CVS model function of the components and avoid possible contributions to CVS dynamics from more complex driver profiles. However, further development to make the driver function more physiologically accurate could produce better simulation results. The parameters used to define the shape of the driver profile in Equation (2.4) could also be used as variables in the optimisation routine.

11.3 Optimisation

Chapters 6 and 7 show how optimisation can be used to manipulate the minimal model parameters to achieve target model performance dynamics and create a patient specific model. The application of optimisation techniques to the minimal model can be further extended by modifying the optimisation routine and by adding additional parameters and more objective functions. Examples of potential modifications to the optimisation routine include:

- The importance of the difference between the maximum ventricle pressure and the maximum afterload pressure is illustrated in Chapter 9, relating to valvular dysfunction. The difference in these two maximum values could be added as an objective function in the optimisation routine. Thus, the optimisation of the minimal model may show a significant increase in aortic resistance, which is characteristic of aortic stenosis.

- When plotting cardiac output as a function of heart rate in Chapter 9, the plot of optimised parameters was found to reach a peak at a heartrate that is too low. If the peak heartrate value is known, or estimated, it could be used as an objective function in the optimisation.

- Only the average ventricle filling pressures (Avg P_{vc} and Avg P_{pu}) were used, and no restraint was placed on the amplitude of the variation in these variables. If this pressure information was available it could be added as additional objective functions.

- Model parameters such as the elastance and relaxed volume of the pericardium and the septum could be added as additional optimisation variables, particularly if the focus is on ventricular interaction.

However, care should be taken when choosing appropriate parameters to be used as optimisation variables. Too many parameters will cause large computation time and potentially non-unique solutions. Conversely, if not enough parameters are used, the optimisation routine may not be able to satisfy all of the objective functions.

The optimisation settings and routine could also be modified to accelerate the time taken to find a solution. Many of the optimisation routine settings could be adjusted to produce faster results. For example, Chapter 7 discusses how relaxing the target error to 1% would still produce accurate results, but

take significantly less computational time. Additionally, the generic optimisation routine used could be modified to be more specifically suited to this application.

11.4 Application as a Diagnostic Aid

One of the key initial aims of this research is to create a model that is of direct use to medical staff to help in understanding, diagnosis and treatment selection. This thesis offers a proof of concept of the minimal model to simulate specific patient CVS function. Further development should be focused on the application of the minimal model as a teaching and diagnostic aid. The next stage should involve two areas of development to make the model more useful to medical staff. One area involves investigating the application of the model, how medical staff will use it, and clinical verification. The other area is in decreasing the computational time to find a solution, most directly achieved by converting the model to a faster language, such as C\C++. The result would be increases in the speed of the simulations by an order of 10 to 100 times, and a reduction in the time required for patient specific optimisation to a matter of minutes.

11.5 Summary

The minimal model has been shown to capture a wide range of CVS dynamics. However, further developments in the model structure and governing equations could enable more specific and subtle dynamics to be captured. In particular, the driver function profile could be investigated to make it more physiologically accurate. The optimisation routine could also be further developed by adding more objective functions to create more accurate patient specific models. Finally, further investigation is needed into how the model can be of direct use to medical staff, perhaps by carrying out specific clinical verification and accelerating the computational solution time.

Appendix A

ODE Calculations

Defined below are the equations used at each step of the ODE solver to determine the state derivative of the state vector. Equations labeled [CR] are used when assuming constant resistance and equations labeled [TVR] are used when assuming time varying resistance. All parameters and variables listed below are non-dimensionalised.

If resistance is assumed constant, the state vector ($\underline{x}$) is defined:

$$[\text{CR}] \qquad \underline{x} = [V_{pu}, Q_{mt}, V_{lv}, Q_{av}, V_{ao}, V_{vc}, Q_{tc}, V_{rv}, Q_{pv}, V_{pa}] \tag{A.1}$$

Otherwise, if simulating time varying resistance then the state vector is defined:

$$[\text{TVR}] \qquad \underline{x} = [V_{pu}, \underline{u}_{mt}, V_{lv}, \underline{u}_{av}, V_{ao}, V_{vc}, \underline{u}_{tc}, V_{rv}, \underline{u}_{pv}, V_{pa}] \tag{A.2}$$

$$[\text{CR\&TVR}] \qquad e = e(t) = \sum_{i=1}^{N} A_i e^{-B_i(t-C_i)^2} \tag{A.3}$$

$$[\text{CR\&TVR}] \qquad P_{th} = f(t) \tag{A.4}$$

$$[\text{CR\&TVR}] \qquad V_{pcd} = V_{lv} + V_{rv} \tag{A.5}$$

$$[\text{CR\&TVR}] \qquad P_{pcd} = P_{0,pcd}(e^{\lambda_{pcd}(V_{pcd}-V_{0,pcd})} - 1) \tag{A.6}$$

$$[\text{CR\&TVR}] \qquad P_{peri} = P_{pcd} + P_{th} \tag{A.7}$$

Determine V_{spt} by solving [CR & TVR]:

$$\begin{aligned} &eE_{es,spt}(V_{spt} - V_{d,spt}) + (1-e)P_{o,spt}(e^{\lambda_{spt}(V_{spt}-V_{o,spt})} - 1) \\ &= eE_{es,lvf}(V_{lv} - V_{spt} - V_{d,lvf}) + (1-e)P_{o,lvf}(e^{\lambda_{lvf}(V_{lv}-V_{spt}-V_{o,lvf})} - 1) \\ &-eE_{es,rvf}(V_{rv} + V_{spt} - V_{d,rvf}) - (1-e)P_{o,rvf}(e^{\lambda_{rvf}(V_{rv}+V_{spt}-V_{o,rvf})} - 1) \end{aligned} \tag{A.8}$$

$$[\text{CR\&TVR}] \qquad V_{lvf} = V_{lv} - V_{spt} \tag{A.9}$$

$$[\text{CR\&TVR}] \qquad V_{rvf} = V_{rv} + V_{spt} \tag{A.10}$$

$$[\text{CR\&TVR}] \qquad P_{lvf} = eE_{es,lvf}(V_{lvf} - V_{d,lvf}) + (1-e)P_{o,lvf}(e^{\lambda_{lvf}(V_{lvf}-V_{o,lvf})} - 1) \tag{A.11}$$

$$[\text{CR\&TVR}] \qquad P_{rvf} = eE_{es,rvf}(V_{rvf} - V_{d,rvf}) + (1-e)P_{o,rvf}(e^{\lambda_{rvf}(V_{rvf}-V_{o,rvf})} - 1) \tag{A.12}$$

$$[\text{CR\&TVR}] \qquad P_{lv} = P_{lvf} + P_{peri} \tag{A.13}$$

$$[\text{CR\&TVR}] \qquad P_{rv} = P_{rvf} + P_{peri} \tag{A.14}$$

$$[\text{CR\&TVR}] \qquad P_{pu} = E_{pu}(V_{pu} - V_{d,pu}) + P_{th} \tag{A.15}$$

$$[\text{CR\&TVR}] \qquad P_{pa} = E_{pa}(V_{pa} - V_{d,pa}) + P_{th} \tag{A.16}$$

$$[\text{CR\&TVR}] \qquad P_{vc} = E_{vc}(V_{vc} - V_{d,vc}) \tag{A.17}$$

$$[\text{CR\&TVR}] \qquad P_{ao} = E_{ao}(V_{ao} - V_{d,ao}) \tag{A.18}$$

$$[\text{CR\&TVR}] \qquad Q_{sys} = \frac{P_{ao} - P_{vc}}{R_{sys}} \tag{A.19}$$

$$[\text{CR\&TVR}] \qquad Q_{pul} = \frac{P_{pa} - P_{pu}}{R_{pul}} \tag{A.20}$$

$$[\text{CR}] \qquad \dot{Q}_{mt} = \frac{480\nu}{\bar{r}^2 HR} \times \frac{P_{pu} - P_{lv} - Q_{mt}R_{mt}}{L_{mt}} \tag{A.21}$$

$$[\text{CR}] \qquad \dot{Q}_{av} = \frac{480\nu}{\bar{r}^2 HR} \times \frac{P_{lv} - P_{ao} - Q_{av}R_{av}}{L_{av}} \tag{A.22}$$

$$[\text{CR}] \qquad \dot{Q}_{tc} = \frac{480\nu}{\bar{r}^2 HR} \times \frac{P_{vc} - P_{rv} - Q_{tc}R_{tc}}{L_{tc}} \tag{A.23}$$

$$[\text{CR}] \qquad \dot{Q}_{pv} = \frac{480\nu}{\bar{r}^2 HR} \times \frac{P_{rv} - P_{ao} - Q_{pv}R_{pv}}{L_{pv}} \tag{A.24}$$

$$[\text{CR\&TVR}] \qquad \dot{V}_{pv} = Q_{pul} - Q_{mt} \tag{A.25}$$

$$[\text{CR\&TVR}] \qquad \dot{V}_{lv} = Q_{mt} - Q_{av} \tag{A.26}$$

$$[\text{CR\&TVR}] \qquad \dot{V}_{ao} = Q_{av} - Q_{sys} \tag{A.27}$$

$$[\text{CR\&TVR}] \qquad \dot{V}_{vc} = Q_{sys} - Q_{tc} \tag{A.28}$$

$$[\text{CR\&TVR}] \qquad \dot{V}_{rv} = Q_{tc} - Q_{pv} \tag{A.29}$$

$$[\text{CR\&TVR}] \qquad \dot{V}_{pa} = Q_{pv} - Q_{pul} \tag{A.30}$$

$$[\text{CR}] \qquad \frac{d\underline{x}}{dt} = \left[\dot{V}_{pu}, \dot{Q}_{mt}, \dot{V}_{lv}, \dot{Q}_{av}, \dot{V}_{ao}, \dot{V}_{vc}, \dot{Q}_{tc}, \dot{V}_{rv}, \dot{Q}_{pv}, \dot{V}_{pa}\right] \tag{A.31}$$

$$[\text{TVR}] \qquad \frac{d\underline{x}}{dt} = \left[\dot{V}_{pu}, \dot{\underline{u}}_{mt}, \dot{V}_{lv}, \dot{\underline{u}}_{av}, \dot{V}_{ao}, \dot{V}_{vc}, \dot{\underline{u}}_{tc}, \dot{V}_{rv}, \dot{\underline{u}}_{pv}, \dot{V}_{pa}\right] \tag{A.32}$$

References

Amoore, J., Santamore, W., Corin, W., and George, D. (1992). Computer simulation of the effects of ventricular interdependence on indices of left ventrilcular systolic function. *J. Biomed. Eng*, 14:257–262. [P-V relations].

Avanzolini, G., Barbini, P., Cappello, A., Cevenini, G., Pohl, V., and Sikora, T. (March 1989). Tracking time-varying properties of the systemic vascular bed. *IEEE Trans. Biomed. Eng.*, 3(3):373–381.

Avanzolini, G., Barbini, P., Cappello, A., and Cevese, A. (Oct 1985). Time-varying mechanical properties of the left ventricle - a computer simulation. *IEEE Trans. Bio. Eng.*, BME-32(10):756–763. Time-varying mechanical properties, good paper.

Bartlett, B. and Fyfe, D. (1974). *Handbook of mathematical formulae for engineers and scientists.* Denny publications ltd, London.

Bellhouse, B. J. and Talbot, L. (1969). The fluid mechanics of the aortic valve. *J. Fluid Mech.*, 35(4):721–735.

Beyar, R., Hausknecht, M. J., Halperin, H. R., Yin, F. C., and Weisfeldt, M. L. (1987). Interaction between cardiac chambers and thoracic pressure in intact circulation. *Am. J. Physiol.*, 22(253):H1240–H1252.

Bove, A. A. and Santamore, W. P. (Mar/Apr 1981). Ventricular interdependence. *Prog. Cardio. Disease*, 265(5):365–387.

Braunwald, E. (1997). *Heart Disease, A text book of cardiovascular medicine, 5th edition.* W.B. Saunders Company, Philadelphia.

Buda, A. J., Pinsky, M. R., Ingels, N. B., J., Daughters, G. T., n., Stinson, E. B., and Alderman, E. L. (1979). Effect of intrathoracic pressure on left ventricular performance. *N Engl J Med*, 301(9):453–9.

Buist, M., Pullan, A., and Hunter, P. (1999). Modelling electrical activity from cell to body surface. In *IEEE: Proceedings of the first joint BMES/EMBS Conference*, page 1174, Atlanta, GA, USA.

Burkhoff, D. and Tyberg, J. V. (1993). Why does pulmonary venous pressure rise after onset of lv dysfunction: a theoretical analysis. *Am. J. Physiol.*, 265:H1819–H1828.

Campbell, K. B., Kirkpatrick, R. D., Knowlen, G. G., and Ringo, J. A. (Jan 1990). Late-systolic pumping properties of the left ventricle. *Circ. Res.*, 66(1):218–233. time-varying properties such as elactance and resistance.

Chung, D. (1996). *Ventricular Interaction in a Closed-Loop model of the canine circulation.* Master of science, Rice University.

Chung, D., Niranjan, S., Clark, J., Bidani, A., and Johnston, W. (1997). A dynamic model of ventricular interaction and pericardial influence. *Am. J. Physiol.*, 14(272):H2924–H2962.

Conn, A. R., Gould, N. I. M., and Toint, P. L. (2000). *Trust-Region Methods.* Society for Industrial and Applied Mathematics, Philadelphia, PA.

Denault, A. Y., Gasior, T. A., Gorcsan, J., r., Mandarino, W. A., Deneault, L. G., and Pinsky, M. R. (1999). Determinants of aortic pressure variation during positive-pressure ventilation in man. *Chest*, 116(1):176–86. 0012-3692 Journal Article.

Denault, A. Y., Gorcsan, J., r., and Pinsky, M. R. (2001). Dynamic effects of positive-pressure ventilation on canine left ventricular pressure-volume relations. *J Appl Physiol*, 91(1):298–308. 8750-7587 Journal Article.

Frazier, O. H., Myers, T. J., Jarvik, R. K., Westaby, S., Pigott, D. W., Gregoric, I. D., Khan, T., Tamez, D. W., Conger, J. L., and Macris, M. P. (2001). Research and development of an implantable, axial-flow left ventricular assist device: the jarvik 2000 heart. *Ann Thorac Surg*, 71(3 Suppl):S125–32; discussion S144–6.

Fung, Y. (1990). *Biomechanics: Motion, flow, stress, and growth.* Springer-Verlag, San Deigo.

Fung, Y. (1993). *Biomechanics: Mechanical properties of Living Tissues, 2nd Edition.* Springer-Verlag, San Deigo.

Fung, Y. (1997). *Biomechanics: Circulation.* Springer-Verlag, New York.

Funk and Wagnalls (1960). *Funk and Wagnalls Standard Dictionary of the English Language.* Funk and Wagnalls Co., New York.

Ganong, W. F. (1979). *Review of Medical Physiology, 9th Edition.* Lange Medical Publications, Los Altos, California.

Glantz, S. A. and Parmley, W. W. (1978). Factors which affect the diastolic pressure-volume curve. *Circ Res*, 42(2):171–80.

Glass, L., Hunter, P., and McCulloch, A. (1991). *Theory of Heart, Biomechanics, Biophysics, and Nonlinear Dynamics of Cardiac Function.* Springer-Verlag New York, Inc.

Groeneveld, A. and Thijs, L. (1995). Hypovolemic shock. In Parrillo, J. E. and Bone, R. C., editors, *Critical Care Medicine, Principles of diagnosis and management.* Mosby, St. Louis, Missouri.

Guyton, A. C. (1991). *Textbook of medical physiology.* W.B. Saunders Company, Philadelphia, 8 edition.

Hancock, E. W. (1995). Pericardial tamponade. In Parrillo, J. E. and Bone, R. C., editors, *Critical Care Medicine, Principles of diagnosis and management.* Mosby, St. Louis, Missouri.

Hardy, H. H. and Collins, R. E. (1982). On the pressure-volume relationship in circulatory elements. *Med Biol Eng Comput*, 20(5):565–70.

Hardy, H. H., Collins, R. E., and Calvert, R. E. (1982). A digital computer model of the human circulatory system. *Med Biol Eng Comput*, 20(5):550–64.

Hoit, B. D., Shao, Y., Gabel, M., and Walsh, R. A. (1993). Influence of pericardium on left atrial compliance and pulmonary venous flow. *Am J Physiol*, 264(6 Pt 2):H1781–7.

Hoppensteadt, F. C. and Peskin, C. S. (2002). *Modeling and Simulation in Medicine and the Life Sciences.* Springer-Verlag, New York.

Hunter, P., Hookings, A., LeGrice, I., and Smaill, B. (1991). Activation of the heart with a 3d finite element model. In *Annual International Conference of the IEEE Engineering in Medicine and Biology Society*, volume 13, 2, pages 681–983.

Hunter, W. C., Janicki, J. S., Weber, K. T., and Noordergraff, A. (1983). Systolic mechnical properties of the left ventricle. *Circulation Research*, 52(3):319–327.

Hurst, J. W. (1966). *The heart, arteries and veins (3rd edition).* McGraw-Hill, Kogakusha Ltd, Tokyo.

Janicki, J. S. and Weber, K. T. (1980). The pericardium and ventricular interaction, distensibility, and function. *Am J Physiol*, 238(4):H494–503.

Katz, A. M. (2002). A modern view of heart failure: practical applications of cardiovascular physiology. In Page, E., Fozzard, H. A., and Solaro, R. J., editors, *Handbook of medical physiology, Section 2: The cardiovascular system, Volume 1: The heart.* Oxford university press, New York, USA.

Kumar, A. and Parrillo, J. E. (1995). Shock: Classification, pathophysiology, and approach to management. In Parrillo, J. E. and Bone, R. C., editors, *Critical Care Medicine, Principles of diagnosis and management.* Mosby, St. Louis, Missouri.

Lazar, J. M., Flores, A. R., Grandis, D. J., Orie, J. E., and Schulman, D. S. (1993). Effects of chronic right ventricular pressure overload on left ventricular diastolic function. *Am J Cardiol*, 72(15):1179–82. 0002-9149 Journal Article.

Legrice, I., Hunter, P., and Smaill, B. (1997). Laminar structure of the heart: a mathematical model. *Am J Physiol*, 272:H2466–76.

Little, R. C. (1978). *Physiology of the Heart and Circulation.* Year book medical publishers, Inc., New York.

Lu, K., Clark, J., Ghorbel, F., Ware, D., and Bidani, A. (2001). A human cardiopulomonary system model applied to the analysis of the valsalva maneuver. *Am. J. Physiol.*, 281:H2661–H2679.

Marcus, J. T., Vonk Noordegraaf, A., Roeleveld, R. J., Postmus, P. E., Heethaar, R. M., Van Rossum, A. C., and Boonstra, A. (2001). Impaired left ventricular filling due to right ventricular pressure overload in primary pulmonary hypertension: noninvasive monitoring using mri. *Chest*, 119(6):1761–5.

Maughan, W. and Kass, D. A. (1988). The use of the pressure-volume diagram for measuring ventricular pump function. *Automedica*, 11:317–342.

Maughan, W. L., Sunagawa, K., and Sagawa, K. (1987). Ventricular systolic interdependence: volume elastance model in isolated canine hearts. *Am. J. Physiol.*, 253:H1381–H1390. [Ventricular interaction].

Melchior, F. M., Sriniwasan, R. S., and Charles, J. B. (1992). Mathematical modeling of human cardiovascular system for simulation of orthostatic response. *Am. J. Physiol.*, 262:H1920–H1933.

Natanson, C., Hoffman, W. D., and Parrillo, J. E. (1995). Septic shock and multiple organ failure. In Parrillo, J. E. and Bone, R. C., editors, *Critical Care Medicine, Principles of diagnosis and management.* Mosby, St. Louis, Missouri.

Nielsen, P. M., Le Grice, I. J., Smaill, B. H., and Hunter, P. J. (1991). Mathematical model of geometry and fibrous structure of the heart. *Am J Physiol*, 260(4 Pt 2):H1365–78.

Noble, M. I. (1968). The contribution of blood momentum to left ventricular ejection in the dog. *Circ Res*, 23(5):663–70. 0009-7330 Journal Article.

Norton, J. M. (2001). Toward consistent definitions for preload and afterload. *Adv Physiol Educ*, 25(1-4):53–61. 1043-4046 Journal Article Review Review Literature.

Olansen, J., Clark, J., Khoury, D., Ghorbel, F., and Bidani, A. (2000). A closed-loop model of the canine cardiovascular system that includes ventricular interaction. *Comp. Biomed. Res.*, 33:260–295.

Opie, L. H. (1998). *The heart : physiology, from cell to circulation, 3rd ed.* Lippincott-Raven, Philadelphia.

Parrillo, J. E. and Bone, R. C. (1995). *Critical Care Medicine, Principles of diagnosis and management.* Mosby, St. Louis, Missouri.

Parry-Jones, A. and Pittman, J. (2003). Arterial pressure and stroke volume variability as measurements for cardiovascular optimisation. *International Journal of Intensive Care.*

Parsons, R. H. (2002). Human parameters. *http://bio.bio.rpi.edu /Parsons /Universal/2HemorVolume%20Lab /HemPar2.html.*

Peskin, C. S. and McQueen, D. M. (1992). Cardiac fluid dynamics. *Crit Rev Biomed Eng*, 20(5-6):451–9.

Santamore, W. P. and Burkhoff, D. (1991). Hemodynamic consequences of ventricular interaction as assessed by model analysis. *Am. J. Physiol.*, 260:H146–H157.

Santamore, W. P. and Dell'Italia, L. J. (Jan/Feb 1998). Vantricular interdependence: Significant left ventricular contributions to right ventricular systolic function. *Prog. Cardiovascular Diseases*, 40(4):289–308.

Scharf, S. M., Brown, R., Saunders, N., and Green, L. H. (1979). Effects of normal and loaded spontaneous inspiration on cardiovascular function. *J Appl Physiol*, 47(3):582–90.

Scharf, S. M., Brown, R., Saunders, N., and Green, L. H. (1980). Hemodynamic effects of positive-pressure inflation. *J Appl Physiol*, 49(1):124–31.

Scharf, S. M. and Cassidy, S. S. (1989). *Heart-lung interactions in health and disease.* Marcel Dekker Inc, New York.

Schwartz, D. R., Maroo, A., Malhotra, A., and Kesselman, H. (1999). Negative pressure pulmonary hemorrhage. *Chest*, 115(4):1194–7. 0012-3692 Journal Article.

Segers, P., Stergiopulos, N., Schreuder, J. J., Westerhof, B. E., and Westerhof, N. (2000a). Left ventricular wall stress normalization in chronic pressure-overloaded heart: a mathematical model study. *Am J Physiol Heart Circ Physiol*, 279(3):H1120–7.

Segers, P., Stergiopulos, N., and Westerhof, N. (2000b). Quantification of the contribution of cardiac and arterial remodeling to hypertension. *Hypertension*, 36(5):760–5.

Skatssoon, J. (2003). Patient given new type of heart pump. *The Courier-Mail, Queensland Newspapers.*

Slinker, B. K. and Glantz, S. A. (1986). End-systolic and end-diastolic ventricular interaction. *Am J Physiol*, 251(5 Pt 2):H1062–75.

Slinker, B. K. and Glantz, S. A. (1989). Beat-to-beat regulation of left ventricular function in the intact cardiovascular system. *Am J Physiol*, 256(4 Pt 2):R962–75.

Smith, B. W., Chase, J. G., Nokes, R. I., Shaw, G. M., and Wake, G. (2003a). A minimal cardiovascular system haemodynamic model for rapid diagnostic assistance. In *5th IFAC 2003 Symposium on Modelling and Control in Biomedical Systems*, pages 427–432, Melbourne, Australia.

Smith, B. W., Chase, J. G., Nokes, R. I., Shaw, G. M., and Wake, G. (2003b). Minimal haemodynamic system model including ventricular interaction and valve dynamics. *Medical Engineering and Physics*, (Accepted, to be published).

Stergiopulos, N., Segers, P., and Westerhof, N. (1999). Use of pulse pressure method for estimating total arterial compliance in vivo. *Am J Physiol*, 276(2 Pt 2):H424–8.

Stevens, C. and Hunter, P. J. (2003). Sarcomere length changes in a 3d mathematical model of the pig ventricles. *Prog Biophys Mol Biol*, 82(1-3):229–41. 0079-6107 Journal Article Review Review, Tutorial.

Suga, H., Sagawa, K., and Shoukas, A. A. (March 1973). Load independence of the instantaneous pressure-volume ratio of the canine left ventricle and effects of epinephrine and heart rate on the ratio. *Circulation Res.*, 32:314–322.

Sun, Y., Beshara, M., Lucariello, R. J., and Chiaramida, S. A. (1997). A comprehensive model for right-left heart interaction under the influence of pericardium and baroreflex. *Am J Physiol*, 272(3 Pt 2):H1499–515.

Tsitlik, J. E., Halperin, H. R., Popel, A. S., Shoukas, A. A., Yin, F. C., and Westerhof, N. (1992). Modeling the circulation with three-terminal electrical networks containing special nonlinear capacitors. *Ann Biomed Eng*, 20(6):595–616.

Ursino, M. (1999). A mathematical model of the carotid baroregulation in pulsating conditions. *IEEE Trans Biomed Eng*, 46(4):382–92.

VentrAssist (2003). http://www.ventrassist.com/.

Vis, M. A., Sipkema, P., and Westerhof, N. (1997). Modeling pressure-flow relations in cardiac muscle in diastole and sysole. *Am. J. Physiol.*, 272:H1516–H1526.

Weber, K. T., Janicker, J. S., Hunter, W. C., Shroff, S., Pearlman, E. S., and Fishman, A. P. (March/April 1982). The contractile behaviour of the heart

and its functional coupling to the circulation. *Prog. Card. Dis.*, 24(5):375–400. Good general summary of heart stuff.

Weber, K. T., Janicki, J. S., Shroff, S., and Fishman, A. P. (1981). Contractile mechanics and interaction of the right and left ventricles. *Am J Cardiol*, 47(3):686–95.

West, J. B. (1985). *Respiratory Physiology - the essentials, 3rd Edition.* Waverly Press, Inc., Baltimore.

Westaby, S., Banning, A. P., Jarvik, R., Frazier, O. H., Pigott, D. W., Jin, X. Y., Catarino, P. A., Saito, S., Robson, D., Freeland, A., Myers, T. J., and Poole-Wilson, P. A. (2000). First permanent implant of the jarvik 2000 heart. *Lancet*, 356(9233):900–3.

Westerhof, N. (2003). Special issue on mechanics of the cardiovascular system. *J. Biomech.*, 36(5):621–622.

White, F. M. (1991). *Viscous Fluid Flow, Second Edition.* McGraw-Hill, Inc, USA.

Wijkstra, H. and Boom, H. B. (Dec 1991). Left-ventricular dynamic model based on constant ejection flow periods. *IEEE Trans. Biomed. Eng.*, 38(12):1204–1212. [Time varying mechanical properties].